THE EROSIVE CHARACTERISTICS OF SOUTH AFRICAN PULVERIZED COALS

by

Torill Marie Karlsen

A thesis submitted to the Faculty of Engineering, University of Cape Town, in fulfilment of the degree of Master of Science in Applied Science

Department of Materials Engineering
University of Cape Town
1985

ABSTRACT

A characterization and comparison of the erosive characteristics of four power generation pulverized fuels and several pure abrasives - quartz, silicon carbide, alumina and zircon - was undertaken in order to select a suitable substitute for the pulverized fuels for use in accelerated erosion tests.

A study of the influence of particle parameters on erosion rate established that the effects of these parameters corresponded reasonably well with those predicted by the theoretical models of erosion. The particle size exponents obtained in this study are in close agreement with those predicted theoretically and the particle density exponent supported the value of 1.20 predicted by the quasi-static model of erosion. The range of velocity exponent values obtained encompassed those predicted by both the dynamic model of erosion ($n = 3.2$) and the quasi-static model ($n = 2.4$), and were comparable to the values obtained by other researchers. A definite velocity exponent-particle size dependence was observed for quartz and silicon carbide, with the exponent decreasing as particle size increased. This dependence may be expressed by a relationship of the form $n = qD^{-p}$.

The erosive characteristics of the pulverized fuels could not be predicted in terms of particle size distribution and X-ray diffraction analysis alone, and hence an investigation of the single impact damage was undertaken. The actual damage created by the abrasive media was examined by means of lineal analysis of the single particle impact sites. It was demonstrated that the range of damage sizes produced by any one abrasive is an order of magnitude larger than the range of particles sizes, a phenomenon which is thought to be the result of particle orientation effects. The results of the single impact study established that only the largest particles are important contributors to the total volume of target material that is removed.

The selection of 115 μm diameter quartz as the most suitable substitute for the pulverized fuels for use in accelerated erosion tests was based upon consideration of both the particle parameters and the damage parameters. The quartz produced erosion rates that were greater than that of the pulverized fuels by factors of 21 to 100 when considering a particle velocity of 35 ms^{-1}.

ACKNOWLEDGMENTS

I would like to thank the following people who assisted me in producing this thesis.

Professor R.O. Heckroodt, my supervisor, for his patience, support and guidance.

Tracey Leveton who did the typing.

Bernard Greeves for the photographic work.

Nic Dreze, Andrew Rapley and Reggie Hendricks for assistance in the workshop.

Anne-Marie Nathan who did the drawings.

Staff and fellow students for their support and encouragement.

The Electricity Supply Commision of South Africa is gratefully acknowledged for their financial assistance.

CONTENTS

CHAPTER 1 : INTRODUCTION

Pneumatic conveying is a widely used technique for transporting pulverized coal in power stations. Pulverized coal can be a particularly erosive material and a well-known problem in power stations is the wear associated with the many right-angled bends that are common in pneumatic conveying systems.

Ceramics have gained acceptance as lining materials to combat this erosive wear and it is necessary to have an increased understanding of the erosion mechanisms of these materials when evaluating their relative merits and when comparing their performance under the conditions thought to pertain to power stations.

It is well known that homogeneous ceramic materials erode predominantly by brittle fracture but that plastic deformation also occurs and plays an important role. The more recent analyses of brittle erosion have encompassed the concepts of elastic-plastic deformation into the erosion models. Both the models which are now generally accepted are based on single impact events and were developed for materials under idealized conditions. Despite differences in the inital underlying assumptions, both models relate erosion rate to particle velocity, particle size, particle density, target fracture toughness and target hardness. Before any assessment of the usefulness of various lining materials for combatting erosion in pulverized fuel pipelines can be made, it was necessary to investigate the validity of the erosion models, to characterize a few of the typical pulverized coals and to select a suitable abrasive to replace the pulverized coal for accelerated erosion tests. Accordingly, a number of objectives were pursued in this investigation.

(i) Since the present research was not concerned with the candidate materials themselves, the influence on the erosion rate of the particle parameters only, were dealt with. Glass microscope slides were used as the target material throughout the testing, thus eliminating the influences of target parameters on erosion rate. Several abrasive media - quartz, silicon carbide, alumina and zircon - were employed.

(ii) It would be unrealistic to test the candidate materials with pulverized coal under the conditions prevailing at the power stations, viz. velocities of 15 to 30 ms^{-1} and angles of impingement of less than 45°, since measureable weight losses would not be obtained within a reasonable time scale. Hence, accelerated testing would be required and therefore the influence of velocity and angle of attack on erosion rate was investigated using pure abrasives and higher velocities (25 to 55 ms^{-1}) as well as angles of 90°.

(iii) The pulverized fuels were characterized in terms of their erosion rates, bulk mineralogical compositions and particle size distributions. The selection of a suitable replacement for the pulverized fuels was based upon a comparison of the erosive characteristics of the pulverized fuels with those of quartz, silicon carbide, alumina and zircon particles.

(iv) Finally, since the models of brittle erosion pertain to single impact events, the possibility of determining the volume of material removed by a particular particle type by analysis of the single impact events, was investigated.

CHAPTER 2 : A REVIEW OF EROSION BY SOLID PARTICLES

The erosion behaviour of a brittle material was studied in order to assess the effect of impact parameters and particle parameters on solid particle wear. In addition, the validity of the elastic-plastic models of erosion was investigated. Since solid particle erosion is thought to be a discrete, accumulative process, it was also considered important to understand the single impact event as well as multiple particle effects.

The above-mentioned issues, which are relevant to the present investigation, will be addressed in the sections which follow.

2.1 THE IMPACT PARAMETERS

2.1.1 Velocity

Investigations of the effect of velocity on erosion have all yielded a relationship of the form

$$E \propto \text{constant} \cdot V^n \quad (1)$$

where E = the erosion rate
V = the impacting particle velocity
n = the velocity exponent

Evans et al (1978) and Evans (1979) have both derived expressions for a critical threshold velocity (V_c) below which fracture does not occur. Both expressions predict a reciprocal dependence on target hardness, particle size and particle density and a direct dependence on the fracture toughness of the target. Although the expressions determine a threshold velocity for the occurrence of radial fracture (responsible for strength degradation), it is

reasonable to assume that lateral fracture (responsible for material removal) would exhibit the same dependencies. However, as stated by Evans, results supporting the equations are sparse and much additional study is needed in order to fully comprehend the threshold.

2.1.2 The Velocity Exponent

The velocity exponents of brittle materials generally range from 2 to 3 although both higher and lower exponents have been reported (Table 2.1).

TABLE 2.1 : Summary of Particle Velocity Exponents from Literature

TARGET MATERIAL	PARTICLE TYPE	PARTICLE SIZE (μm)	VELOCITY (ms^{-1})	ANGLE (°)	VELOCITY EXPONENT	REFERENCE
Fibre glass, glass	Quartz	125 - 150	61 - 549	90	2.3	Goodwin et al (1969)
Plate glass	SiC	200 100	61 & 183	90	3	Sheldon & Finnie (1966a)
"	steel-shot	400	38 & 107	90	4.37	
Pyrex glass	Al_2O_3	30	28 - 65	90	2.2	Sargent et al (1979)
	Al_2O_3	10	58 - 84	90	2.7	
Soda lime silica glass	SiC	150	37 - 94	90	2.5	Wiederhorn & Hockey (1983)
Vitreous silica	SiC	150	37 - 94	90	2.9	
PPG float glass at 440° - 770°C	glass-spheres	3000	-	90	2.3-2.7	Kirchner & Gruver (1978)
MgF_2, Si_3N_4	Quartz, SiC	10 - 1000	61 - 275	-	3.2	Gulden (1981)
Al_2O_3, steel	SiO_2,SiC	172, 80	40, 46	-	3.0	Dimond et al (1983)
HP SiC	Al_2O_3	130	108 - 151	40	1.2	Routbort & Scattergood (1980)
HP SiC	Al_2O_3	130	108 - 151	90	1.8	
HP SiC	Al_2O_3	270	108 - 151	40	1.7	
HP SiC	Al_2O_3	270	108 - 151	60	1.5	
HP SiC	Al_2O_3	270	108 - 151	90	1.5	

Continued/...

TARGET MATERIAL	PARTICLE TYPE	PARTICLE SIZE (μm)	VELOCITY (ms^{-1})	ANGLE (°)	VELOCITY EXPONENT	REFERENCE
RB SiC	Al_2O_3	130	54 - 151	40	2.5	Routbort et al (1980b)
RB SiC	Al_2O_3	130	54 - 151	90	2.3	
RB SiC	Al_2O_3	270	54 - 151	40	2.2	
RB SiC	Al_2O_3	270	54 - 151	60	2.2	
RB SiC	Al_2O_3	270	54 - 151	90	2.0	
11% Cr Steel	Quartz	125 - 150	61 - 549	90	2.3	Goodwin et al (1969)
11% Cr Steel	Glass sphere	125 - 150	61 - 549	90	3.4	Tilly & Sage (1970)
11% Cr Steel	Diamond		61 - 549	90	2.3	
Aluminium alloy	Glass sphere		61 - 549	90	2.4	
Aluminium alloy	Diamond		61 - 549	90	2.3	
Silicon single crystal	Al_2O_3	23, 37, 130 & 270	32 - 151	90	3.4 (23 μm) 2.6 (170 μm)	Scattergood & Routbort (1981)
MgF_2	Quartz	10 - 385	15 - 343	90	4	Gulden (1979)
RB Si_3N_4	Quartz (high veloc.)	10 - 385	15 - 343	90	4	
HP Si_3N_4	SiC	10 - 385	15 - 343	90	4	
HP Si_3N_4	Quartz	10 - 385	15 - 343	90	1	
GB Al_2O_3	Quartz	10 - 385	15 - 343	90	1 to 3	
MgO	SiC	200 and 100	61 & 183	90	2.74	Sheldon & Finnie (1966a)
Graphite	SiC	200 and 100	61 & 183	90	2.69	
Al_2O_3	SiC	200 and 100	61 & 183	90	2.62	
MgO	Steel-shot	400	38 & 107	90	2.73	
Graphite	Steel-shot	400	38 & 107	90	2.67	
Silicon single crystal	SiC	38	100	90	3	Marshall et al (1981)
95% Al_2O_3 castable refractory	SiC	150	10 - 100	90	2.8	Wiederhorn & Roberts (1976)
MgO	SiC	150	37 - 94	90	2.2	Wiederhorn & Hockey (1983)
Sapphire	SiC	150	37 - 94	90	2.3	
Sintered Al_2O_3 (30μm)	SiC	150	37 - 94	90	2.3	
HP Al_2O_3 (3 - 4 μm)	SiC	150	37 - 94	90	2.3	
Si	SiC	150	37 - 94	90	2.9	

Continued/...

HP SiC HP Si_3N_4	SiC SiC	150 150	37 - 94 37 - 94	90 90	1.8 2.1	Wiederhorn & Hockey (1983)
Castable refractories	SiC	150	15 - 50	90	2.3-3.9	Wiederhorn et al (1977)
Mild steel Mild steel	Quartz Glass-spheres	100 100	20 20	45-90 45-90	3.5 3.5	Raask (1969)
Sintered Alumina HP Al_2O_3 HP Al_2O_3 HP Si_3N_4 HP Si_3N_4	SiC SiC SiC SiC SiC	150 150 150 150 150	30 - 200 30 - 200 30 - 200 30 - 200 30 - 200	90 15 90 15 90 15	2.4 2.6 1.9 2.0 2.0 1.7	Hockey et al (1978)
Cemented WC	Coal slurry	18	100	90	3.5	Shetty et al (1982)

The velocity exponent does not appear to be influenced in any consistant way by the composition and microstructure of the target material or by the nature of the impacting particle. Castable refractories [Wiederhorn et al (1977)] exhibit the same range of velocity exponents as do dense, homogeneous ceramics [Hockey et al (1978)], and hot pressed silicon carbide, whether impacted with Al_2O_3 particles [Routbort and Scattergood (1980)] or with SiC [Wiederhorn and Hockey (1983)], has a velocity exponent of 1.8.

By contrast, independent researchers have obtained significantly different velocity exponent values for the target/particle system HP Si_3N_4/SiC (see Table 2.1). It is thus evident that caution should be exercised when comparing the velocity exponent values obtained by different researchers, since interlaboratory differences in experimental technique are likely to affect the determination of velocity exponent values.

(i) Variation in the value of the velocity exponent

Several suggestions have been put forward as to why the value of the velocity exponent is not 2.0, as suggested by arguments based on kinetic energy. As shown in Table 2.1, a wide range of velocity exponent values have been obtained experimentally.

In the case of the following target/particle systems:

hot-pressed SiC/Al_2O_3 [Routbort & Scattergood (1980)]
hot-pressed SiC/SiC [Wiederhorn & Hockey (1983)]
hot-pressed Si_3N_4/quartz [Gulden (1979)]
glass-bonded Al_2O_3/quartz [Gulden (1979)]

velocity exponents lower than 2 were obtained, which could be explained neither in terms of the existing erosion models nor in terms of postulates based on kinetic energy. Routbort and Scattergood (1980) suggested that, in the case of hot-pressed SiC, weak grain boundaries requiring less momentum and energy transfer in order to remove material were present, thus lowering the velocity exponent values. Similarly, Gulden (1979) explained the experimental values of velocity exponent in terms of microstructure.

Hockey et al (1978) suggested that the differences between experimental and theoretically predicted values of velocity exponent were the result of the assumptions made by Evans et al (1978) and Ruff and Wiederhorn (1979) when predicting the amount of material removed by an impact. They assumed that the maximum amount of material removed per impact was proportional to C_r^2h (see also Section 2.5), where C_r is the length of the radial cracks (which are proportional to length of the lateral cracks) and h is the depth to which lateral cracking occurs. According to Hockey, however, the prediction does not take into account the following:

i) not all the particles striking the target surface may cause material removal.
ii) The impacting particles may not cause the same amount and type of damage.
iii) Particle velocity and orientation on impact and the condition of the target surface as erosion progresses, may vary, thus influencing material removal mechanisms and hence the velocity exponent value may also be affected.

Scattergood and Routbort (1981) who found that the velocity exponent value increased as particle size decreased, could not explain the phenomenon but suggested that there might be a change in erosion mechanism, or, alternatively, a change in particle or erosion surface morphology.

(ii) The effect of angle on the velocity exponent

There is some controversy as regards the effect of angle on the value of the velocity exponent. Routbort et al (1980b), investigating the effect of impacting reaction-bonded SiC with angular Al_2O_3 particles, reported that the velocity exponent did not appear to vary in any consistent manner as the angle was altered. Sheldon and Kanhere (1972), however, stated that higher velocity exponent values would be obtained at 20° than at 90°. (The authors obtained velocity exponent values of 2.83 at 20° and 2.41 at 90° for annealed aluminium alloys impacted with glass shot). It should, however, be borne in mind that a brittle and a ductile material are being compared and that this could account for the differing results.

(iii) The effect of particle size on the velocity exponent

Goodwin et al (1969) impacted 11 per cent chromium steel with quartz particles ranging in size from 25 to 210 μm, and found that the value of the velocity exponent (n) tended to increase as the particle size increased. The reverse was found to be true for brittle materials e.g. silicon single crystals impacted with Al_2O_3 particles [Scattergood and Routbort (1981)] (Figure 2.1).

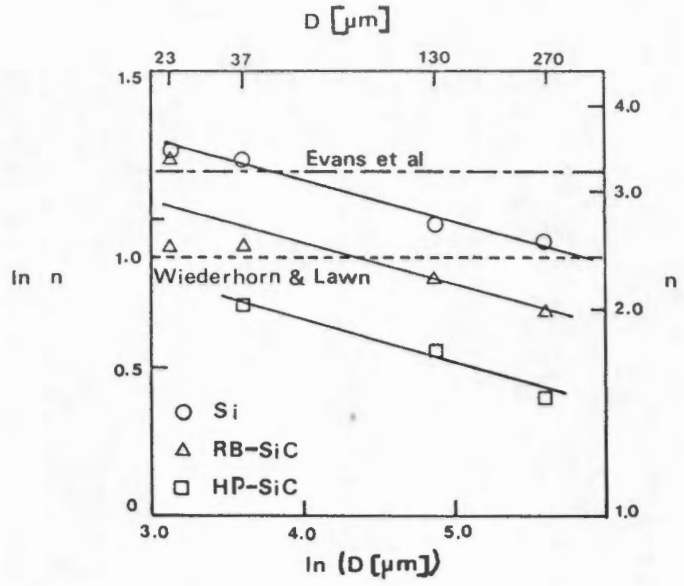

FIGURE 2.1 : The influence of Al_2O_3 particle size on the velocity exponent values for silicon single crystals [From Scattergood and Routbort (1981)]

2.1.3 The Effect of Angle on Erosion Rate

Numerous studies have shown that erosion by a brittle mechanism is characterised by a maximum erosion rate at an impact angle of 90° and by a decrease in erosion rate as the impact angle is decreased. Ductile erosion, by contrast, has a maximum erosion rate at 15 to 20°, with a decrease in erosion rate at both higher and lower impact angles (Figure 2.2). Most materials, however, undergo combined modes of erosion, and classifying material behaviour as either completely ductile or completely brittle is an over-simplification. The erosion characteristics of a material are determined by the test conditions and can, for example, vary with particle size (see also section 2.2.2).

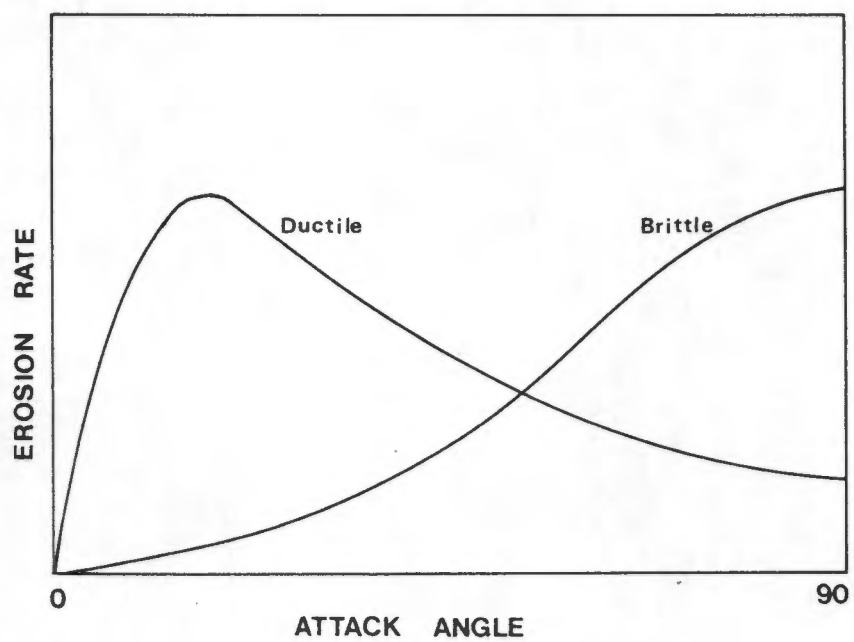

FIGURE 2.2 : Schematic diagram illustrating the effect of angle on the erosion rate of a ductile and brittle material [Ruff and Wiederhorn (1979)].

The models of erosion developed by Evans et al (1978) and Ruff and Wiederhorn (1979) pertain to normal particle incidence. It has been suggested that the models can be extended to oblique angles

of impact by taking into consideration the normal component of the particle velocity and thus velocity, V_o, is modified to $V_o \sin\alpha$ where α is the angle between the target surface and the path of the impinging particles. Hockey et al (1978) found that their experimental data for hot pressed Si_3N_4 agreed with the values predicted by $E_\alpha = E_{90}(\sin\alpha)^n$ for angles up to 30° but that at 15°, the measured erosion rate was five times more than the predicted value. Routbort et al (1980b), Dimond et al (1983) and Shetty et al (1982) also found that the erosion rate was underestimated, particularly at low angles of impact.

Sheldon (1970) plotted erosion rate, expressed as mass loss per mass particles (g/g), as a function of $\sin\alpha$, and although straight lines were obtained, the slopes of the lines did not agree with the values of the velocity exponents, n. In view of this, it does not appear correct to consider erosion rate exclusively in terms of the normal component of the particle velocity. Hockey et al attributed the deviation to the importance of a shear mechanism of erosion at low angles.

Microscopic examination, by Hockey et al (1978), of brittle materials impacted by particles at low angles of impingement revealed the formation of shallow surface impressions (attributed to plastic flow) frequently elongated along the horizontal component of particle motion, and a decrease in the extent of surface cracking.

2.1.4 The Effect of Temperature on Erosion Rate

Since the present investigation is not concerned with the effect of temperature on erosion, it will only be discussed briefly.

Although there appear to have been relatively few studies of the effect of temperature on the erosion rate of brittle materials, the results obtained by researchers seem to be essentially the same.

Wiederhorn (1979), who studied hot-pressed silicon nitride and polycrystalline aluminium oxide and Routbort et al (1980a), who studied silicon single crystals, demonstrated that the erosion rate of materials was substantially the same at temperatures of 500° to 1000°C as at room temperature. Hockey et al (1978) and Kirchner and Gruver (1978) studied the surface damage produced in alumina and glass respectively, at high temperatures (1000°C and 770°C) and found that the extent of plastic deformation had increased despite the fact that erosion rate remained constant.

2.2 THE IMPACTING PARTICLES

Quartz is commonly used as the impacting particle type in erosion studies, since it is the major erosive component occurring in natural dusts, fly ash and pulverized coal. Investigators have also made use of angular silicon carbide and alumina particles, both of which are harder than quartz particles. Single impact studies have tended to use large spheres of glass or steel in order to facilitate the study of the sequence of events occurring on particle impaction.

In the following sections the effects of several particle parameters on erosion will be discussed.

2.2.1 The Particle Size Exponent

The erosion of brittle materials such as glass exhibits a power law dependence on particle size:

$$E \propto \text{constant}.D^m \qquad (2)$$

where E = the erosion rate
D = the impacting particle radius
m = the particle size exponent

Table 2.2 lists a few of the particle size exponents which have been reported.

TABLE 2.2 : Particle Size Exponents

TARGET	IMPACTING PARTICLE TYPE	PARTICLE SIZE EXPONENT	REFERENCE
HP Si_3N_4 HP Si_3N_4 GB Al_2O_3	SiC Quartz Quartz	4 3 3	Gulden (1979)
- -	Round particle Angular particle	3m'/(m'-2) 3.3m'/(m'-2)	Sheldon & Finnie (1966a) (section 2.5)
Plate glass Plate glass	SiC Steel shot	4.25 5.12	Sheldon & Finnie (1966a) (section 2.5)
Glass	Quartz	2	Sage & Tilly (1969)

Routbort et al (1980b) found that m (the particle size exponent) tended to vary with velocity and angle of impact, although not in a consistent manner.

2.2.2 Particle Size

The erosion rate of brittle materials is, in theory, expected to increase monotonically as particle size increases and erosion studies commonly support this assumption (Figure 2.3).

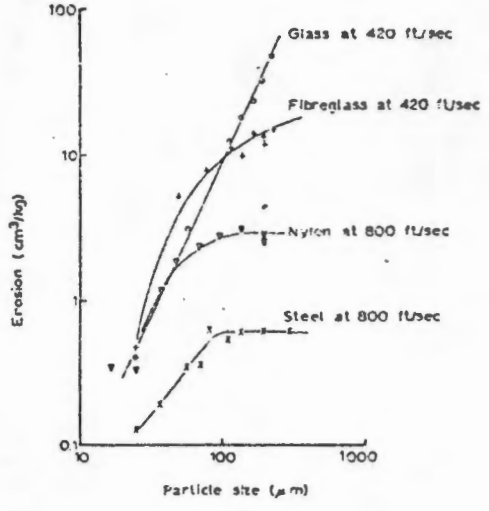

FIGURE 2.3 : Influence of quartz size on erosion of different types of materials [Tilly and Sage (1970)]

Note that for materials other than those which are inherently brittle in nature, there appears to be a critical particle size above which erosion is not influenced by size.

Routbort and Scattergood (1980), however, found that for hot-pressed silicon carbide impacted with 37 - 270 μm alumina particles, the erosion rate remained either constant, or decreased (Figure 2.4). The decrease in erosion rate appears to occur with the larger particle sizes and also appears to be more marked at a lower angle of incidence. This observation was, however, thought to be due to the influence of the eroded surface morphology rather than a particle size effect.

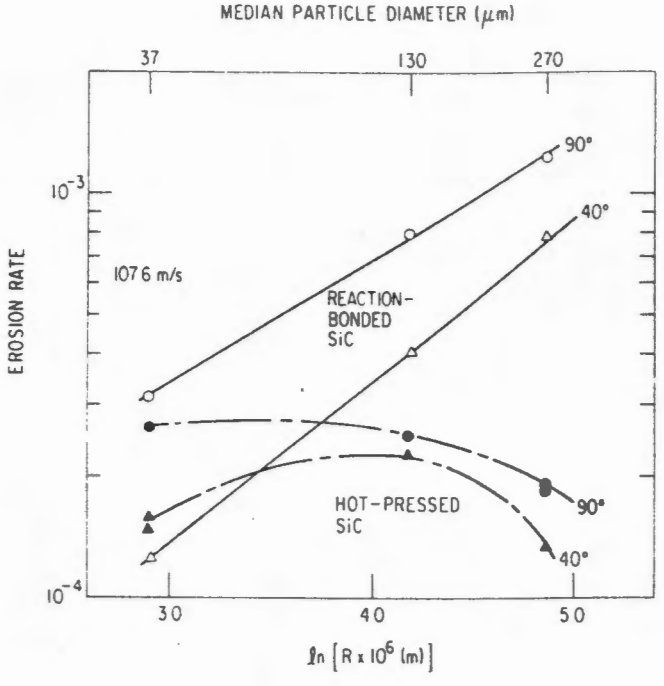

FIGURE 2.4 : Steady-state erosion rate as a function of the logarithm of the radius of impacting alumina particles at a velocity of 108 ms^{-1} and impact angles of 40° and 90° for reaction-bonded and hot-pressed silicon carbide [Routbort and Scattergood (1980)]

Figure 2.5 illustrates the effect on erosion of reducing the impacting particle size from 127 μm to 9 μm. The plate glass exhibits a ductile mechanism of erosion when impacted with small diameter particles, displaying a maximum in erosion at an angle of 20°.

In addition to maximum erosion occurring at a low angle, the surface appearance of the target material (plate glass) also indicates a ductile erosion mechanism (Sheldon and Finnie (1966b)].

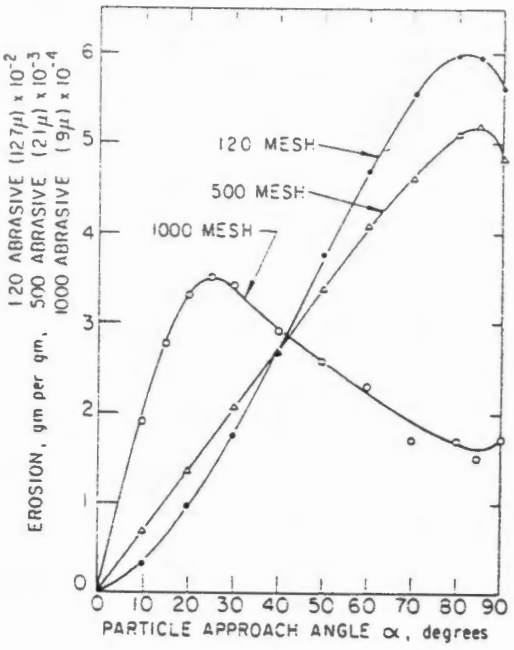

FIGURE 2.5 : Weight removal as a function of particle approach angle for plate glass eroded by angular silicon carbide particles at 150 ms^{-1} [Sheldon and Finnie (1966b)]

Particle size was found to have a significant influence on the erosion of pipe bends [Mills and Mason(1977)]. The authors found that sand particles of 70 μm mean diameter wore the bends into a pattern of steps or ridges, whereas the 230 μm diameter sand particles produced a smooth and rounded surface (devoid of ridges or steps). A more important result which emerged from the tests conducted by Mills et al (1983), was the fact that the 70 μm particles removed less material (by weight) than the 230 μm particles, although the depth of penetration of the 70 μm particles was greater than that of the 230 μm particles (Figure 2.6).

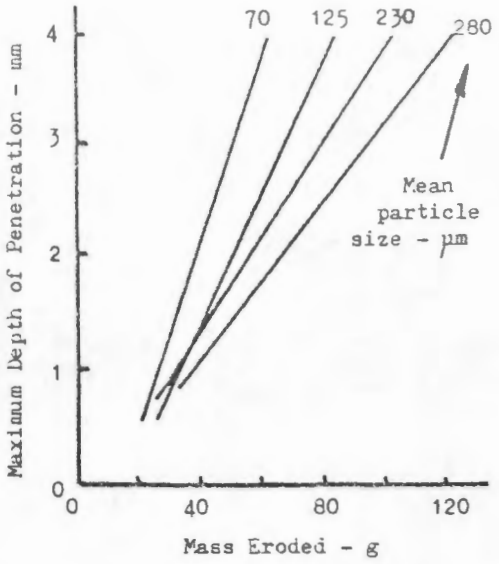

FIGURE 2.6 : Influence of particle size on rate of penetration [Mills et al (1983)]

Marshall et al (1981) conducted a series of experiments in which the particle size range of silicon carbide was varied and impacted against single crystal silicon. They found that the rate of material removal was sensitive to the particle size range and thus it would appear that an in-service erosion rate may be seriously underestimated if the particle size distribution employed experimentally is too narrow around the mean size.

A threshold particle size (D_0), below which no erosion occurs, may exist, although conclusive evidence verifying this existence has, as yet, not been reported.

2.2.3 Hardness

The hardness of the particles may be expressed by Moh's scale of hardness, or may be determined by the Vicker's microhardness test.

The widely held opinion that hard particles are more erosive than softer particles [supported by Raask (1969)], was clearly demonstrated by Head et al (1973) to be untrue. They eroded 302 stainless steel and 6061-T6 aluminium with fluorite particles (Moh's hardness 4.0) and with alumina particles (Moh's hardness 9.0). The fluorite particles of 70 μm diameter were significantly more erosive than the alumina particles of 70 μm diameter. (See Figure 2.7).

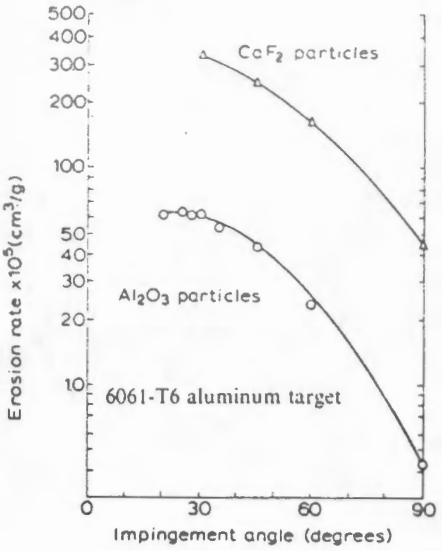

FIGURE 2.7 : Experimental erosion rates versus impingement angle for 6061-T6 aluminium alloy eroded by alumina and fluorite [Head et al (1973)]

Tilly and Sage (1970) obtained one set of results which supported those of Raask and one set which supported those of Head et al (Figure 2.8).

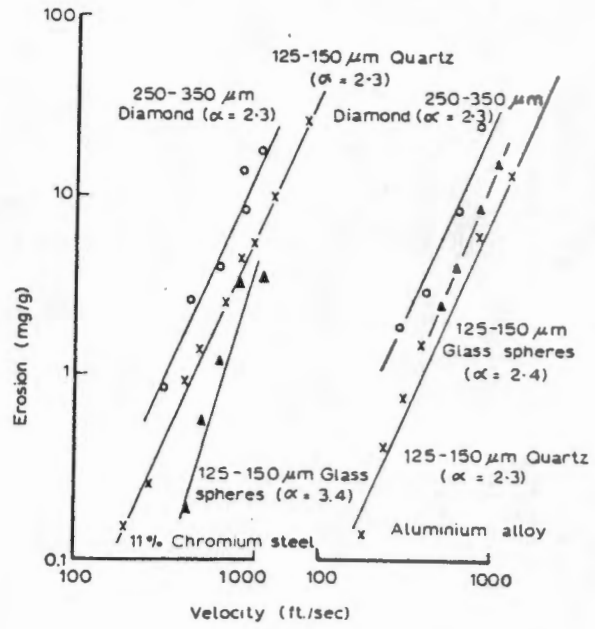

FIGURE 2.8 : Effect of velocity and type of abrasive on erosion for 90° impacts [Tilly and Sage (1970)]

When the three particle types, diamond (Moh's hardness 10.0), quartz (Moh's hardness 7.0) and glass (softer than quartz) were impacted against an aluminium alloy, the glass appeared to be more erosive than the quartz. It is thought that the degree of fragmentation and hence the amount of secondary erosion occurring in the glass particles is greater than that of the quartz particles. This result supports the results obtained by Head et al (1973). Alternatively, the results obtained when the three particle types were impacted against an 11 per cent chromium steel support the results obtained by Raask (1969) who compared the erosiveness of quartz and glass when impacted against a mild steel target. It is thus important that the relative hardness of the target materials be known when comparisons of this nature are made, since target hardness may influence the fragmentation and erosive ability of the impacting particles. Furthermore, Head et al (1973) did not take into account the difference in shape of the impacting particles. The alumina particles are angular in shape, whilst the fluorite particles are rhomboidal in shape. It is likely that , although the fluorite particles have a low Moh's hardness value (4.0), their erosive ability will be positively influenced by their shape. In addition, the angle at which the particles struck the target should be borne in mind since fragmentation is reported to be influenced by impingement angle. (Raask (1969) conducted his tests at an angle of 45°, whereas Tilly and Sage (1970) used an angle of 90°). See Figure 2.9.

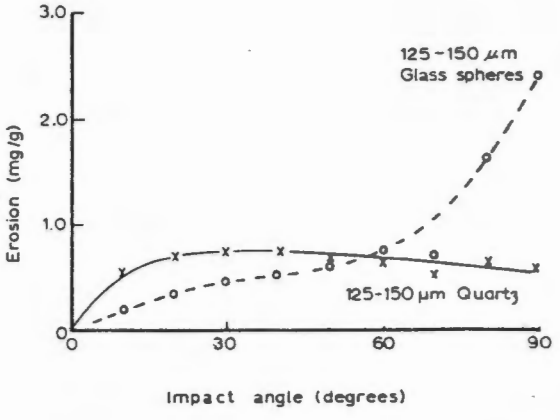

FIGURE 2.9 : Angle dependence for an aluminium alloy tested at 240 ms^{-1} [Tilly and Sage (1970)]

It would appear that angular particles are potentially more erosive than rounded particles, and thus Dimond et al (1983) feel that a term reflecting the shape of the particles (which by inference is related to their hardness) should be included in the erosion models.

2.2.4 Aerodynamic Effects

The aerodynamic behaviour of particles is important, since both the velocity and angle of impact may be influenced by this behaviour. Tilly (1969) studied the influence of airflow on the trajectories of particles ranging in size from 5 to 60 μm and concluded that particles greater than 20 μm in size were virtually undeflected by the airflow, whereas smaller particles (5 μm) impacted the target material at modified angles and velocities, or failed to strike the target at all.

2.2.5 Particle Fragmentation

Tilly and Sage (1970) studied the damage incurred by 3000 μm glass spheres, which, on striking the steel target at a normal angle of incidence, disintegrated and glass fragments flowed across the surface in a radial wash at a speed of $1.7V_0$ (where V_0 represents the inital impact velocity). At higher (unspecified) impact velocities, the particle fragments may be radially ejected at velocities up to four times the initial velocity of the particles [Uuemois and Kleis (1975)].

Tilly and Sage (1970) also found that the radial scarring produced by the glass spheres was very similar to the damage produced by irregular quartz particles impacting against both ductile and brittle materials.

Tilly and Sage (1970) report that the extent of particle fragmentation increased with increasing particle size and with increasing impact velocity. No fragmentation appeared to occur for particles smaller than a certain threshold size, which, in the case of quartz, is 10 to 20 μm.

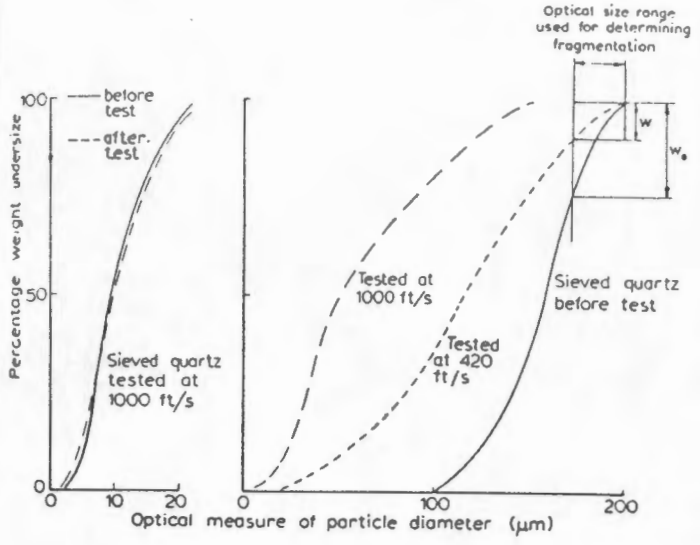

FIGURE 2.10 : Quartz particle size distributions before and after testing. [Tilly (1973)]

Contrary to expectation, fragmentation also occurs in materials of greater hardness (and strength) than quartz particles. See Figure 2.11.

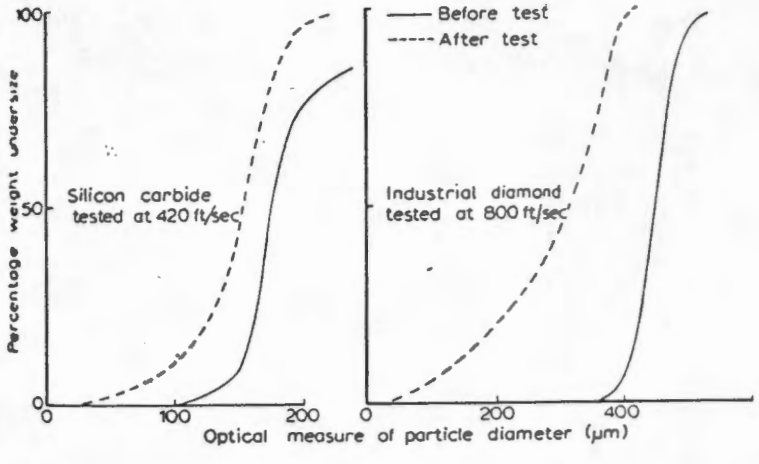

FIGURE 2.11 : Size distributions for silicon carbide and industrial diamond before and after testing [Tilly (1973)]

2.2.6 Particle Concentration

Although particle concentration is often interpreted as "percentage content by weight or volume of particles in a gaseous or fluid stream" [Uuemois and Kleis (1975)], it is more accurately described by a relationship of the form:

$$\psi = \frac{G}{F.t} \qquad (4) \text{ [Uuemois and Kleis (1975)]}$$

where ψ = particle concentration ($g.cm^2s$)
G = the mass of impacting particles (g)
F = the area of wear (cm^2)
t = the duration of the test (s)

The authors found that for small particles ($< 30\ \mu m$), an increase in particle concentration had no effect on erosion rate, whereas for larger particles an increase in concentration (from 2 to $200 g/cm^2s$) led to a decrease in erosion rate for metals, alloys and ceramic materials.

The effect of particle concentration on erosion is primarily due to the increased probability of collision between the incident and rebounding particles as particle concentration is increased. The velocity and angle of impingement of the incident particles also tend to be influenced.

Uuemois and Kleis (1975) also concluded that the effect of particle concentration was dependent upon particle velocity, e.g. at 165 ms^{-1} the influence of concentration is 2.1 times greater than at 56 ms^{-1}. They also found that the concentration effect tended to be greater at the higher angles of particle impingement. Most investigators [eg. Tilly and Sage (1970)] found that particle concentration has little or no effect on erosion rate . Uuemois and Kleis (1975) attributed this to the fact that the ranges of particle concentration used result in negligible concentration effects.

Mills et al (1983) found that a large increase in particle concentration led either to a decrease in the mass eroded, or had no effect. However, it was found that particle concentration had a significant effect on the rate of penetration. As particle concentration increased, the depth of penetration by the particles increased, and therefore the amount of material which could be sent through a bend before failure occurred, would decrease as particle concentration increased.

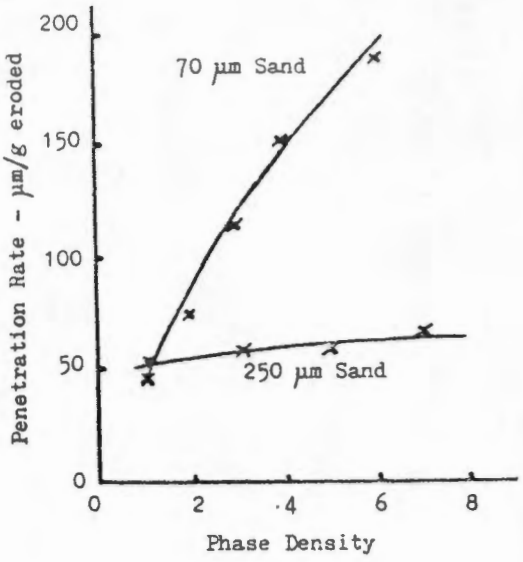

FIGURE 2.12 : The influence of particle size on the variation of penetration rate with phase density [Mills et al (1983)]

2.2.7 Synergistic Effects

Although the impacting particles used in erosion tests are usually pure and dry, in practice the particles are generally impure, and contain moisture. Small percentages of $Ca(OH)_2$ and water present in abrasives acted as effective intensifiers of the erosive wear of metals and alloys [Uuemois and Kleis (1975)]. However, with hard and high strength materials such as ceramics, the influence of impurities on erosion was found to be either very low, or to result in less damage.

Routbort et al (1980a) conducted a series of experiments using mixtures of 37 μm and 270 μm Al_2O_3 particles in order to determine a "rule of mixing" for erosion. Their results showed positive deviations from the results predicted for a linear "rule of mixing". (See Figure 2.13).

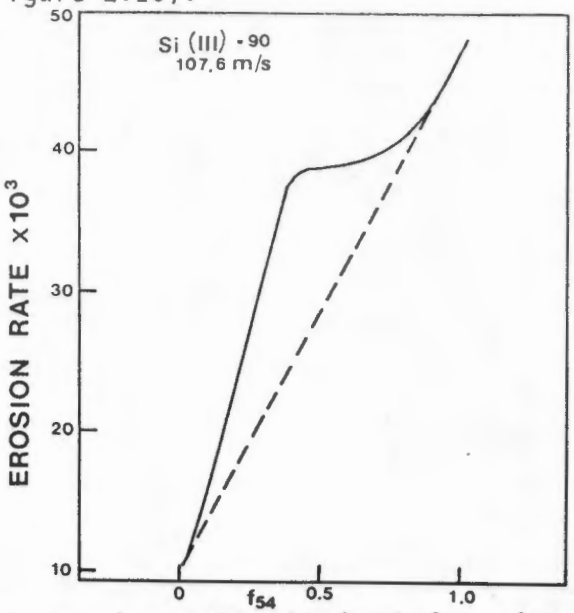

FIGURE 2.13 : The erosion rate obtained for mixtures of 37 and 270 μm Al_2O_3 particles. The dashed line indicates the predicted erosion rate [Routbort et al (1980a)].

2.3 TARGET CHARACTERISTICS

2.3.1 Hardness and Fracture Toughness

Hardness (H) and fracture toughness (K_c) are the critical material parameters governing erosion. However, since their influence on erosion rate was not investigated in the present study, they will only be briefly discussed in the present section.

Hardness represents the resistance of the target material to plastic flow and fracture toughness represents its resistance to fracture.

Since fracture toughness and hardness are determined by the inherent properties of the target material, they cannot be varied independently, and are thus compared with the erosion models in a combined form. Evans et al (1978) investigated the effect of hardness and fracture toughness on the erosion rate of several

target materials. They impacted the target materials with 115 μm quartz particles at velocities less than 200 ms^{-1} and plotted the volume of material removed as a function of $K_c^{4/3}$ $H^{1/4}$ and found a direct, albeit non-linear, correlation, suggesting that erosion rate may not be defined uniquely by fracture toughness and hardness. Wiederhorn and Hockey (1983) impacted 150 μm SiC particles against a number of materials which had widely differing fracture toughness and hardness values. The authors compared the experimentally obtained data with the dynamic [Evans et al (1978)] and quasi-static [Ruff and Wiederhorn (1979)] models of erosion and it appeared that the data compared more favourably with the dynamic model. By means of dimensional analysis and multiple regression analysis, the authors obtained the following expression for erosion rate:-

$$E \propto \text{constant } K_c^{-1.9} H^{+0.48} \qquad (5)$$

Erosion rate appears to exhibit a greater dependence on the parameters K_c and H than suggested by either of the elastic-plastic response régime models.

Most erosion theories predict a decrease in erosion rate as the hardness increases. The authors explain their positive hardness exponent as follows. Hardness determines both depth of penetration and the maximum load during impact and the penetration and load tend to oppose one another. The authors suggest that hardness affects the load terms to a greater extent than the penetration terms, as suggested by the quasi-static erosion model. ($H^{+0.11}$).

The fracture toughness exponent may be due to the effects of target microstructure or the orientation of the particles on impact. It is generally assumed that the particles strike the target with their sharp corners, that each impact event results in geometrically similar damage and that resultant cracks propagate to the surface. This, however, is not true, since the particles may strike the target in any orientation and only a fraction of the impacting particles effectivly remove material. The tougher the material, the fewer the impacts resulting in material

removal. It appears [Hockey and Wiederhorn (1979)] that hardness and fracture toughness are unaffected by increases in temperature.

2.3.2 Microstructure

The microstructure of the target material may greatly influence the erosion behaviour of a material. For example, Wiederhorn and Hockey (1983) and Hockey et al (1978) found that grain size affected erosion rate. Hot-pressed Al_2O_3 has a grain size of 3 to 4 μm (smaller than the lateral cracks which form on particle impact), and thus, the lateral cracks interact with many grains, and their propagation is resisted by the grain boundaries, whilst with polycrystalline Al_2O_3 which has a 30 μm grain size, the lateral cracks are contained within one grain.

Wiederhorn and Hockey (1983) found that MgO had an anomalously high erosion rate relative to the other materials tested, since the impact damage incurred by this material was different. The MgO appeared to crack along the grain boundaries, forming loosely connected aggregates of grains which were readily removed on subsequent particle impacts.

Besides the influence of grain size on erosion, porosity also has an effect on the response of the target material to particle impact. Pores tend to inhibit the propagation of cracks through a blunting mechanism.

2.4 IMPACT DAMAGE IN BRITTLE MATERIALS

Comprehensive investigations have been made of the sequence of events taking place when brittle materials are damaged by either spherical or angular particles. Dynamic solid particle studies were conducted by Evans and Wilshaw (1979), Knight et al (1977), Chaudhri and Brophy (1980) and Chaudhri and Walley (1978). Swain and Hagan (1976), Evans and Wilshaw (1976) and Lawn and Fuller (1975) followed the sequence of crack formation and propagation in materials which had been indented with either spheres or Vickers indenters. The table below summarizes the target materials and particle types employed in the above-mentioned investigations.

TABLE 2.3 : Target materials and particle types used in a few investigations of the sequence of events taking place in impacted materials

NATURE OF TEST	TARGET MATERIAL	PARTICLE TYPE	PARTICLE DIAMETER	REFERENCE
Dynamic solid particle damage	ZnS	Nylon, glass spheres	1 mm	Evans & Wilshaw (1979)
Dynamic solid particle damage	Borosilicate and soda lime glass	Steel spheres	0.8-1 mm	Knight et al (1977)
Dynamic solid particle damage	Fused silica	Spherical WC Conical WC	1 mm Apex radius 5 mm	Chaudhri & Brophy (1980)
Dynamic solid particle damage	Borosilicate and soda lime glass	Glass spheres Steel spheres	1 mm	Chaudhri & Walley (1978)
Indentation damage	Various glasses	WC spheres Diamond spheres	0.39-1mm 0.40 mm	Swain and Hagan (1976)
Indentation damage	A range of materials with differing hardness and K_c values	Spherical WC Vickers indenter	- -	Evans & Wilshaw (1976)
Indentation damage	Soda lime float glass	WC cones WC spheres	- -	Lawn and Fuller (1975)

These studies have elucidated two charateristic forms of impact fracture damage which may be summarised as follows:

2.4.1 Fully Elastic Response

In this system the target material (eg. ZnS) is hard relative to the highly deformable impacting particle (eg. nylon sphere, water droplet). Plastic deformation is not detectable and short circumferential surface cracks are observed outside the central undamaged zone. As distance from the central zone increases, the length of the cracks increases and the density of cracks decreases. The cracks are usually inclined at 50° to the surface. Additional cracks, approximately parallel to the surface, have also been detected.

2.4.2 Elastic-plastic response

This type of damage pertains to relatively hard spherical and angular particles, and both single and multiphase target materials. The morphology of the damage can be divided into two groups, depending on whether the particles are classified as "blunt" or "sharp". Impact with "sharp" particles is characterised by a central deformed zone (often indistinct or lost due to chipping of the contact area) which is the point of contact between the particle and target. Associated radial and lateral cracks (Figures 2.14 and 2.15 respectively) propagate away from the central zone.

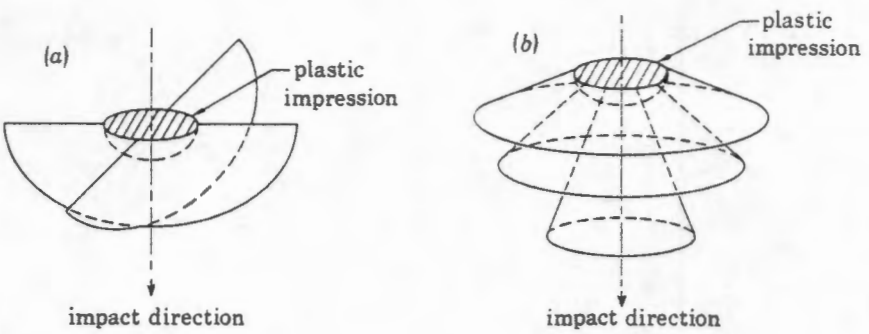

FIGURE 2.14 : A schematic diagram indicating the morphology of (a) radial and (b) conical cracks [Evans et al (1978)]

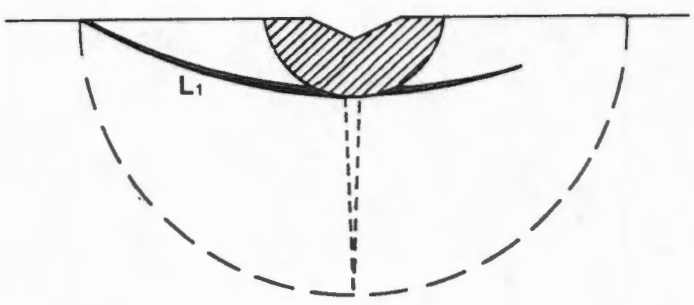

FIGURE 2.15 : The lateral crack system. The shaded area represents the plastically deformed zone. L_1 represents a lateral crack which has broken out to the surface. Dashed lines indicate the median-radial crack system

The radial cracks extend outward from the damage crater and are generally perpendicular to the surface. The lateral cracks, which also extend from the central zone, run on planes approximately parallel to the surface. Material loss from the surface occurs when the lateral cracks extend to form surface chips. This type of damage has been observed by numerous researchers such as Ritter et al (1985), Gulden (1979 and 1980) and Evans et al (1978) during the impact erosion testing of a variety of target-particle systems. Hockey et al (1978) and Hockey and Wiederhorn (1979) have pointed out that the damage morphology is analagous to that produced quasi-statically in brittle materials using "sharp" indenters, eg. the Vickers diamond pyramid. The sequence of events for an indentation cycle is illustrated by Figure 2.16 [Lawn and Marshall (1978)].

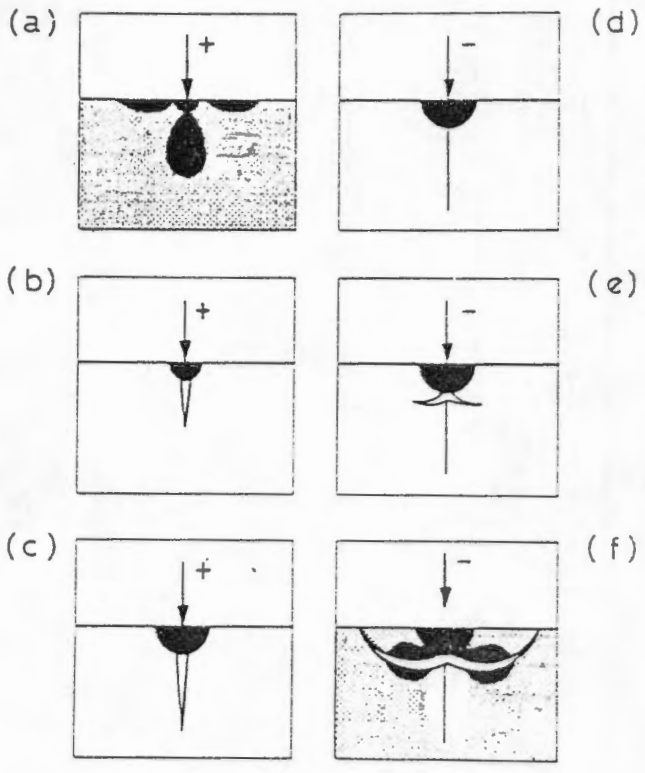

FIGURE 2.16 : Evolution of median/lateral crack system during one loading (+) and unloading (-) cycle. Dark regions represent the plastic zone. Point-loading and residual stress fields indicated in (a) and (f) respectively [Lawn and Marshall (1978)]

The sequence of events is:

(a) The tensile field peaks directly below the indenter point where the greatest concentration of deformation and elastic-plastic constraint occurs.

(b) One or more flaws grow into subsurface penny-like cracks which are called median cracks.

(c) Increased loading expands the contact area, driving median cracks downwards and outwards. At peak loading, the median cracks break through to the specimen surface ("pop-in"), the compressive hoop stresses no longer containing the expanding pennies.

(d) As unloading begins, the walls of the median cracks begin to move together, fracture debris and residual tension preventing total closure. A "hoop" tension develops in the near surface region, allowing the poorly developed pennies (radial cracks) to develop into near-symmetrical, stably propagating half-pennies centred on the contact point.

(e) During unloading, residual stresses at the point of contact set up a system of saucer-shaped lateral cracks which run parallel to the surface.

(f) Lateral cracks continue to grow and may intersect with the free surface, thus allowing a chip of material to be removed. Note: a well-developed radial crack will tend to inhibit the formation of well-developed lateral cracks and vice versa.

In the case of "blunt" particles, the contact between the particle and target is exclusively elastic and Hertzian cone cracks are formed. The sequence of events for an indentation cycle is illustrated in Figure 2.17 [Lawn and Marshall (1978)].

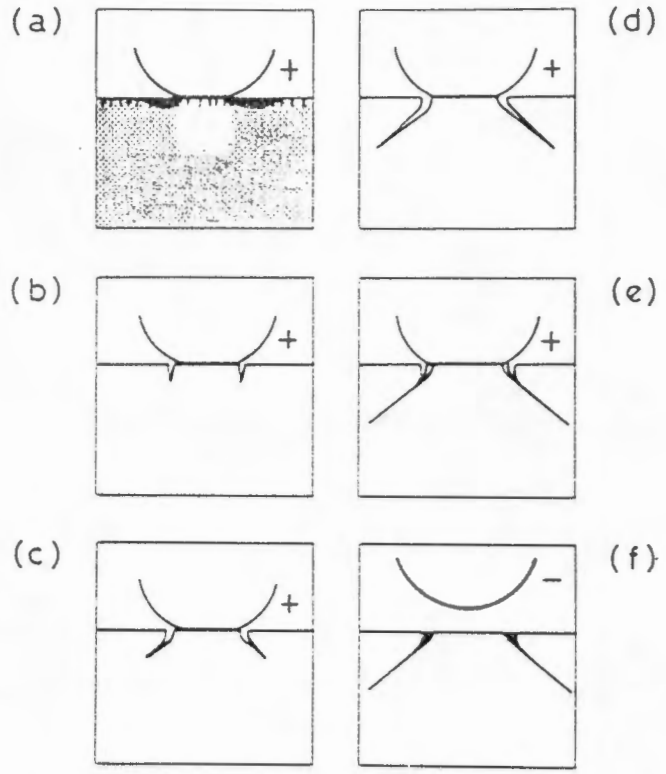

FIGURE 2.17 : Evolution of a cone crack during one complete loading (+) and unloading (-) cycle. Stress field indicated in (a) [Lawn and Marshall (1978)]

The sequence of events can be described as follows:

(a) The sphere subjects surface flaws to increased tensile stress outside the expanding contact circle.

(b) An unstable flaw propagates around the contact, forming a surface ring crack, in conjunction with downward growth.

(c) The crack continues to grow downward, avoiding the compressive zone.

(d) A full cone crack develops.

(e) The cone crack continues its extension.

(f) On unloading, the cone crack attempts to close in order to recover stored elastic and surface energy, but is prevented from doing so completely as a result of mechanical obstruction at the interface.

As the contact load increases above a level determined by the hardness of the target material, plastic deformation occurs beneath the contact zone and radial cracks normal to the impact surface form [Swain and Hagan (1976), Chaudhri and Brophy (1980) and Evans (1979)]. During unloading, a system of lateral cracks forms and these radial and lateral cracks are identical to the crack types formed when impact by a "sharp" particle takes place.

The transition from fully elastic crack formation to elastic-plastic indentation occurs when the radii of curvature of the particles decrease below a critical value, R_c. (Figure 2.18).

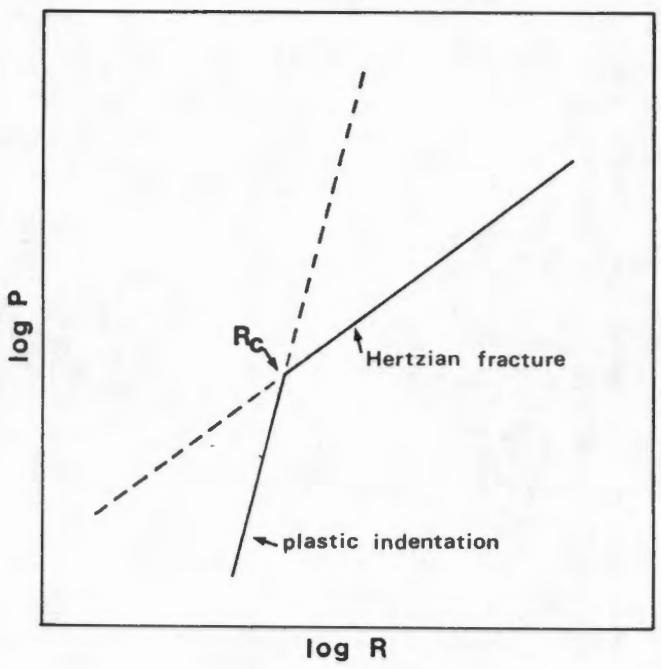

FIGURE 2.18 : The effect of particle radius on the indentation load for Hertzian fracture and plastic indentation [From Evans and Wilshaw (1976)]

The initial fracture caused by a particle of a size greater than R_c is completely elastic, whilst that by a particle smaller than R_c is elastic-plastic in nature. The value of R_c can be determined by the expression [Evans and Wilshaw (1976)]:

$$R_c \simeq \frac{B_1}{B_2} \left(\frac{E^2}{k}\right) \frac{1}{H^3}$$

where B_1 = a constant dependent upon fracture toughness (and sometimes on pre-existing surface flaw size)

B_2 = a constant

E = Young's Modulus

k = a constant

H = target hardness

2.4.3 Plastic Deformation

As early as 1966 Sheldon and Finnie (1966b) noted that plastic deformation could occur in nominally brittle materials. Since then, several researchers [eg. Gulden (1979) and Hockey and Wiederhorn (1979)] have observed plastic deformation as well as cracking of brittle target materials. It is now recognised that plastic deformation plays an important role in the erosive wear of brittle materials. Radial and lateral cracks form as a result of stresses caused by the plastic deformation at the impact site and the models of erosion are based on a characterization of the plastic processes occurring during impact. The model elucidated by Evans et al (1978) places more emphasis on dynamic effects, with the plasticity effect playing a secondary role, whereas in the model proposed by Wiederhorn and Lawn (1979), the plastic processes play the important role.

Hockey and Wiederhorn (1979) found that the extent of plastic deformation and the morphology of the cracks were dependent upon the crystal structure of the impacted material. In MgO, which is

ionically bonded, extensive deformation occurred at the impact sites with the cracking always confined to the plastic zone. In the case of Si and Ge, which are covalently bonded materials and more brittle than MgO, plastic deformation was confined to the vicinity of the impact site and cracks propagated some distance into the crystal. SiC and Al_2O_3, which have both ionic and covalent bonding, displayed an intermediate type of behaviour, with the extent of deformation about twice the size of the residual plastic impression and the cracks extending beyond the deformation zone.

2.5 MODELS FOR THE EROSION OF BRITTLE MATERIALS

Three models of erosion which have been developed for brittle materials will be discussed in the following section. The models assume that the impinging particles strike the target surface at a normal angle of incidence, and that erosion rate is the result of a direct summation of the volume of material removed per impact.

2.5.1 The Sheldon and Finnie Model

Sheldon and Finnie (1966a) predicted that the volume of material removed during erosion processes was:

$$E = K R^m V^n \qquad (7)$$

where E = erosion rate (the volume of material removed)
K = a constant involving material properties
R = the radius of the impacting particle
V = the velocity of the impacting particle
m = 3m'/(m'-2) for spherical particles, or
3.6m'/(m'-2) for angular particles
n = 2.4m'/(m'-2) for both spherical and angular particles
m' = the flaw parameter of the Weibull fracture strength distribution

The authors tested a variety of brittle materials (glass, graphite, alumina, magnesium oxide) using both angular silicon carbide particles and spherical steel shot and the results yielded

erosion rates in general agreement with the above equation. Sheldon (1970) found reasonably good agreement between the theoretical and experimental values of K, the materials constant involving Young's Modulus.

2.5.2 The Evans, Gulden and Rosenblatt Model

Evans et al (1978) analysed the impact damage in brittle materials in the elastic-plastic response régime by means of postulates based on impact dynamics and basic fracture mechanics concepts. The two damage characteristics of greatest import in their model are the maximum radial crack extension, Cr, and the maximum depth, h, at which extensive lateral fracture occurs.

(a) The radial or conical cracks

The lengths, Cr, of the largest radial or conical cracks were found to be proportional to the impression radius, a (Figure 2.19).

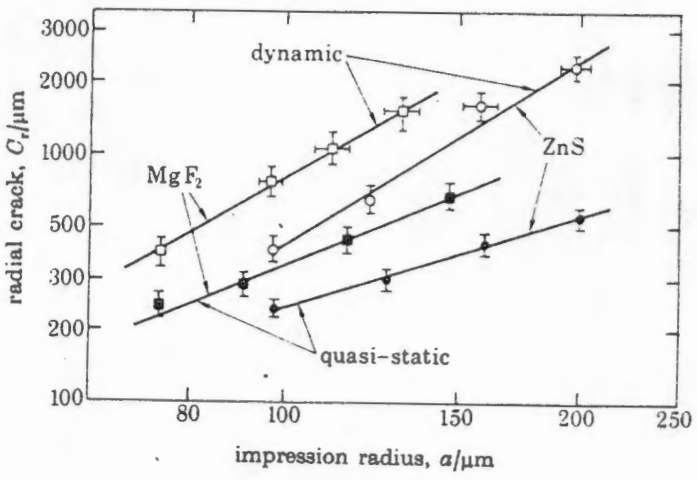

FIGURE 2.19 : A comparison of the radial crack length for dynamic and quasi-static penetration in ZnS and MgF_2 [Evans et al (1978)]

It was noted that the cracks formed dynamically were longer than those obtained quasi-statically for equivalent impact radii. The radial crack extension was estimated using dynamic analysis in conjunction with experimental data, thus yielding the expression

$$C_r \approx \lambda[(R_p\ V_o)^2/K_c]^{2/3} \quad (8)$$

where Cr = length of largest radial or conical crack

λ = a weak function of the impedance and density variables

R_p = the radius of the impacting particle

V_o = the velocity of the impacting particle

K_c = the fracture toughness of the target material

The impact damage data for a range of impacting particles (both spherical and angular) and various target materials, indicated that particle shape and density, as well as the hardness of the target material were of secondary importance. Important parameters were, as predicted by equation (8), found to be the particle radius and velocity and the fracture toughness of the target material.

(b) The lateral cracks

The maximum depth at which significant lateral fracture could be detected was found to relate directly to the impression radius (Figure 2.20).

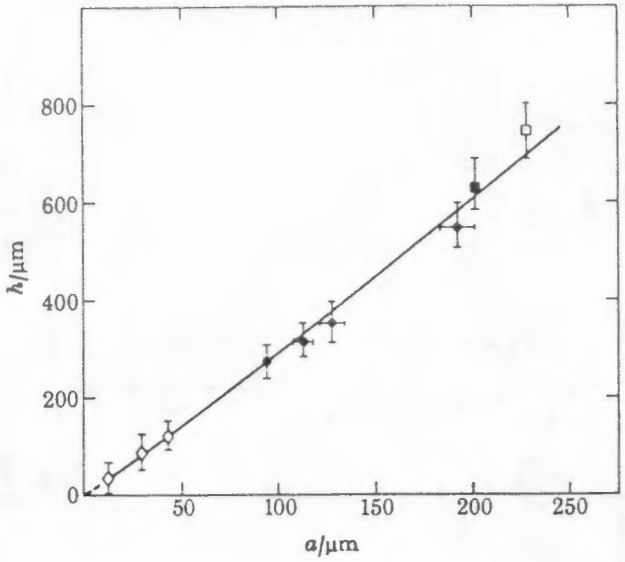

FIGURE 2.20 : The variation in the depth of lateral fracture, h, with the impression radius, a, for ZnS impacted by a variety of projectiles. ●, 400 μm, WC; ■, 1000 μm WC; □, 1000 μm glass; ◇, 350 - 370 μm glass. [Evans et al (1978)]

The damage data for a range of target and particle materials were expressed in the form

$$(h/R_p)^2 \approx \lambda' \, V_o \, \sqrt{(\rho_p/H)} \qquad (9) \text{ [Evans et al (1978)]}$$

where λ' = a constant (~ 3.5)
R_p = particle radius
h = depth of lateral fracture
V_o = particle velocity
ρ_p = density of the impacting particle
H = hardness of the target material

Experimental data gave good quantitative agreement with the above expression.

The authors assumed that the multi-particle erosion of brittle materials is a direct summation of the material removal per impact and that the amount of material removed is some fraction of the volume of material encompassed by the zone of lateral fracture. Therefore, the maximum amount of material which could be removed by an impact is:

$$V \approx \pi C_r^2 h \qquad (10)$$

Substituting for C_r and h with equations (8) and (9) respectively, yields

$$E \propto V_o^{19/6}\ R_p^{11/3}\ \rho_p^{19/12}\ K_c^{-4/3}\ H^{-1/4} \qquad (11a)$$

or, alternatively,

$$E \propto V_o^{3.2}\ R_p^{3.7}\ \rho_p^{0.25}\ K_c^{-1.3}\ H^{-0.25} \qquad (11b)$$

2.5.3 The Ruff and Wiederhorn Model

Wiederhorn and Lawn (1979) assumed that all the kinetic energy of the impinging particle is dissipated in an irreversible plasticity process, such that:

$$P_m = H^{1/3}\ m^{2/3}\ V_o^{4/3} \qquad (12)$$

where P_m = the maximum impulsive load delivered to the target surface by the impacting particle
H = hardness of the target material
m = the mass of the impacting particle
V_o = the particle velocity

By substituting P_m into the expression

$$F/R^{3/2} = \beta_R\ K_c \qquad (13)$$

where F = impulsive load
R = base radius of cone crack
β_R = empirically determined constant
K_c = fracture toughness

With further substitution they obtained the relationship:

$$C_r \propto m^{4/9}\ H^{2/9}\ V_o^{8/9}\ K_c^{-2/3} \qquad (14)$$

where C_r = length of largest radial or conical crack
m = mass of the impacting particle
H = hardness of the target material
V_o = the particle velocity
K_c = the fracture toughness of the target material.

As in the model proposed by Evans et al, Ruff and Wiederhorn (1979) assume that the lateral crack size is proportional to the radial crack size, and that the depth of lateral cracking is proportional to the maximum particle penetration, i.e.:

$$h \propto m^{1/3} V_o^{2/3} H^{-1/3} \qquad (15)$$

and thus the following expression for erosion rate is obtained:

$$E \propto V_o^{22/9} R_p^{11/3} \rho_p^{11/9} K_c^{-4/3} H^{1/9} \qquad (16a)$$

or, alternatively,

$$E \propto V_o^{2.4} R_p^{3.7} \rho_p^{1.2} K_c^{-1.3} H^{0.11} \qquad (16b)$$

Dimond et al (1983) and Gulden (1981) assessed the validity of the erosion models proposed by Evans et al (1978) and by Ruff and Wiederhorn (1979) and found that their experimental data fit the models equally well.

Although the factors influencing solid particle erosion have been discussed separately in this chapter, it is important to realise that the variables interact and affect the relative importance of other parameters.

CHAPTER 3 : EXPERIMENTAL METHODS

Erosion tests at room temperature were performed by impacting a stationary target with particles accelerated in an airstream. The equipment used made it possible to study the influences of velocity, angle of impingement and the nature of the impacting particles on the erosion of glass microscope slides. Multiple particle erosion results are reported in terms of milligrams of material lost per gram of impacting particles, whilst the single particle impact damage was analysed quantitatively by means of optical microscopy and lineal analysis, as well as qualitatively by means of scanning electron microscopy.

3.1 MATERIALS

Glass slides were used as the target material in all the erosion testing. Using glass, which is homogeneous, single phase and isotropic, as the model brittle target material conveniently avoids the microstructural and orientational effects which strongly influence the erosion behaviour of polycrystalline ceramic materials. In addition, since glass slides are relatively "soft", measurable weight losses are obtained within shorter testing times and using smaller amounts of impacting particles.

The particle types employed as the erodent in the tests are listed in Table 3.1, together with their more important properties.

The particle size distributions of the pulverized fuels were determined by means of wet sieve analysis, and the particle size ranges of the commercial abrasives were determined by measuring the average diameters of the particles in scanning electron micrographs. The mineralogical composition of the pulverized fuel samples was established by quantitative X-ray diffraction analysis, using the internal standard method. Details of the method are given in Appendix I.

TABLE 3.1 : The Abrasive Particles

PARTICLE TYPE	AVERAGE SIZE RANGE (μm)	MOH'S HARDNESS	DENSITY g/cm^3	SHAPE	SOURCE
Pulverized Coal : Arnot Duvha Matla Kriel	As received - generally 250 μm See section 5.1	Clay component 2 to 2.5 Quartz component 7.0 Organic component unknown	-	Angular quartz agglomerated material	Power stations, ex ESCOM
Quartz	230 115 41	7.0	2.65	Angular	Prepared in the laboratory using glass sand of high purity
Silicon carbide	115 51 36	9.0	3.22	Angular	Commercial loose grain abrasive
Alumina	120	9.0	3.97	Angular	Commercial loose grain abrasive
Zircon sand	130	7.5	4.56	Rounded	By-product from ilmenite mining

3.2 EROSION TESTING

The erosion of pipe-bends in pulverized fuel lines can be most closely modelled by the particle-gas stream type of erosion tester. Erosion tests were performed using the apparatus illustrated in Figure 3.1.

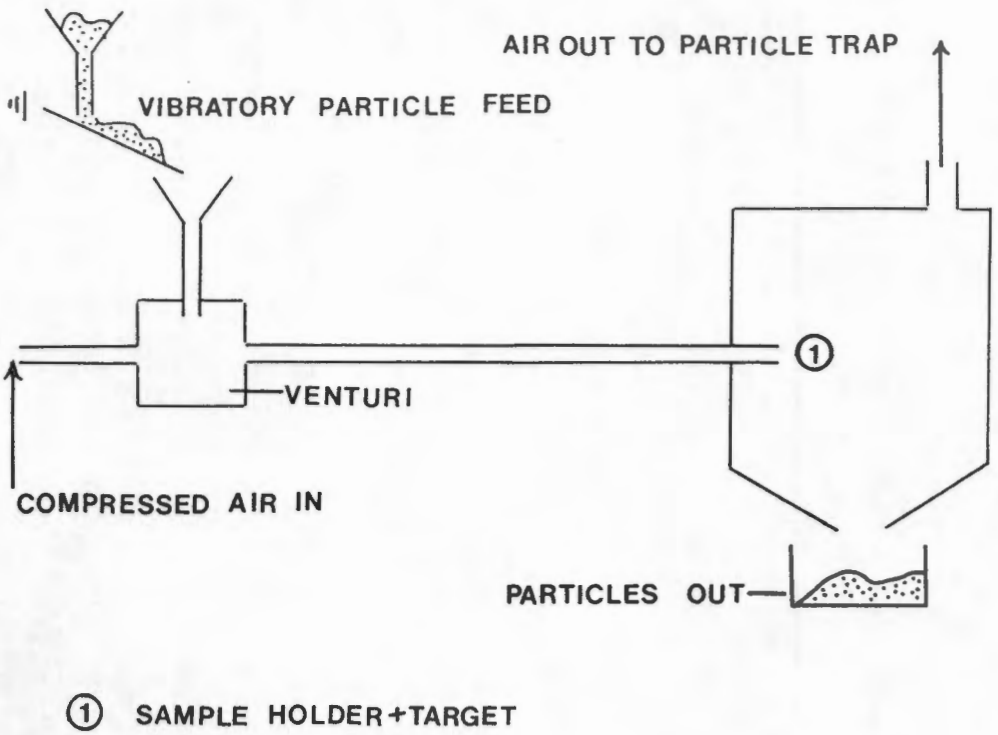

FIGURE 3.1 : A schematic diagram of the erosion apparatus

A predetermined mass of the abrasive particles was fed into the airstream by means of a vibratory particle feeder. The concentration of particles was kept as close as possible to 0.001 g/cm^2s, although the minor fluctuations which occur apparently had no effect on the erosion rate or on the reproducibility of the results. The target was cleaned ultrasonically in alcohol, dried, and weighed on a 5-point balance both before and after testing. The particle velocity was varied between 25

and 55 ms^{-1} and was measured using the rotating double disc method developed by Ruff and Ives (1975). (See Appendix II for a description of this method).

Since the pulverized fuel pipelines do not reach significantly high temperatures (ie. the operating temperature is generally less than 200°C), room temperature testing should represent the in-situ conditions adequately. The basic operating parameters of the erosion apparatus are summarized below:

TABLE 3.2 : Operating parameters of the particle-gas stream erosion tester

VARIABLE	RANGE
Particle velocity	from 25 to 55 ms^{-1}
Particle feed rate	approximately 0.01 gs^{-1}
Particle concentration	approximately 0.001 g/cm^2s
Operating temperature	room temperature
Angle of impingement	generally 90° but also 35°, 45° and 60°
Target material	Glass slides (76 x 26 x 1.0-1.2 mm) with finely ground edges, manufactured by Superior, W. Germany.
Particle type	Pulverized fuel, quartz, silicon carbide, alumina, zircon.
Particle sizes	See Table 3.1
Length of accelertion tube	130 cm
Distance between target and exit port of accelertion tube	10 mm
ID of acceleration tube	10 mm
Area of target eroded at 90° impact angle	86.59 mm^2

The results of two separate series of experiments conducted with 230 μm diameter quartz are depicted in Figure 3.2. As is evident from the illustration, the fit is good, indicating that the experimental techniques employed are adequate, with no necessity for higher precision or for a more sophisticated experimental technique.

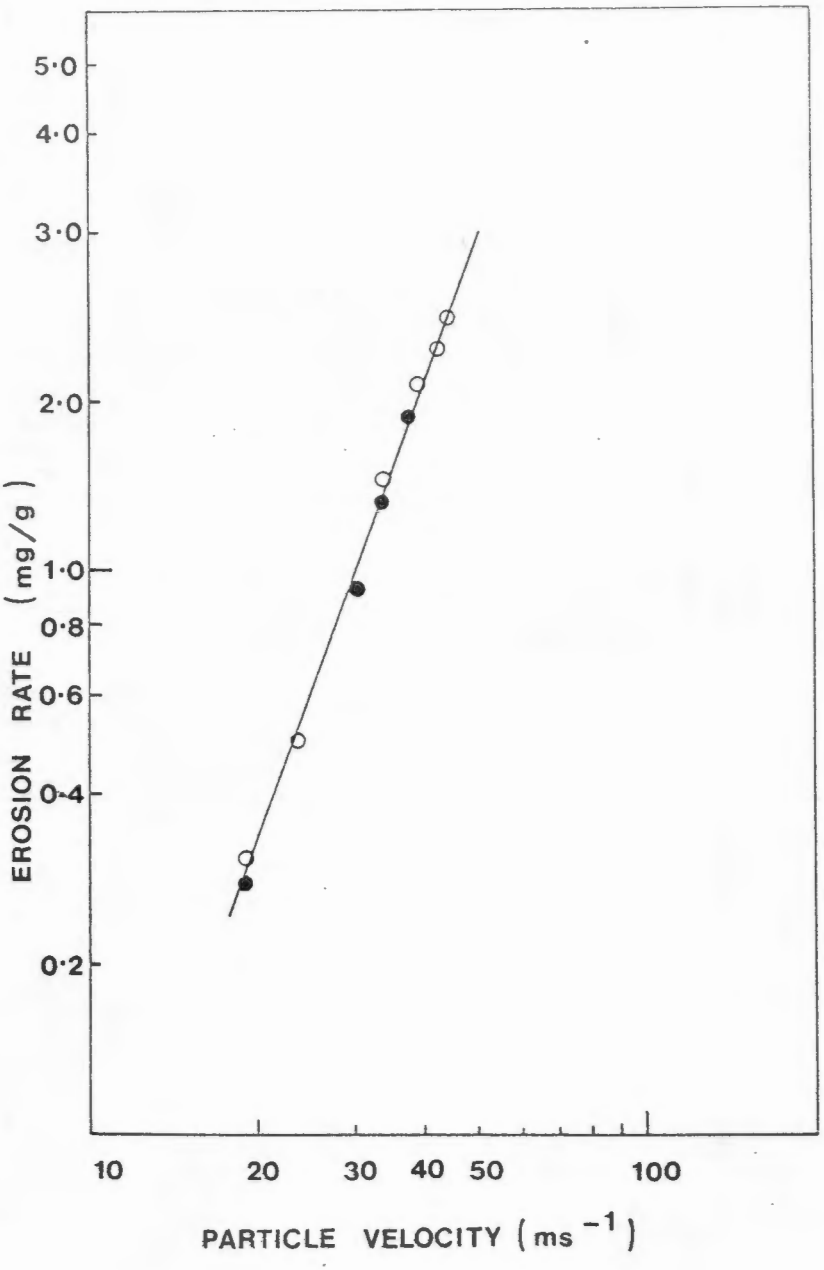

FIGURE 3.2 : Erosion rate versus velocity for 230 μm diameter quartz impacted against glass at an angle of incidence of 90°. ○ represents the first run and ● represents the second run.

Single impact, as well as multiple particle impact erosion tests were conducted and Table 3.3 lists the mass of material used for both types of test.

TABLE 3.3 : Mass of each particle type used in the single and multiple particle impact erosion testing

PARTICLE TYPE	MASS (g) FOR SINGLE PARTICLE IMPACT TEST	MASS (g) FOR MULTIPLE PARTICLE IMPACT TEST
Arnot (< 250 μm)	0.5	20 to 80
Duvha (< 250 μm)	0.5	20 to 80
Matla (< 250 μm)	0.5	20 to 80
Kriel (< 250 μm)	0.5	20 to 80
Quartz (230 μm)	0.02	1 to 3
Quartz (115 μm)	0.01	1 to 3
Quartz (41 μm)	0.01	1 to 3
Silicon carbide (115 μm)	0.01	1 to 3
Silicon carbide (50 μm)	0.0059	1 to 3
Silicon carbide (30 μm)	0.0062	1 to 3
Alumina (115 μm)	0.0118	1 to 3
Zircon sand (120 μm)	0.0237	1 to 3

The semi-automatic image analysis system, developed for use on the Teletronix 4051-Summagraphic digitizer system [Frith and Heckroodt (1984)] was employed in the investigation of the magnitude of the damage craters formed by the single particle impact events.

Optical micrographs were taken of the damage caused by the single particle impacts, whilst higher magnification scanning electron micrographs were taken of the particle types and of the impact damage incurred by the glass slides.

CHAPTER 4 : THE INFLUENCE OF VARIOUS PARAMETERS ON THE EROSION RATE OF GLASS

The main objective of this work is to establish the erosive characteristics of the four pulverized fuels which had been received, and to relate their erosion rates to their particle properties. Prior to commencement of the practical work, during a review of the literature dealing with solid particle erosion, it became evident that much controversy existed as regards the influence of the various impact and particle parameters on the erosion rate of brittle materials.

The two elastic-plastic models of erosion which are in current use both relate erosion rate to particle parameters such as velocity, radius and density, as well as target properties such as critical stress intensity factor and hardness. The relationships for the two models are:

$E \propto V_o^{3.2}\ Rp^{3.7}\ \rho_p^{0.25}\ K_c^{-1.3}\ H^{-0.25}$ [Evans et al (1978)]

$E \propto V_o^{2.4}\ Rp^{3.7}\ \rho_p^{1.20}\ K_c^{-1.3}\ H^{0.11}$ [Ruff and Wiederhorn (1979)]

However, the relative importance of the parameters differ in each of the equations and the opinions of researchers vary as to which expression is more representative of erosion conditions. For example, the velocity exponent (n) incorporated in the two predicted equations for erosion differ, and , as can be seen from Table 2.1, the available experimental data agree equally well with both exponent values and neither exponent can be said to be more applicable. Although both expressions predict the same erosion rate dependence on particle diameter, controversies exist as regards the effect of particle size on the velocity exponent and on the erosion rate. The effect of density on erosion rate also differs in the two models. A particle parameter not included in the expressions is that of particle hardness, and again much controversy exists regarding the effect of this parameter on erosion rate.

This part of the study is concerned primarily with the controversies which exist as regards particle parameters and it also includes an investigation of the influence of the impact parameters of velocity and angle of attack on erosion rate.

Variations in stress intensity factor and hardness of the target could not be investigated since the brittle target material was kept constant throughout the entire investigation. Thus, despite the fact that controversies also exist as regards these parameters, they will not be dealt with in this work.

4.1 THE TARGET AND PARTICLE MATERIALS

4.1.1 The Target

Since the candidate materials for use in the lining of the pulverized fuel pipelines are ceramic materials such as high density alumina, the use of a brittle target material in the present study is required. Glass microscope slides were chosen as the target material for several reasons. Since glass is single phase, homogeneous and isotropic, microstructural effects such as grain size and porosity (see section 2.3.2) are eliminated. By keeping glass as the target material throughout the entire investigation, the target characteristics of hardness and fracture toughness were also kept constant, thus effectively eliminating any influence which these parameters might have had on erosion rates and erosion mechanisms. The hardness and fracture toughness values of the glass slides were not determined experimentally but, according to Evans and Wilshaw (1976) and Ritter et al (1985), soda-lime glass, from which the slides are manufactured, has a hardness value of 5.5 GN/m^2 and a fracture toughness value of 0.7 $MN/m^{3/2}$.

4.1.2 The Particles

Several particle types were used as erodents and differed from one another with respect to density, hardness, shape and/or average size. A list of these properties is given in Table 3.1. By employing particles with different properties in the erosion testing, it should be possible to ascertain what effects, if any, these properties would have on the erosion rate and mode of damage incurred by the glass slides.

Quartz was chosen as one of the erodents since it is known to be the major erosive constituent occurring in pulverized coals. High purity glass sand was crushed and screened into three narrow size ranges: 38 to 45 μm, 106 to 125 μm and 212 to 250 μm. These size ranges of quartz are similar to those of the quartz particles occurring in the pulverized fuels and the sizes also provided mass differences of at least three orders of magnitude.

The other particle types used were silicon carbide, alumina and zircon. Because of the narrow size ranges within which these particles were obtained, screen analyses would not be a very effective means of checking the particle size distributions and thus the particle size ranges of these powders were determined by measuring the diameters of the particles from enlarged scanning electron micrographs. All the particles, with the exception of zircon, were angular in shape (see Figure 4.1). The average diameter of the particles was defined as the square root of the product of the "width" and "length" of the particles. It is, however, fully acknowledged that the thickness of the particles may be less than the "width" of the particles. Table 4.1 shows the range of sizes within which 90% of the particles fell, and also the average sizes of the particles. The average particle diameters of the quartz fractions were determined by taking the logarithmic mean.

TABLE 4.1 : Particle size distributions and average particle sizes of quartz, silicon carbide, alumina and zircon

PARTICLE TYPE	SIZE RANGE (μm)	AVERAGE PARTICLE DIAMETER (μm)	PARTICLE SIZE GIVEN BY MANUFACTURER (μm)
Quartz	212-250	230	
Quartz	106-125	115	
Quartz	38-45	41	
Silicon carbide	96-135	115	100
Silicon carbide	33-73	51	50
Silicon carbide	28-43	36	30
Alumina	98-137	120	
Zircon	100-160	130	

No foreign minerals were detected on examination of the powders under the optical and scanning electron microscopes. Figure 4.1 illustrates scanning electron micrographs of all the particle types employed in the investigation. Note that the quartz, silicon carbide and alumina particles all display the same angularity in shape, irrespective of their average size. Although a fraction of the zircon particles are elongated in shape, the ratio of "length" to "width" being approximately 2 to 1, these particles all have rounded edges and thus the zircon particles as a whole may be described as spherical.

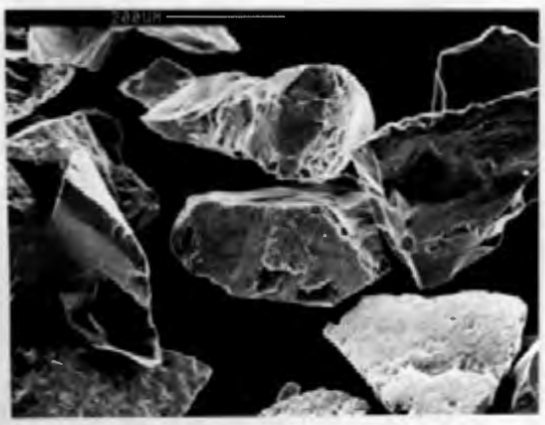

230 μm Quartz

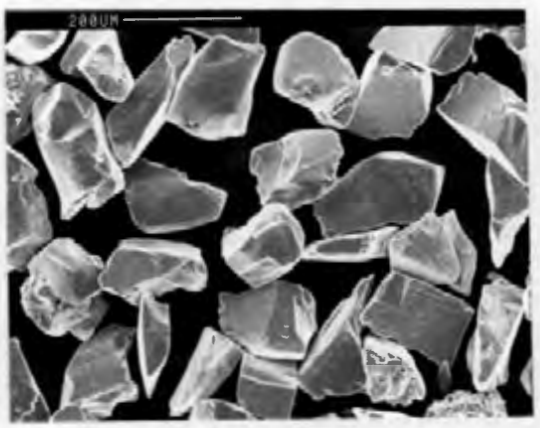

115 μm Silicon carbide

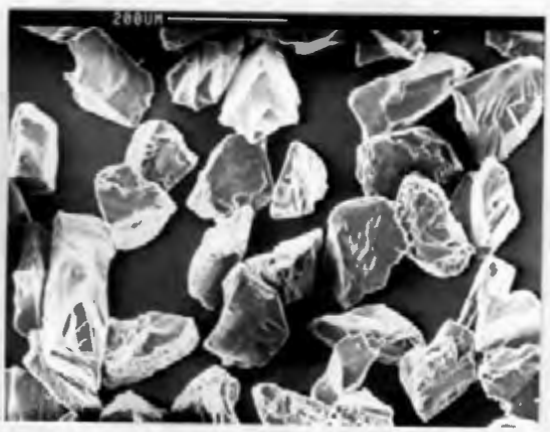

115 μm Quartz

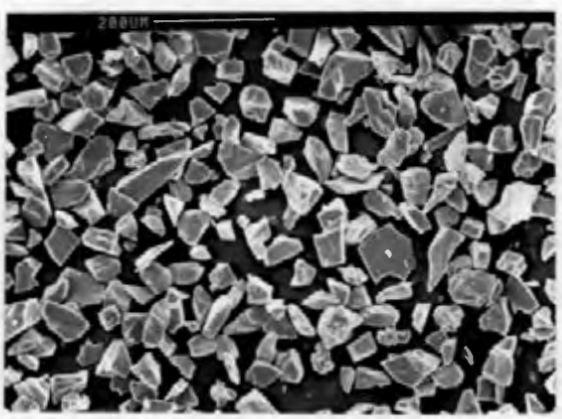

51 μm Silicon carbide

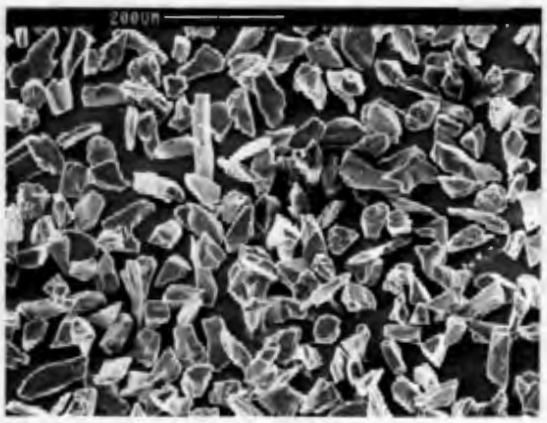

41 μm Quartz

36 μm Silicon carbide

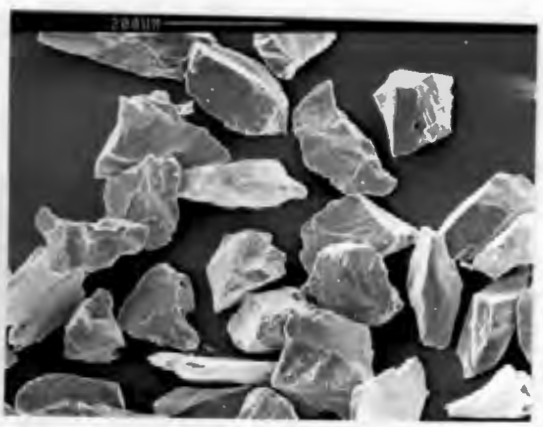

120 μm Alumina

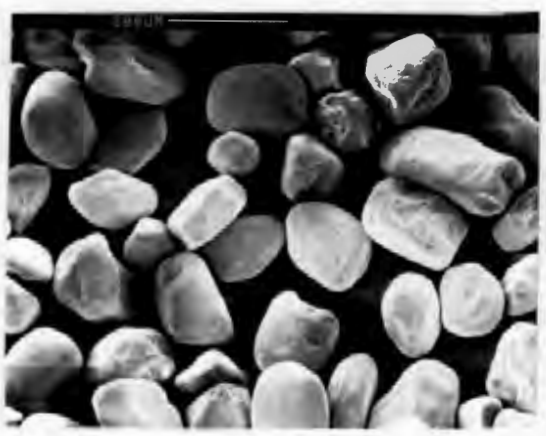

130 μm Zircon

FIGURE 4.1 : Scanning electron micrographs of the particles employed in the study

4.2 EROSION TESTING

Within the pulverized fuel pipelines, the velocity of the particles probably ranges from 15 to 30 ms^{-1} [Raask (1979)], while the angle at which the particles strike the walls of the pipebends has been established as being less than 40° [Mills and Mason (1977)]. The erosion testing, however, was conducted at velocities ranging from 25 to 55 ms^{-1}, and an angle of incidence of 90° was employed. The angle of 90° was

chosen since it is the angle at which maximum material loss occurs for brittle materials, and since erosion rate is proportional to velocity, the use of higher velocities will also increase erosion rate. Accordingly, measurable weight losses were obtained within relatively short testing times using less abrasive material than would have been necessary had lower angles and velocities been used.

The concentration of the pulverized fuels within the pipelines is unknown and thus, for the sake of convenience, an erodent concentration of 0.001 g/cm^2 was selected for use.

4.2.1 Damage Morphology

Prior to commencement of the erosion testing, the nature of the damage produced by the various abrasive particles impinging on the glass target surface was examined.

As discussed in Section 2.4, impacting particles may be classified either as "blunt", in which case the target response is elastic and associated Hertzian cone cracks may form, or "sharp", in which case the fracture damage is characterized by a central, plastically deformed region surrounded by radial and lateral cracking.

The transition from the elastic to the elastic-plastic target response depends upon the radius of curvature (R) of the particles (see Section 2.4.2). The values of the critical particle radius (R_c) for glass impacted with several particle types were calculated by Sargent et al (1979) and are given in Table 4.2.

TABLE 4.2 : Values of the critical particle radius (R_c)

PARTICLE TYPE	CRITICAL PARTICLE RADIUS (R_c) μm
Silicon carbide	782
Alumina	726
SiO_2	249
Steel	600

According to the table, the quartz, silicon carbide and alumina employed in this study are well below the critical particle size and may therefore be regarded as "sharp". Similarly, the zircon particles, which have a small average particle radius - namely 65 μm - may also be regarded as "sharp" despite their rounded appearance.

The target surfaces which had been subject to multiple particle impacts were damaged to an extent where little or no information regarding the nature of the damage was provided. Thus, glass targets which had been subject to single particle impacts were employed in the examination of the damage morphology. The particles struck the target at a velocity of 35 ms^{-1} and a normal angle of incidence.

Since the impacting particles may strike the target surface in any orientation, the individual impact sites were found to differ greatly in their appearance. For example, the magnitude of the damage area varied very much (see Chapter6), as did the amount of laterally cracked material that was removed.

Figures 4.2, 4.3 and 4.4 are typical examples of the type of single impact damage produced by quartz particles, but the appearance of the damage caused by the other particle types is the same.

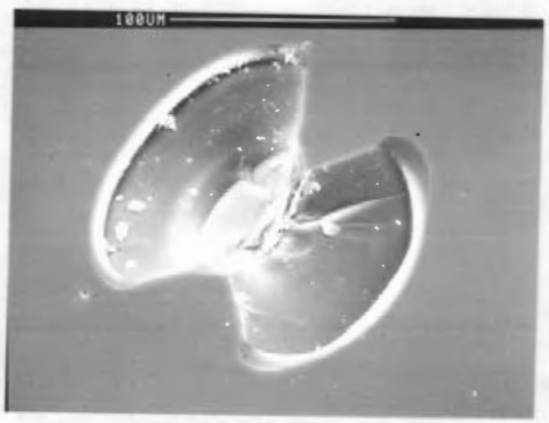

FIGURE 4.2 : Single particle impact damage on glass produced by a 230 μm diameter quartz particle travelling at 35 ms^{-1}

Note the centrally damaged zone, surrounded by two lobes of laterally cracked material which is still in place. It is likely that subsequent particle impaction over the laterally cracked region will have the effect of loosening the material and removing it.

The damage need not be symmetrical about the point of contact, as is clearly illustrated in Figure 4.3. (Three or even four lobes of laterally cracked material may form). Note also the presence of what could be radial cracking on the target surface.

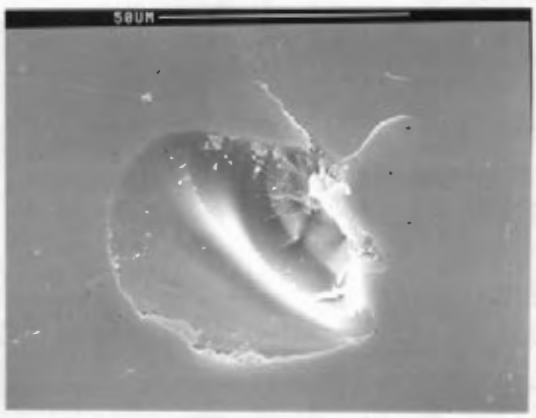

FIGURE 4.3 : Single particle impact damage produced by a 115 μm diameter quartz particle travelling at 35 ms^{-1}

A number of the impact craters produced by the particles were characterized by pits with no evidence of lateral cracks intersecting the target surface (Figure 4.4). These pits were found to occur more frequently on target surfaces which had been damaged by the small diameter particles, namely 41 μm quartz and 36 μm silicon carbide.

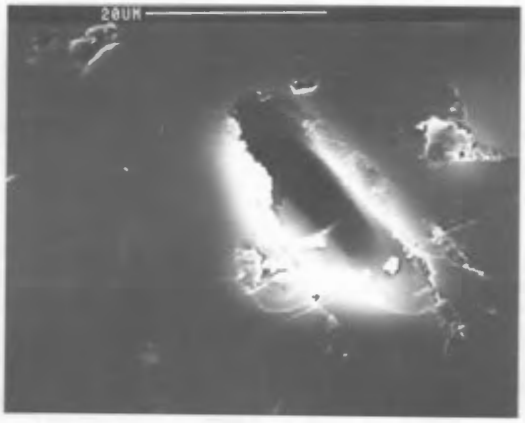

FIGURE 4.4 : Single particle impact damage produced by a 41 μm diameter quartz particle travelling at 35 ms^{-1}

It is thought [Wiederhorn and Hockey (1983)] that pits or plastic impressions in the target surface are a result of the deformation not being sufficiently concentrated to nucleate and propagate surface cracks. Thus not all the impacting particles are effective removers of material.

It should be borne in mind that, although crack formation at the impact craters seems to dominate the erosion process at angles of incidence of 90° and velocities of 35 ms^{-1}, the target response may well alter at lower angles of incidence and lower velocities, perhaps becoming similar to that described for small particles.

4.2.2 Erosion Rates

The erosion rates of all the powders as a function of particle velocities ranging from 25 to 55 ms^{-1} are compared in the figure which appears in Appendix III. As discussed in section 3.2, the reproducibility of the results is good, with the experimentally determined erosion rates of the different particle types at particular particle velocities not varying by more than 2 per cent.

(a) The effect of velocity on erosion rate

The following points regarding the effect of velocity on erosion rate were observed.

At an intermediate velocity of 35 ms^{-1}, the three size fractions of silicon carbide were more erosive than the size fractions of quartz (Table 4.4). However, since the value of n is different for each particle type and each particle size, the relationship between the erosion rates of the particles at 35 ms^{-1} will not remain the same at, for example, 50 ms^{-1}. At 50 ms^{-1}, the quartz particles become more erosive than the silicon carbide particles of equivalent size.

It is suggested by the figure appearing in Appendix III that, at velocities of 60 ms^{-1} and above, the small particles become more erosive than the large particles (also a result of the differing n values). However, whether or not such a velocity-particle size effect does in fact occur, was not investigated since such high velocities do not pertain to the conditions found in the power stations.

An interesting point which emerged from the study of the influence of velocity on erosion rate was the fact that at low particle velocities, the erosion rate of the zircon becomes anomalously low (see Table 4.3 and the figure in Appendix III).

TABLE 4.3 : The influence of velocity (ms^{-1}) on the erosion rate (mg/g) of zircon

VELOCITY (ms^{-1})	50	45	40	35	30	27
EROSION RATE (mg/g)	4.0	2.6	1.95	1.30	0.21	0.01

The effect cannot be explained in terms of a threshold velocity since, as discussed in Section 2.1.1, the threshold velocity below which no fracture occurs is reciprocally dependent upon particle size and density. Thus zircon, which has a higher density than any of the other particle types, should exhibit the lowest threshold velocity. However, the other particle types, which were similar in size to that of

zircon, did not display excessively low erosion rate at the lower velocities. The only other aspect in which the zircon particles differ from the other particles, is morphology, a fact which suggests that shape could be a very important factor when considering erosion rates.

As a first approximation, the relationship between erosion rate and velocity has been proposed to be:

$$E = AV_o^n$$

where A is a constant which is dependent upon target and particle properties.

The values of the velocity exponents n and the constant A determined by least-squares fit, as well as the erosion rates at 35 and 50 ms^{-1}, for the various particle types are listed in Table 4.4.

TABLE 4.4 : Velocity exponent (n), constant (A) and erosion rate (E) as a function of particle material and size

PARTICLE TYPE	AVERAGE PARTICLE DIAMETER (μm)	VELOCITY EXPONENT (n)	CONSTANT A	EROSION RATE (mg/g) AT 35 ms^{-1}	EROSION RATE (mg/g) AT 50 ms^{-1}
Quartz	230	2.6	4.8×10^{-5}	1.45	4.00
Quartz	115	3.2	8.0×10^{-6}	0.70	2.50
Quartz	41	3.7	4.0×10^{-7}	0.26	0.94
Silicon carbide	115	2.3	2.3×10^{-4}	0.90	2.00
Silicon carbide	51	2.6	5.6×10^{-5}	0.39	0.96
Silicon carbide	36	3.8	1.0×10^{-8}	0.13	0.65
Alumina	120	2.6	4.6×10^{-5}	1.30	3.40
Zircon	130	3.3	1.8×10^{-5}	1.30	4.00

The velocity exponent, n, determined for each particle type, did not vary by more than 0.1 when using repeat sets of data to determine the value.

A comparison between the theoretically predicted values of n and an exponent value which was obtained empirically is depicted in Figure 4.5.

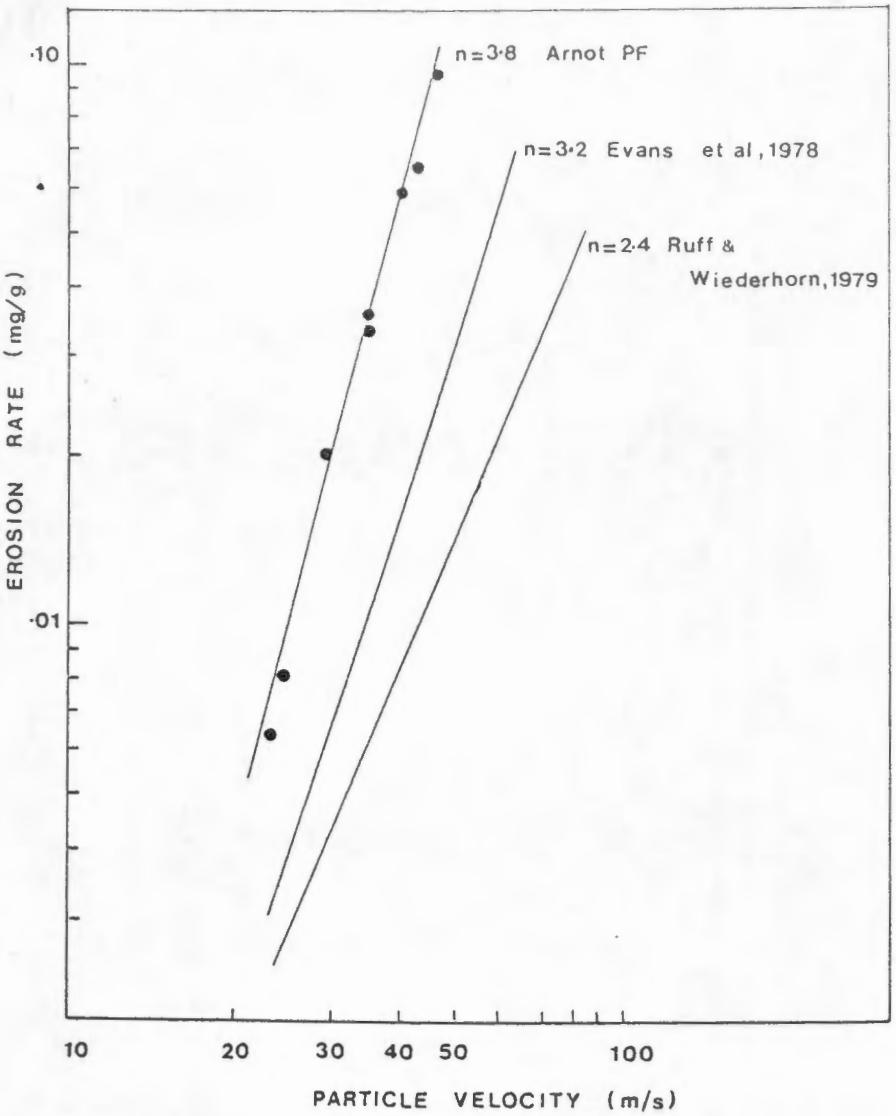

FIGURE 4.5 : Experimentally determined relationship between erosion rate and particle velocity of a pulverized fuel compared to theoretical relationships based on the models of Evans et al and Ruff and Wiederhorn

The values of n obtained in this investigation bracket those predicted by Evans et al (1978) and Ruff and Wiederhorn (1979) and are also in reasonable agreement with those obtained by other researchers who used similar target materials (namely glass) and particle types (see Table 2.1).

The 230 μm quartz, the 115 μm silicon carbide, the 51 μm silicon carbide and the 120 μm alumina all have comparatively low velocity exponent values, similar to the value of 2.4

which is used in the quasi-static model of erosion, while the velcity exponents of the 115 μm quartz, the 41 μm quartz, the 36 μm silicon carbide and the 130 μm zircon were closer to the velocity exponent value of 3.2 predicted by the dynamic model of erosion. The particle types could not be grouped together in terms of their n values according to their physical properties, nor could they be grouped together in terms of size. One point which emerged clearly was the fact that no velocity exponent values of less than 2 were obtained in the present work. Thus the suggestions of Gulden (1979) and Routbort and Scattergood (1980) that such low exponent values are the result of microstructural effects, which did not enter into the present study, could not be verified.

A consistent trend which was immediately apparent when considering the velocity exponents reported in Table 4.4 was that the velocity exponent increases with decreasing erodent particle size. These trends are shown in Figure 4.6.

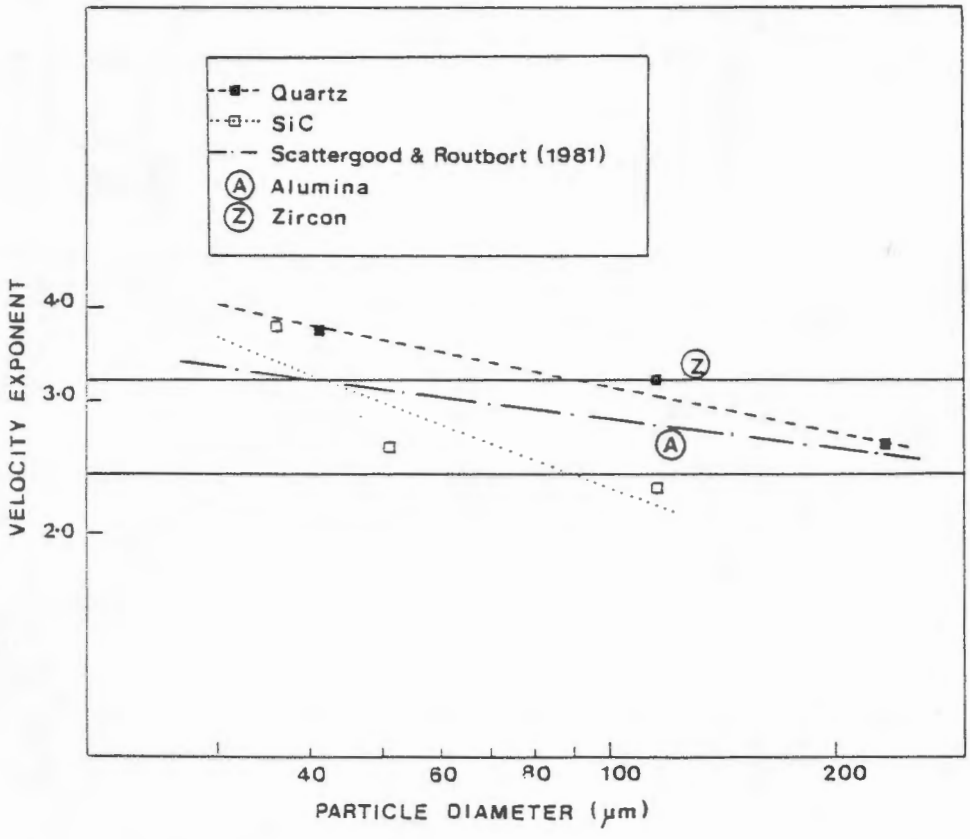

FIGURE 4.6 : The effect of particle size on the velocity exponent.

This result is not peculiar to the target-particle systems soda-lime glass-quartz and soda-lime glass-silicon carbide, as is pointed out in Table 4.5.

TABLE 4.5 : The effect of particle size on the velocity exponent for several target-particle systems

TARGET MATERIAL	PARTICLE TYPE	PARTICLE SIZE (μm)	VELOCITY EXPONENT n	REFERENCE
Pyrex glass	Alumina	30	2.2	Sargent et al (1979)
Pyrex glass	Alumina	10	2.7	
Reaction-bonded SiC	Alumina	270	2.0	Routbort et al (1980b)
Reaction-bonded SiC	Alumina	130	2.3	
Silicon single crystal	Alumina	270	2.55	Scattergood & Routbort (1981)
		130	2.70	
		37	3.35	
		23	3.40	

The same trend was not observed by Routbort and Scattergood (1980) who impacted hot-pressed silicon carbide with 270 μm alumina (n = 1.8) and 130 μm alumina (n = 1.5). However, the behaviour of this target material was anomalous in other respects too, as discussed in section 2.2.2.

In view of the results obtained in this investigation and of those reported in Table 4.5, a term incorporating the particle size dependence of the velocity exponent should be included in the erosion models. As yet, too few data points are available to allow a reliable prediction of the general form which such a dependence should take, although it does seem that particle size is related to n by a power law, i.e. $n = q\ D^{-p}$, or $\log n = \log q - p \log D$. The values of q and p, obtained in this investigation for glass impacted with quartz and silicon carbide and from the data reported by Scattergood and Routbort (1981) for silicon single crystals impacted with alumina, are given in Table 4.6.

TABLE 4.6 : The values of the constants p and q

TARGET MATERIAL	IMPACTING PARTICLE TYPE	q	p
Glass	Quartz	8	-0.2
Glass	SiC	13.5	-0.4
Si single crystal	Al_2O_3	5	-0.1

The fit was found to be good for the data of Scattergood and Routbort (1981) and for glass impacted with quartz particles, whilst there was some scatter in the results for glass impacted with silicon carbide particles.

Scattergood and Routbort (1981) suggested that the phenomenon of increasing velocity exponent with decreasing particle size was due to a change in the particle impact mechanism, with large particles appearing quasi-static (n = 2.4) and small particles appearing dynamic (n = 3.2). They could not, however, offer an explanation as to why such a change should occur.

Alternatively, the particle size-velocity exponent dependence could be explained in terms of fragmentation effects. Large particles are statistically more likely to contain flaws than are small particles, which will increase the probability of the large particles shattering on impact with the target surface. Energy is expended in the process, with less energy being available for the propagation of lateral cracks. As a result, the large particles will exert less influence than expected on erosion rate and the resultant velocity exponent will not be as great as that of smaller particles.

When two teams of researchers [Routbort et al (1980a) and Routbort et al (1980b)] investigated the manner in which angle of incidence influenced the value of the velocity exponent, they obtained differing results. When impacting reaction-

bonded silicon carbide with 270 μm alumina particles, Routbort et al (1980b) found that n varied inconsistently as angle was altered, whereas Routbort et al (1980a), who impacted silicon single crystals with alumina found that n was independent of angle.

In this investigation, the effect of angle on the velocity exponent of silicon carbide was briefly investigated. The results are tabulated below:

TABLE 4.7 : The effect of angle of incidence on velocity exponent

PARTICLE DIAMETER (μm) OF SiC	115	51	36
n at 90°	2.28	2.55	3.80
n at 45°	2.35	2.36	3.80

Since the difference in n may vary by about 0.1, the differences reported in Table 4.7 are not really significant and thus these results favour those of Routbort et al (1980a). Since homogeneous single-phase materials were employed in this study and in that of Routbort et al (1980a), it may well be that the varying n values obtained with the reaction-bonded silicon carbide were due to microstructural influences.

b) <u>The effect of angle on erosion rate</u>

For brittle materials, maximum material loss is expected to occur at high angles of incidence (at or near 90°) and, accordingly, a normal angle of incidence was used in the evaluation of the erosivity of all the particle types.

Since in the pulverized fuel pipelines, particles strike the walls at angles of less than 40°, it was necessary to study what effect lower angles of incidence would have on erosion rate. Furthermore, the effect of angle on erosion rate was

used as a means of determining whether or not the 41 μm diameter quartz particles or the 36 μm diameter silicon carbide particles would illicit a ductile target response, in which case the maximum in erosion rate would occur at an angle of about 20°.

The effect of angle on the erosion of the particles was investigated using angles of 90°, 60°, 45° and 35° and a particle velocity of 47 ms^{-1}. In Figure 4.7 the erosion rates are plotted as a function of angle for all the particle types.

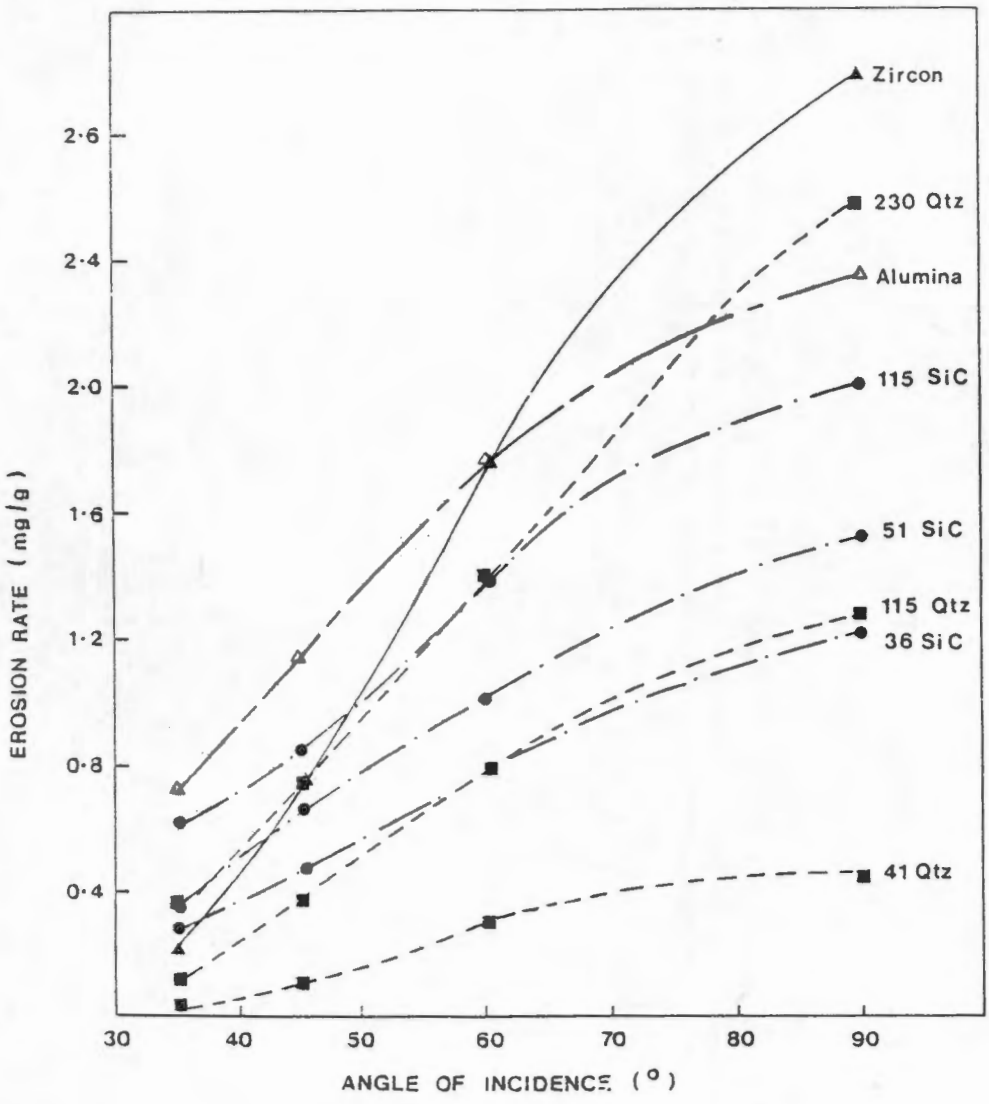

FIGURE 4.7 : The effect of angle of incidence on the erosion rate

The response of the glass target was typical of the behaviour of a brittle material, with the maximum material removal

occurring at an angle of 90°. This was found to be true for all the particles, irrespective of size.

The degree to which angle influenced the erosivity of the four abrasive media was not the same, although the particles existing within a group (eg. the three size fractions of quartz) followed a similar trend. Note also the erosive behaviour of the zircon abrasive. At an angle of 90°, the erosivity of the zircon particles was three times that of the 36 μm diameter silicon carbide particles, whilst at 35°, the silicon carbide became twice as erosive as the zircon. This latter effect may yet again be an illustration of the importance of the shape of the zircon particles.

Because of the angular dependence of the experimentally determined erosion rates, it was suggested [Hockey et al (1978) and Shetty et al (1982)] that only the velocity component normal to the target surface might be relevant to the erosion process.

The theoretically predicted models of erosion assume the angle of particle impingement to be 90°. The models may be modified so as to include oblique or low angles of incidence by incorporating the normal component of particle velocity into the expressions, viz:

$$V = V_0 \sin\alpha \qquad (17)$$

where α = the angle of incidence

V_0 = the particle velocity at a normal angle of incidence

or, alternatively, since $E \propto V_0^n$:

$$E = E_{90} (\sin\alpha)^n \qquad (18)$$

A brief comparison was made between the experimentally determined erosion rates and the erosion rates calculated by means of Equation 18. There is acceptable agreement between the calculated and experimental erosion rates for most of the abrasives at angles of incidence as low as 35°. Two examples are illustrated in Figure 4.8.

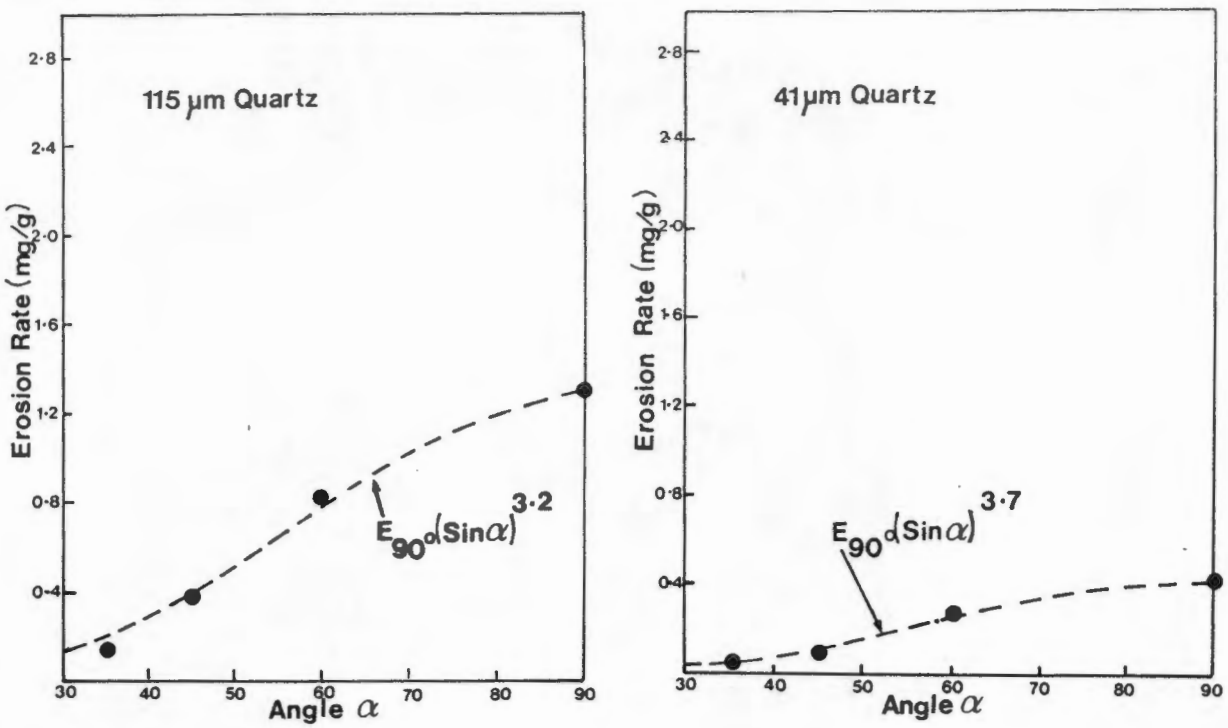

FIGURE 4.8 : A comparison of the predicted (dashed line) and experimentally determined erosion rates (●) for 41 μm diameter and 115 μm diameter quartz at 60°, 45° and 35°.

These results are in agreement with those predicted by Dimond et al (1983) and Hockey et al (1978) who found that the comparison between the predicted and experimental erosion rates was satisfactory for angles on impingement greater than 40° and 35°, respectively.

Some systematic deviations from the predicted curves were found for a few of the abrasives, i.e., the predicted erosion rates either consistently over or under estimated the experimentally determined erosion rates. Examples are given in Figure 4.9.

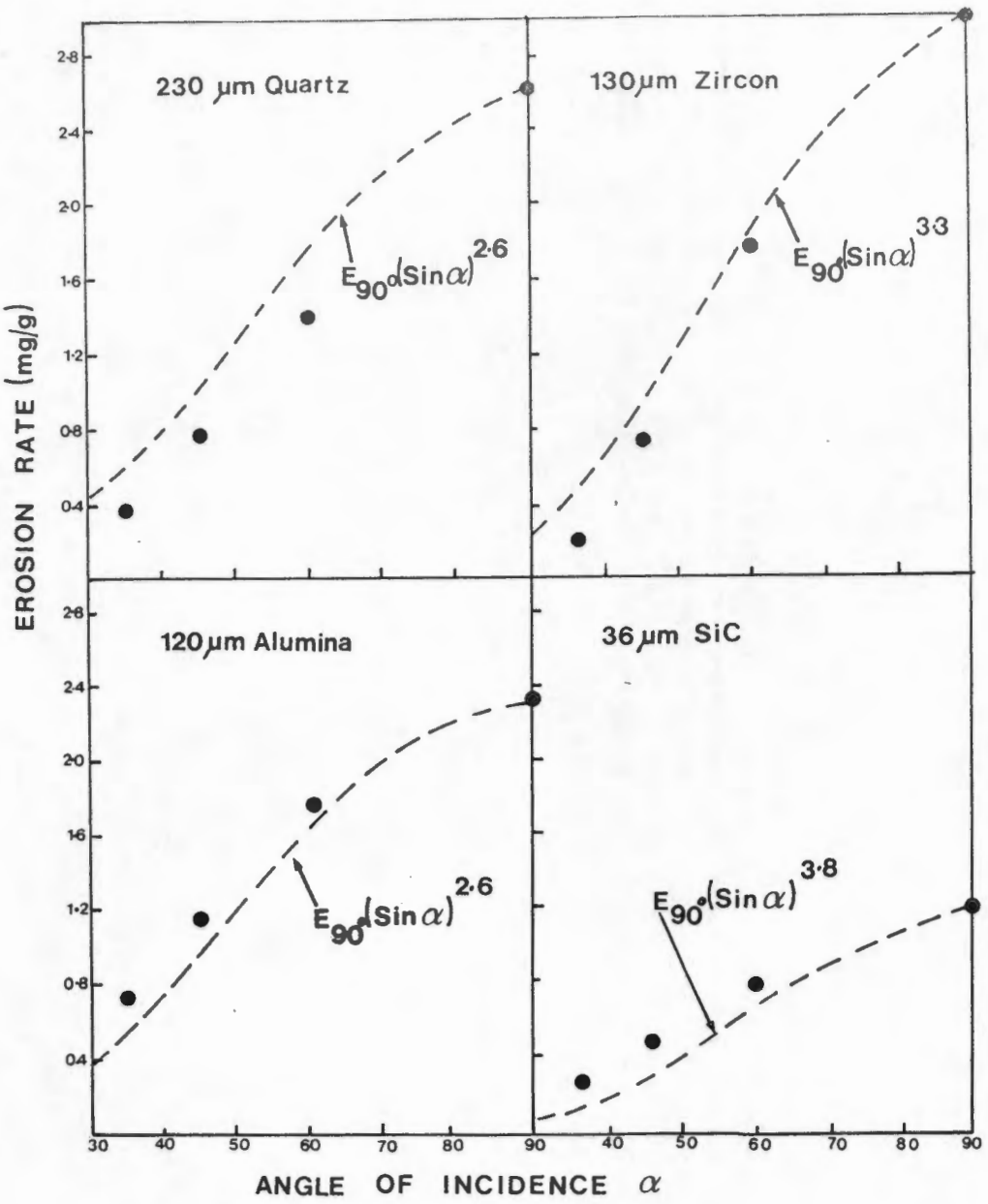

FIGURE 4.9 : The systematic deviations observed for 230 μm diameter quartz, 130 μm diameter zircon, 120 μm diameter alumina and 36 μm diameter silicon carbide.

In the case of 130 μm diameter zircon, an explanation for overestimation of the calculated erosion rates could perhaps be found in the particle shape and the anomalously low erosion rates which occur for these particles at low velocities (See Section 4.2.2(a)). A similar deviation was observed for the 230 μm diameter quartz, which is the coarsest of all the erodents employed in this study and it may be that size is

responsible for the differences between the predicted and experimental erosion rates.

In the case of the very fine 36 μm diameter silicon carbide, as well as the 120 μm diameter alumina, the predicted erosion rates consistently underestimated the experimentally determined erosion rates.

The results of this study indicate that particle size and shape may have an influence on erosion rate at the lower angles of incidence. This study did not warrent any further work since it would be necessary and advisable to re-examine the effect of angle on erosion rate when the candidate materials themselves are being investigated. It will also be necessary to examine the effect which angles of incidence as low as 15° have on the erosion rate of the candidate materials since, according to Hockey et al (1978), it is only at these very low angles of incidence that the plastic flow processes become important.

4.3 THE PARTICLE PARAMETERS

The influence of several particle parameters on erosion rate was studied, using the powders described in Section 4.1.

4.3.1 Particle Size

According to the predictions of Evans et al (1978) and Ruff and Wiederhorn (1979), the particle size is an important parameter when assessing erosion rate. The models imply that a doubling of particle diameter will result in a 13-fold increase in erosion rate when expressed as volume of material removed per particle impact. Furthermore, there seems to be no limit in erosion rate with an increase in particle size, as is apparently the case for metals (See Figure 2.4).

Since the quartz and silicon carbide were both available in three size fractions, they were used in the investigation of the influence of particle size on erosion rate (See Figure 4.10).

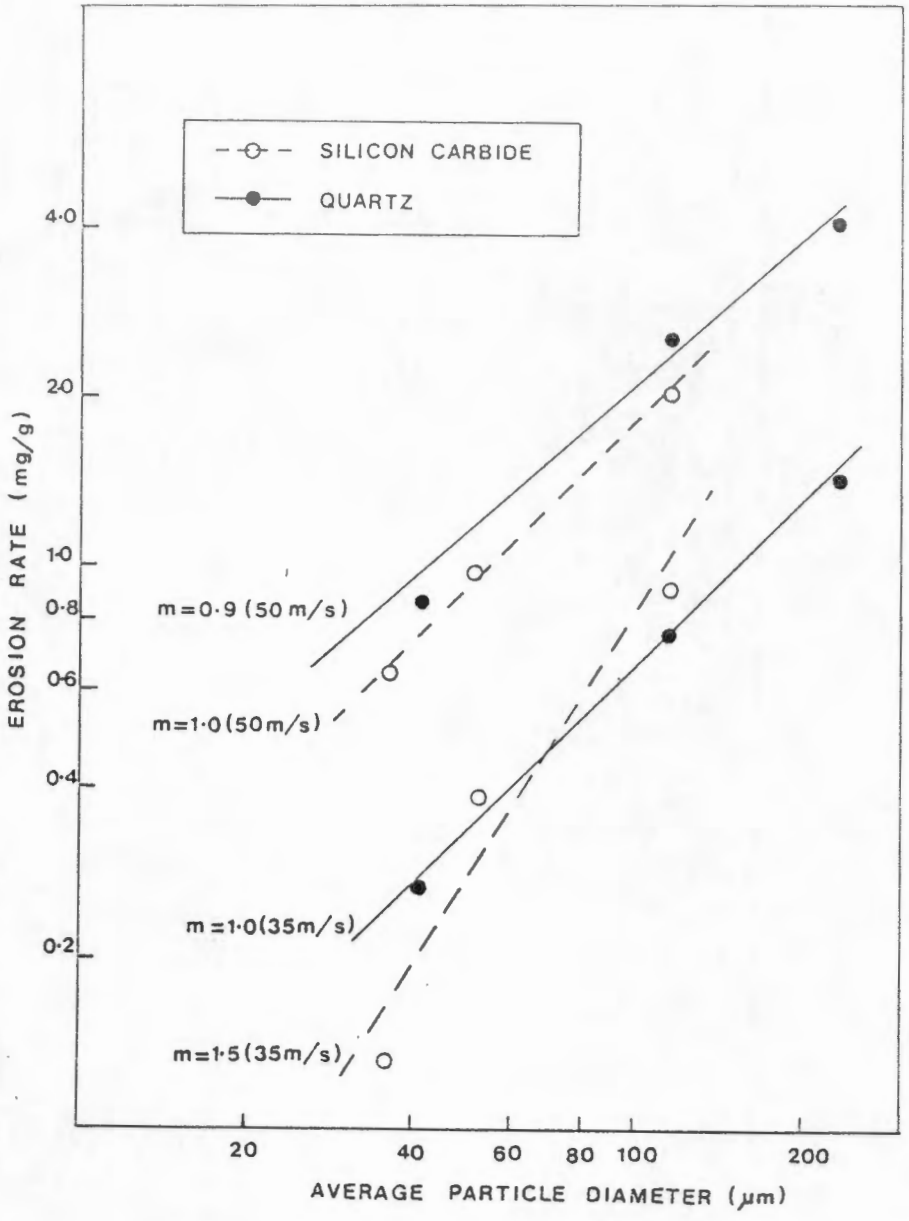

FIGURE 4.10 : Erosion rate (mg/g) versus average particle size (μm). Particle velocities are 35 and 50 ms^{-1} and angle of incidence is 90°

As intuitively expected, erosion rate is observed to increase as particle size increases. The results are supported by those of Goodwin et al (1969) who also eroded glass with quartz particles and by those of Routbort et al (1980b) who obtained increases in the erosion rate of reaction-bonded silicon carbide impacted with increasing sizes of alumina particles at a normal angle of incidence.

The results discussed above contradict those reported by Routbort and Scattergood (1980) who impacted hot-pressed silicon carbide with alumina particles and found that erosion rate decreased as particle size increased. They attributed this phenomenon to eroded surface morphology, that is, a microstructural effect, as opposed to a particle size effect, and since no such trend was observed in the present study where glass was employed as the target material, their assumption appears to be reasonable although in view of the results obtained by Routbort et al (1980b), the phenomenon is probably peculiar to hot-pressed silicon carbide. If the erosion rate is expressed as mg of material lost per g of erodent (mg/g), the particle size exponents obtained from Figure 4.10 were m = 0.9 for quartz and m = 1.0 for silicon carbide, at an impingement angle of 90˚.

In order to compare the values of m appearing in the models with the values of m obtained for this study, volume loss per particle was plotted versus particle diameter and the slopes of these lines yielded the particle size exponents. The values of m obtained for quartz and silicon carbide were 3.8 and 3.9 respectively. Both values are in close agreement with the theoretical value of 3.7.

Routbort et al (1980b) found variations in m as particle velocity and angle of incidence altered but were unable to state whether or not the variations were significant due to "experimental uncertainties". The variations in m with angle of incidence and particle velocity for the present work are reported in Table 4.8.

TABLE 4.8 : The variation of particle size exponent (m) with angle and velocity

PARTICLE TYPE	VARIATION OF m WITH ANGLE (˚)				VARIATION OF m WITH VELOCITY (ms^{-1}) AT 90˚		
	35	45	60	90	35	45	50
Quartz	1.1	1.2	0.9	0.9	1.0	0.9	0.9
Silicon carbide	0.6	0.4	0.5	1.0	1.5	1.0	1.0

Since only 3 data points were employed in the determination of each of the m values, the variation in value (m = 0.9 to 1.2) which occurs for quartz may be regarded as insignificant and it can be said that varitions in angle and velocity do not affect the particle size exponent of quartz. This does not apply to silicon carbide, however. At angles of incidence of less than 90°, the value of m decreases sharply to 0.5, suggesting that , at the lower angles of incidence the effect of particle size on erosion rate is lessened. At a velocity of 35 ms^{-1}, the particle size exponent increases to 1.5, an effect which may be attributed to the very low erosion rate of the 36 μm diameter particles.

4.3.2 Particle Density

Although particle density is an essential factor of all theoretical and empirical analyses of material loss by erosion, there has been no systematic study of its effect. The models predict an increase in erosion rate with increase in density : by increasing the particle density from, say, 2.65 g/cm^3 (quartz) to 3.22 g/cm^3 (silicon carbide), the model derived by Evans et al (1978) predicts a 5.5 per cent increase in erosion rate, since the particle density exponent is 0.25, whereas the effect of such an increase in density is greater (26 per cent) when accepting the Ruff and Wiederhorn (1979) model, where the particle density exponent is 1.20.

The influence of density on the erosion rate of 130 μm diameter quartz and silicon carbide (from extrapolation), 130 μm diameter zircon and 120 μm diameter alumina, is illustrated in Figure 4.11.

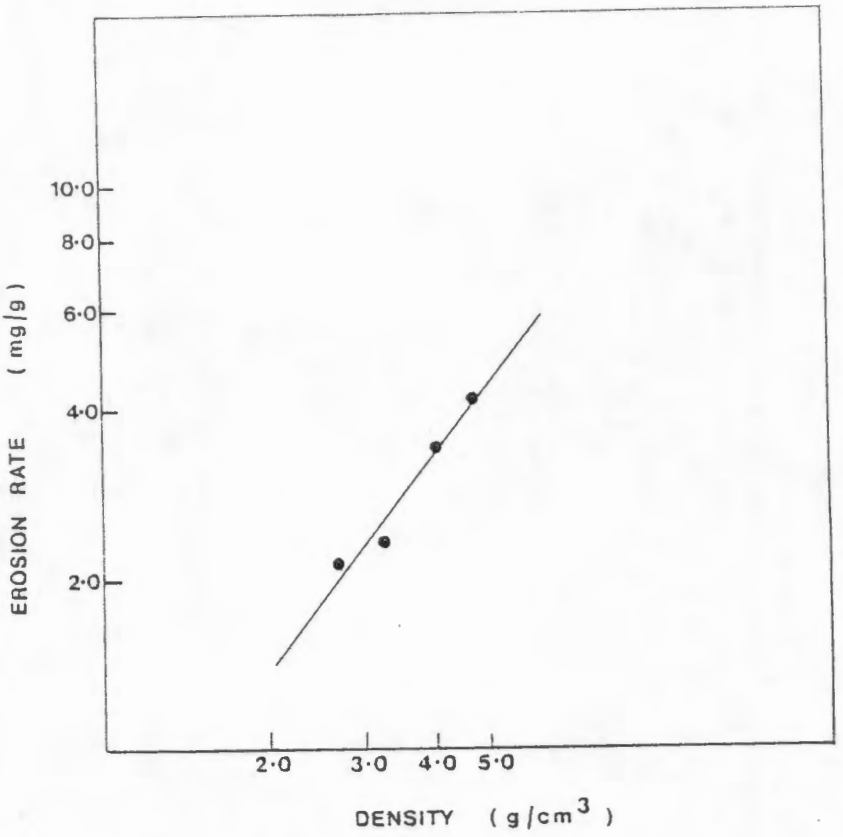

FIGURE 4.11 : Erosion rate (mg/g) at 50 ms^{-1} versus density (g/cm^3). The average particle diameter is 130 μm

The value of the exponent was 1.3 which is in close agreement with the value of 1.20 predicted by Ruff and Wiederhorn's quasi-static model of erosion.

4.3.3 Particle Hardness

Yet another controversy, which was reviewed in Section 2.2.3, regards the influence of particle hardness on erosion rate. In general, an increase in erosion rate with particle hardness is predicted for a given target material. Gulden (1979) has shown that if the same hot-pressed silicon nitride was eroded under identical conditions with quartz particles (Moh's hardness 7.0) and silicon carbide particles (Moh's hardness 9.0), the silicon carbide particles resulted in an erosion rate that was two orders of magnitude greater than that of the quartz, an effect which could be attributed to the fact that quartz is softer than the target material.

The particles used in the present investigation to study the effect of hardness on the erosion rate of the glass targets had Moh's hardness values ranging from 7.0 to 9.0.

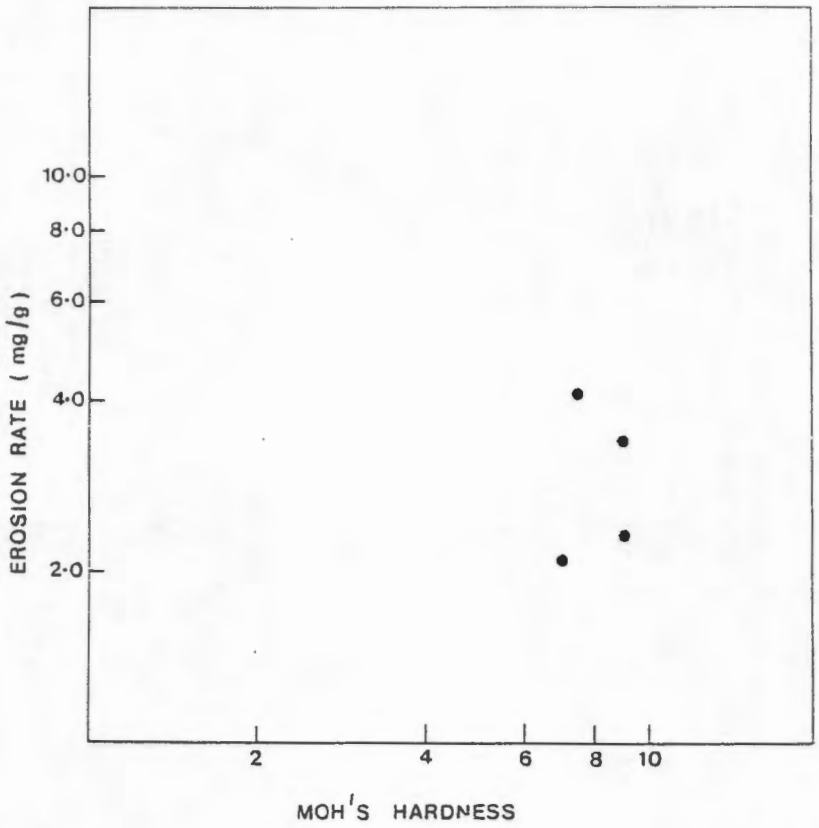

FIGURE 4.12 : The influence of particle hardness on erosion rate (mg/g) at 50 ms^{-1}

The scatter of the data in Figure 4.12 indicates that, for the glass target material, the hardness of the erodent has no influence on erosion rate. It should be noted that all the abrasives are considerably harder than the target.

Similar results to those obtained here and by Gulden (1979) were observed by Dimond et al (1983). When impacting glass targets with silicon carbide and quartz, little difference in erosion rate was noted, whereas when impacting alumina with quartz (softer than the target) and silicon carbide particles (harder than the target), a definite hardness effect was observed, with silicon carbide being the more erosive particle type.

4.3.4 Synergistic Effects

The subject of particle interaction effects has been addressed in three prior studies. The experiments of Marshall et al (1981) and Routbort et al (1980a), discussed in Sections 2.2.2 and 2.2.6 respectively, both employed silicon single crystals as the target material, and demonstrated that erosion rate is dependent upon the particle size distribution of the erodent. Gulden (1980) impacted 50 μm diameter quartz particles against an MgF_2 target surface which had been predamaged by 270 μm quartz particles and obtained a result which was consistent with those obtained by Marshall and Routbort.

Routbort et al (1980a) suggest that the greater erosivity of a mixture of particle sizes could be due to the increased efficiency of the smaller particles in removing material because when the smaller particles strike the target, there is already a pre-existing network of cracks caused by the larger particles.

Since the pulverized fuels consist of a range of particle sizes much wider than those employed in the experiments conducted so far, it was decided to establish whether or not the results of the above-mentioned authors should be taken into account when considering the selection of an abrasive to replace the pulverized fuels.

Several mixtures consisting of different ratios of small (41 μm) quartz particles and large (230 μm) quartz particles were blended together thoroughly in order to ensure homogeneity and impacted against glass slides at a velocity of 38 ms^{-1}. The results are presented in Figure 4.13.

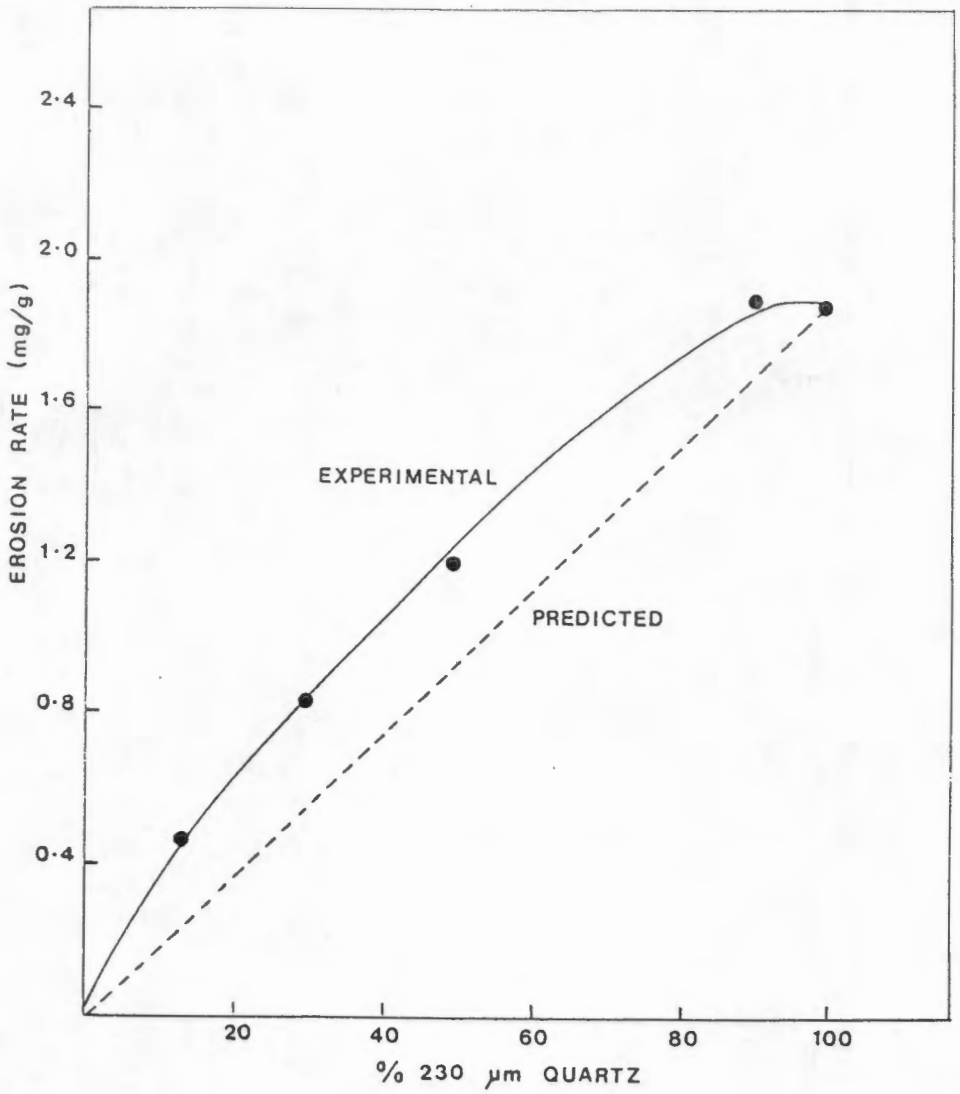

FIGURE 4.13 : Erosion rate (mg/g) versus percentage fraction of 230 μm diameter quartz particles

A range of particle sizes is clearly a more efficient erodent than one particle size and this should be borne in mind when selecting a suitable substitute for the pulverized fuel.

A brief summary of the points which emerged from this study is given below:

(i) All the erodents, irrespective of size, produce surface damage typical of that associated with the impact of "sharp" particles against brittle target surfaces.

(ii) In general the theoretically predicted erosion rates compare favorably with the experimentally obtained erosion rates for angles of incidence as low as 35° when glass is employed as the target material.

(iii) The values of the velocity exponent, n, differ for each particle type and each particle size and values both higher and lower than those theoretically predicted are obtained. A definite velocity exponent - particle size dependence was observed for quartz and silicon carbide, with the small particles having exponent values greater than that predicted by Evans et al and the large particles having exponents near to the exponent value predicted by Ruff and Wiederhorn.

(iv) The particle size exponents of quartz and silicon carbide are in agreement with the value of 3.7 predicted by both erosion models. In general, velocity and angle of incidence do not influence the size exponent.

(v) The particle density exponent is 1.3, which is similar to the value of 1.20 which is found in the quasi-static model of erosion.

(vi) Particle hardness has no effect on the erosion rate of the soft glass target.

(vii) A definite synergistic effect for particle size is observed when a mixture of coarse and fine particles constitute the erodent. The resultant erosion rates deviate positively from the erosion rates predicted by a linear "rule of mixing".

CHAPTER 5 : THE PULVERIZED FUELS

Impact erosion of the right-angled bends of the pneumatic pipelines conveying pulverized fuel is a well-known problem in power station operation. In order to assess the erosion resistance of ceramics, which are gaining acceptance as lining materials to combat the wear, they have to be eroded under conditions that can reliably be related to those prevailing in the pipelines.

Since large quantities of the pulverized coal are required to produce measurable weight losses in an erosion test, it was necessary to find an alternative abrasive for use in the testing. In order to do this, it was necessary first to characterize the pulverized coals and then to compare their erosivity with that of the abrasives which were discussed in Chapter 4.

Four samples of pulverized coal were all received in April 1983 and may be considered as representative of the average monthly coal quality. Additional information regarding the pulverized fuels was supplied by ESCOM and this information (not directly relevant to the present study), as well as the locations of the power stations from which the samples were taken, are reported in Appendix IV.

5.1 THE PULVERIZED FUEL PARTICLES

As was established in Section 4.3.1, particle size is an important parameter affecting the erosion rate of any abrasive material.

The particle size distributions of the pulverized fuels, which had been milled at the power stations to particle diameters of less than 250 μm, are illustrated in Figure 5.1. Since the fraction of particles less than 38 μm in diameter is small, and since the small particles will not contribute significantly to the erosion of the glass targets, it was not necessary to determine the size distribution of this fraction.

The size fractions of the pulverized fuels are also presented in Figure 5.2, in the form of histograms.

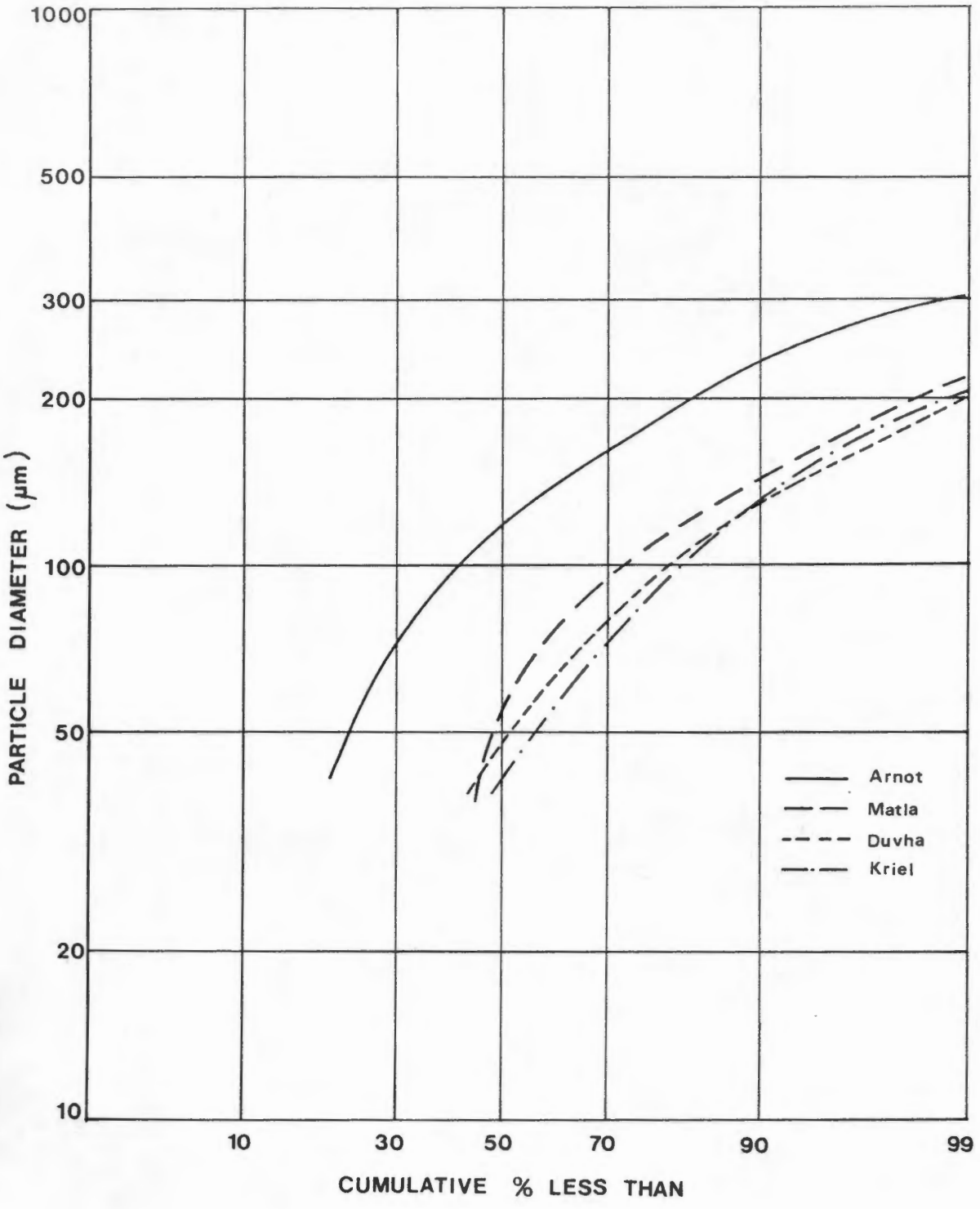

FIGURE 5.1 : Cumulative presentation of the wet screen analyses of the pulverized fuels

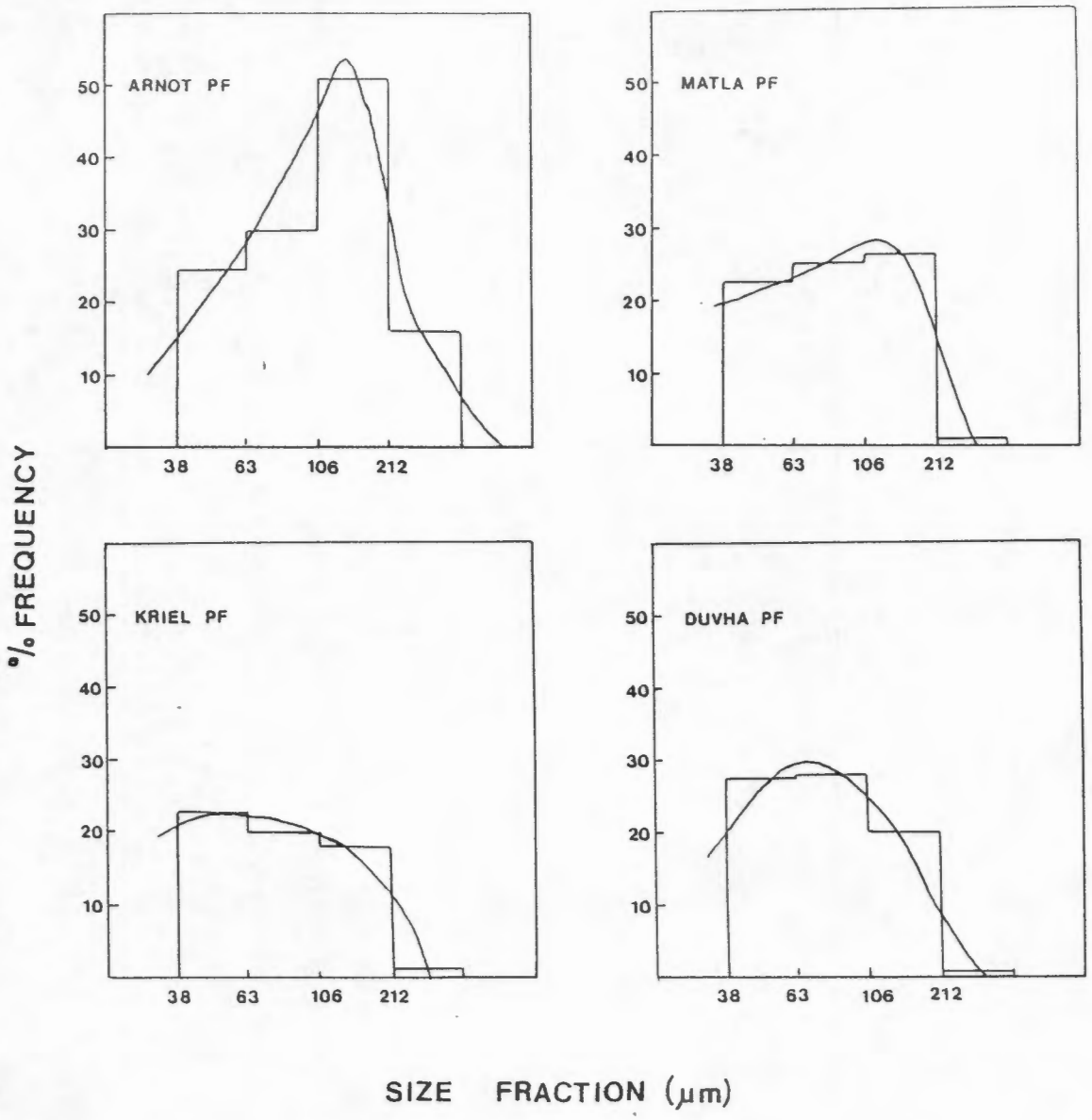

FIGURE 5.2 : Histogram presentation of the wet screen analyses of the pulverized fuels

For the Arnot pulverized fuel, the distribution is quite sharp, with the largest fraction of the particles having diameters lying within the range 106 to 212 μm, whilst for the three other pulverized fuels, the distributions are much broader.

Particle size analysis alone is not an adequate means of predicting the erosivity of the pulverized fuels because the majority of the particles within each screen fraction are coal particles. Since it is the foreign minerals present within a fuel, such as quartz and pyrite, which are responsible for its erosive nature, it is also necessary to determine the mineralogical composition of each fraction.

5.2 MINERALOGICAL ANALYSIS

It is generally accepted that the abrasive properties of a pulverized coal depend mainly on its quartz (Moh's hardness 7.0) and pyrite (Moh's hardness 6 to 7) contents.

Preliminary X-ray diffraction analysis was performed on the samples of coal and it was found that, as with British coals [Raask (1979)], soft, non-abrasive clay minerals (Moh's hardness 2 to 2.5) appear to be the dominant non-organic phase in the South African coals. Quartz was found to be the other main mineral class occurring in the South African coals. Pyrite was only present in trace amounts and was thus expected to contribute very little to the erosivity of these coals.

Quantitative X-ray diffraction analysis, by means of the internal standard method, was performed on the coarse size fractions of each of the pulverized fuels in order to determine the relative quantities of quartz present within each fraction. The fractions, which were prepared by wet screening, were 250 - 212 μm, 212 - 106 μm, 106 - 63 μm and 63 - 38 μm. As discussed in Section 5.1, the particles less than 38 μm in diameter were not considered particularly important and were thus not analysed.

The weight percentages of quartz present in the coal fractions are given in Table 5.1.

TABLE 5.1 : The percentage weight fractions of quartz present in the four size fractions of the pulverized fuels

PULVERIZED FUEL	SIZE FRACTION (μm)	% SIZE FRACTION BY WEIGHT	WEIGHT % QUARTZ IN FRACTION	WEIGHT % QUARTZ IN TOTAL FUEL
Arnot	250 - 212	15.09	3.5	0.5
	212 - 106	51.06	3.7	2.0
	106 - 63	29.29	2.5	0.7
	63 - 38	24.74	4.0	1.1
Matla	250 - 212	1.05	5.5	0.01
	212 - 106	26.71	1.75	1.1
	106 - 63	25.75	1.5	0.3
	63 - 38	22.81	0.75	0.4
Kriel	250 - 212	0.89	2.5	0.02
	212 - 106	18.00	6.25	1.2
	106 - 63	20.03	6.50	1.3
	63 - 38	23.02	4.0	1.2
Duvha	250 - 212	0.44	5.5	0.02
	212 - 106	20.12	1.75	0.4
	106 - 63	28.16	1.5	0.4
	63 - 38	27.61	0.75	0.1

The ditributions of quartz within the pulverized fuels are illustrated in Figure 5.3.

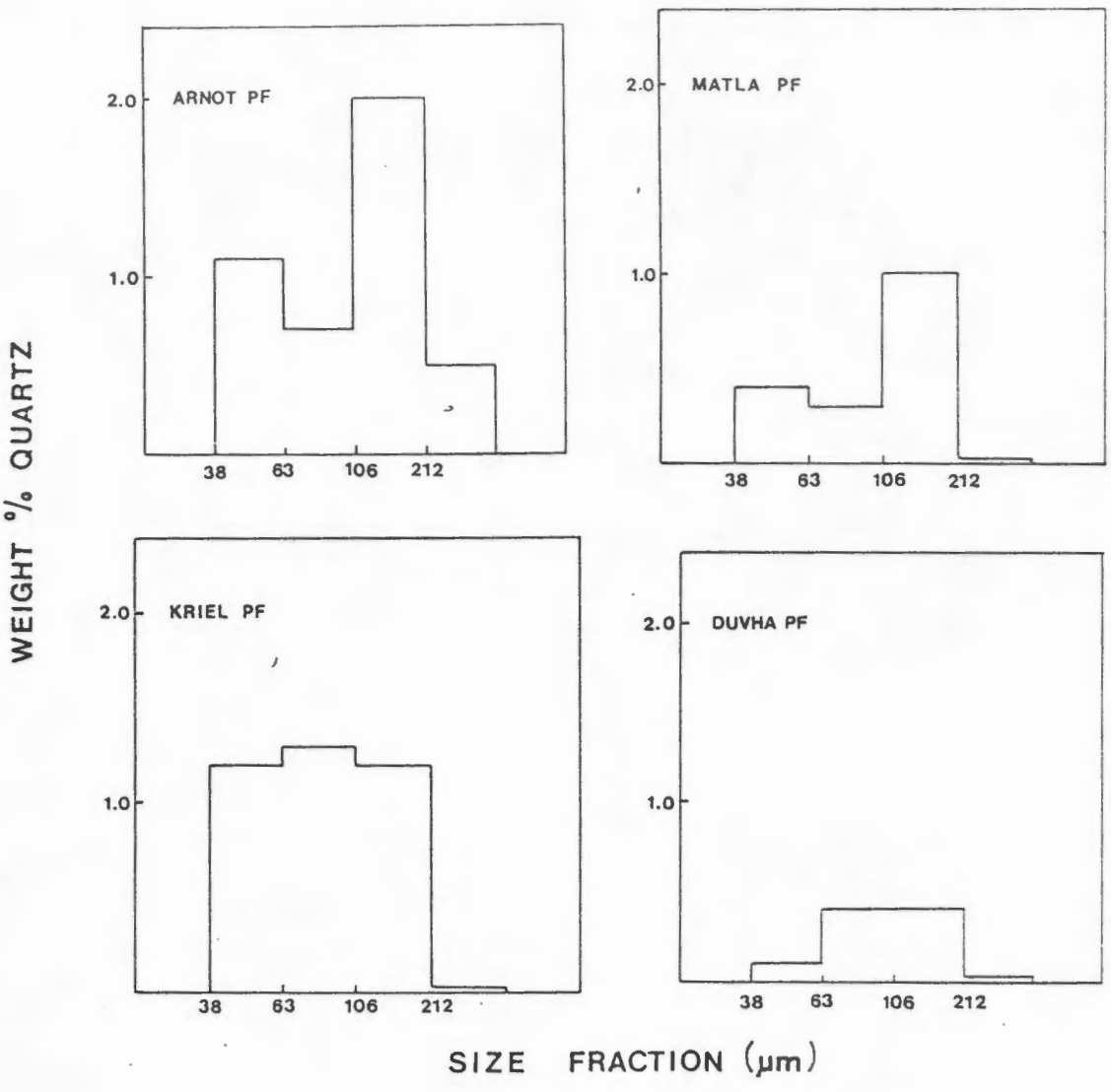

FIGURE 5.3 : The distribution of quartz in the coarse fractions of the pulverized fuels

In terms of particle size distribution and the quartz content of the two largest size fractions (250 - 212 μm and 212 - 106 μm), the four pulverized fuels may be ranked as follows in terms of erosivity: Arnot, Matla, Kriel, Duvha.

Scanning electron micrographs of the pulverized fuels showed that the quartz in the pulverized fuels is present as discrete particles which displayed the same angularity as the laboratory prepared quartz. (See Figure 5.4).

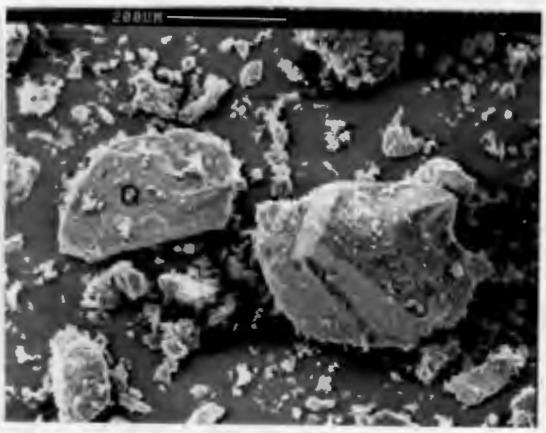

Arnot pulverized fuel

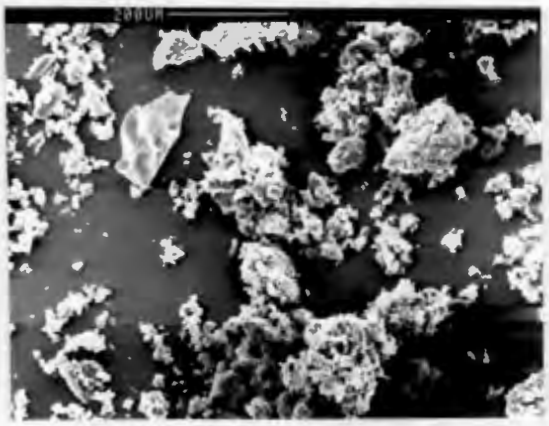

Matla pulverized fuel

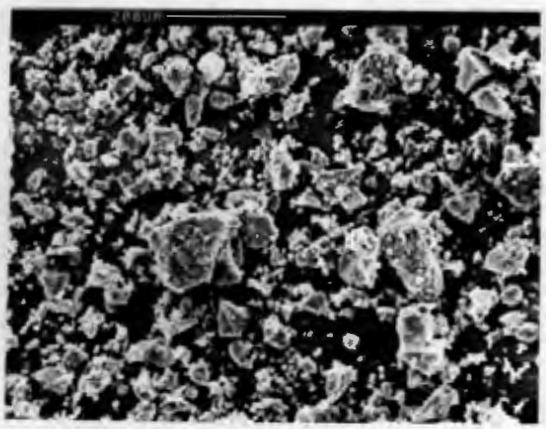

Kriel pulverized fuel

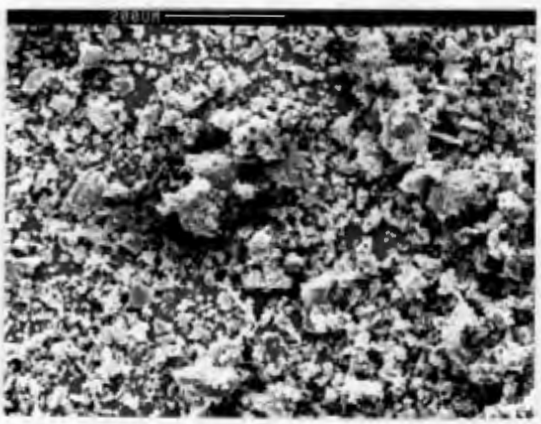

Duvha pulverized fuel

FIGURE 5.4 : Scanning electron micrographs of the four pulverized fuels. Note the quartz particles (Q)

5.3 THE EROSIVITY OF THE PULVERIZED FUELS

The experimental conditions described in Chapter 4 were maintained for the testing of the pulverized fuels, so that comparisons can be made, thus establishing a relationship between the erosive power of the small amount of quartz present in the coals and the 100 per cent pure abrasives.

Tables 5.2 compares the erosivity of the four pulverized fuels with that of the 100 per cent pure abrasives at an intermediate velocity of 35 ms^{-1}, at 50 ms^{-1} and a normal angle of incidence. The values of the velocity exponent, n, are also tabulated.

TABLE 5.2 : The erosion rate (at 35 ms^{-1} and 50 ms^{-1}), the velocity exponent and the constant (A) of the four pulverized fuels and the 100 per cent pure abrasives.

PARTICLE TYPE	VELOCITY EXPONENT (n)	CONSTANT A	EROSION RATE (mg/g) AT 35 ms^{-1}	EROSION RATE (mg/g) AT 50 ms^{-1}
Arnot PF	3.8	4.7×10^{-8}	0.033	0.12
Duvha PF	3.5	3.7×10^{-8}	0.012	0.039
Matla PF	3.7	1.3×10^{-8}	0.0072	0.0227
Kriel PF	3.9	6.0×10^{-9}	0.0070	0.0220
230 μm Quartz	2.6	4.8×10^{-5}	1.45	4.00
115 μm Quartz	3.2	8.0×10^{-6}	0.70	2.50
41 μm Quartz	3.7	4.0×10^{-7}	0.26	0.94
115 μm Silicon carbide	2.3	2.3×10^{-4}	0.90	2.00
51 μm Silicon carbide	2.6	5.6×10^{-5}	0.39	0.96
36 μm Silicon carbide	3.8	1.0×10^{-8}	0.13	0.65
120 μm Alumina	2.6	4.6×10^{-5}	1.30	3.40
130 μm Zircon	3.3	1.8×10^{-5}	1.30	4.0

Contrary to the predicted order of erosivity of the pulverized fuels, Duvha pulverized fuel, which, according to the screen analysis has a relatively low weight percentage of large particles, and the least amount of quartz in the coarsest fractions, is more erosive than either the Matla and Kriel pulverized fuels. By comparing the erosivity of the four pulverized fuels at an intermediate velocity of 35 ms^{-1}, they may be ranked as follows in order of decreasing erosivity : Arnot, Duvha, Matla, Kriel.

From Table 5.2, it can be seen that Arnot pulverized fuel is five times as erosive as Kriel pulverized fuel and the erosivity of the Duvha pulverized fuel is double that of Kriel. The ranking order described above remains fixed for all the velocities likely to be encountered in normal in-service situations.

In order to select a suitable substitute for the pulverized fuels, the influence of the impact parameters on the erosion rates of the fuels must be considered and compared with that of the alternative abrasives.

The impact parameters, such as the effect of angle on erosion rate was found to be the same for the pulverized fuels as for the abrasives, with the maximum erosion rate taking place at an angle of 90°. (See Figure 5.5).

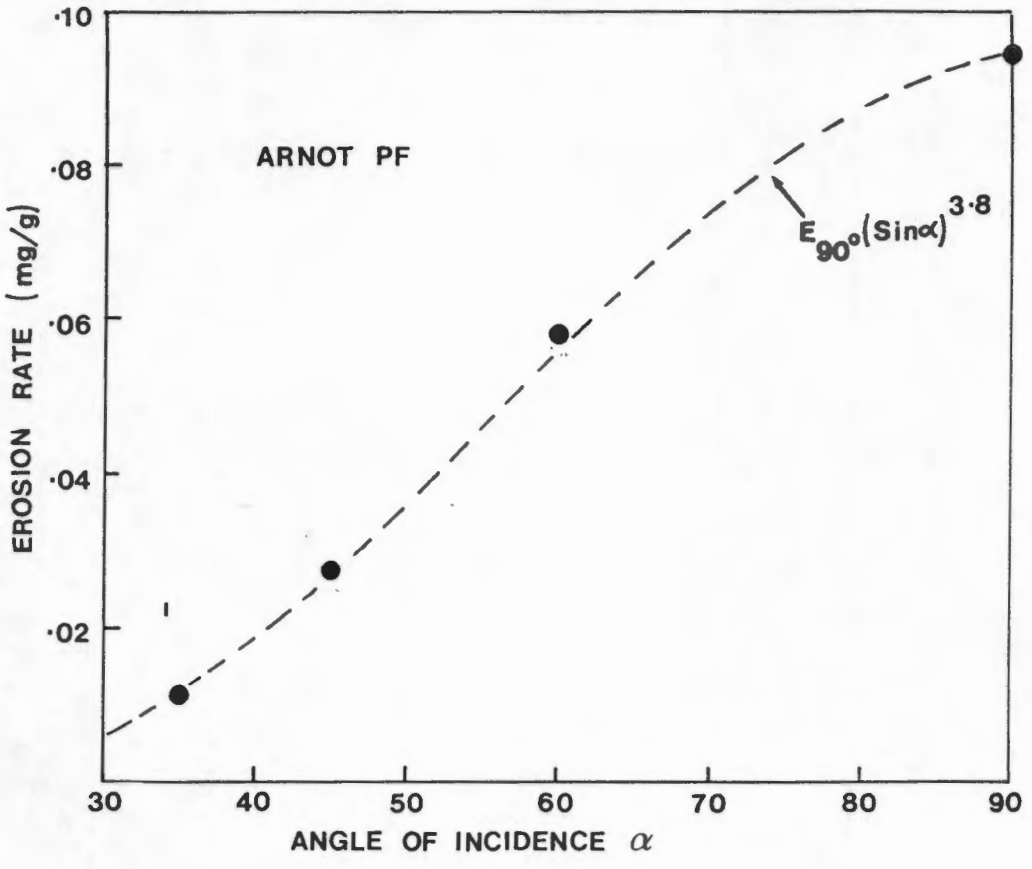

FIGURE 5.5 : The effect of angle on the erosion rate of Arnot pulverized fuel

It was established in Section 4.2.2 that the velocity exponent is dependent upon the particle size of the abrasive. In order to compare the dependence of the velocity exponent on the particle size of the pulverized fuels with those of the 100 per cent pure abrasive, the velocity exponents and the nominal particle sizes (the peaks in the size distributions are shown in Figure 5.2) of the pulverized fuels are shown in Figure 5.6.

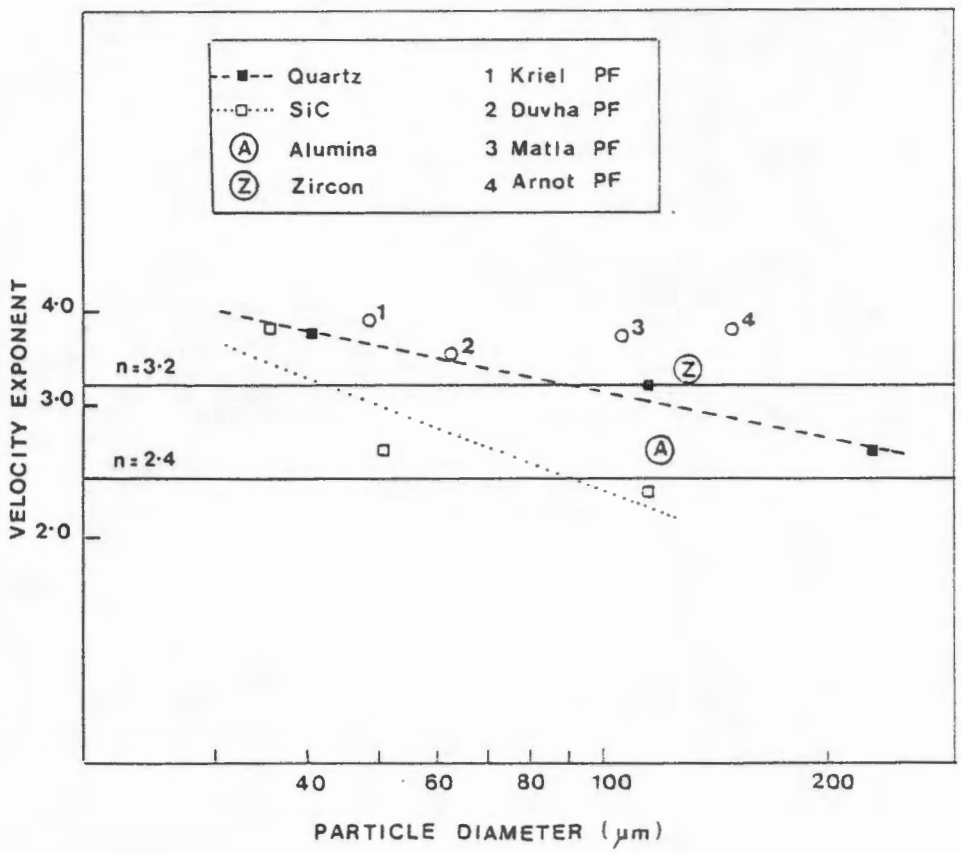

FIGURE 5.6 : The relationship between the velocity exponents and the nominal particle sizes of the pulverized fuels

It is apparent that the velocity exponent-particle size dependences of the Matla and Arnot pulverized fuels most closely resemble those of the 115 μm diameter quartz and the 130 μm zircon, whilst Kriel and Duvha

pulverized fuel most closely resemble those of the 41 μm diameter quartz and the 36 μm diameter silicon carbide. Accordingly, the suitability of these abrasives as the replacements for the pulverized fuels should be considered.

Since the morphology of zircon particles is appreciably different from that of the erosive quartz particles present in the pulverized fuels, this abrasive was eliminated from further consideration, leaving the quartz and silicon carbide.

The silicon carbide particles have both a higher density and a greater hardness than the quartz particles present in the pulverized fuels. Since increased density only has the effect of increasing erosion rate (see Section 4.3.2), silicon carbide may still be considered a suitable substitute for the pulverized fuels. Increased hardness was not found to have any effect on the erosion rate of the glass targets (see Section 4.3.3). However, Dimond et al (1983) implied that hardness only becomes important if the target has a hardness more comparable to that of the particles. This condition could not be verified in this study.

An important question still remained, and that was why the order of erosivity of the pulverized fuels did not follow the same trend as predicted when considering particle size and quartz content. It was evident that this discrepancy warranted further study, and before an alternative abrasive could be recommended with confidence, it would be necessary to study and compare the character of the damage of the pulverized fuels and the pure erodents.

CHAPTER 6 : SINGLE PARTICLE IMPACT DAMAGE

In Section 4.2.1, it was established that the damage produced by all the abrasives, including the pulverized coals, can be described as elastic-plastic. Figure 6.1 summarizes the crack types commonly observed for this damage process.

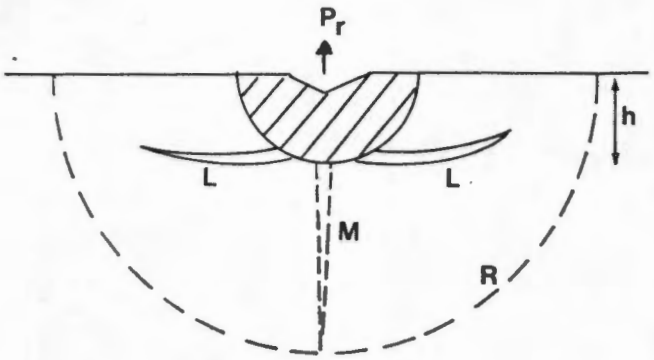

FIGURE 6.1 : The lateral crack system. The residual load, Pr, which is exerted by the radially expanded plastic zone determines the crack driving force. The shaded area represents the deformation zone. L = lateral cracks. M and R = the median and radial crack systems, respectively [From Marshall et al (1982)].

Lateral cracking initiates near the base of the deformation zone, spreads out on planes nearly parallel to the specimen surface and eventually intersects the surface. The volume of material lost will depend upon the depth (h) of the plastically deformed region and the length (L) of the fully developed lateral crack. The erosion models (Section 2.5) assume that the potential volume (V_i) of material removed per particle impact will be $V_i = \pi L^2 h$. The models also assume that the total volume of material removed as a result of particle impacts involves a simple summation of the single particle impact events.

In this Chapter, the results of an investigation to determine the actual volume of material removed per impact as a result of single particle impacts (by means of measuring the single impact events) are presented. The reasons as to why the erosion rates of the four pulverized fuels (see Section 5.3) did not correlate directly with their bulk mineralogical compositions (Section 5.2) and particle size distributions (Section 5.1) are also discussed.

6.1 METHOD OF APPROACH

The simplest way of estimating the amount of material removed per particle impact was to measure the sizes of single particle impact events. Accordingly, the forming of damage craters as discrete entities on the impacted area of the target would facilitate this measuremnt. In order to achieve discrete craters, small amounts (see Table 3.3) of the impacting particles were fed into the airstream at a very slow rate ($\ll 0.001$ g/cm^{2}s), thus minimizing possible particle interactions in the gas steam or on the target surface. The particles struck the glass targets at a velocity of 35 ms^{-1} and a normal angle of incidence. Eight to nine different areas of the central impacted zone were photographed, the magnification used depending upon the dimensions of the damage sites. The semi-automatic image analysis system, mentioned in Section 3.2 and discussed in detail by Frith and Heckroodt (1984), was employed in measuring the dimensions of the damage sites or craters. The total area damaged by the particles was equal to 86.59 mm^2. This value was determined by measuring the area eroded under conditions of multiple particle impact.

In order to compare the amounts of material removed from the target surface by each particle type, the results were normalized as follows:

$$\frac{1}{x} \cdot \frac{86.59}{y} = CF$$

where x = the actual weight of abrasive particles used
y = the damage area actually measured
CF = a correction factor, which is the number of impacts which would have been counted had the entire eroded area been measured and if 1g of particles were used.

The number of particles present in 1 g of material was calculated by using the average particle diameters listed in Table 4.1 and in addition, assuming that each particle was spherical in shape. It was also assumed that every particle striking the target surface created a damage site which resulted in a certain volume of material being removed and that there were no particle interactions.

The maximum diameter (2L') of each crater was estimated (see Figure 6.2) since this would give an indication of the maximum amount of material which could be removed by each impact. The maximum measured diameters (2 L') of all the measurable craters were assigned to classes using a logarithmic scale. The volume (V_i) of material removed per particle impact was assummed to be conical ($V_i = {}^1/_3 \pi L^2 h$) as opposed to cylindrical ($V_i = \pi L^2 h$). Furthermore, it was assumed that the ratio of h (the depth to which lateral cracking occurs) to the radius of the crater (L) remained constant for each particle type and for each particle size, in other words that the ratio h/L was a constant, f. Thus, the volume (V_i) of material removed per particle impact could be expressed as ${}^1/_3 \; f L^3$.

If all the craters are measured and then all the volumes associated with the craters summed, the erosivity of a particle type can be ascertained.

6.2 RESULTS AND DISCUSSION

A typical example of the resultant impact damage is illustrated in Figure 6.2. Note that the damage sites are generally non-interacting.

The percentage frequency distributions of the numbers and volumes are presented in the form of histograms, an example of which is given in Figure 6.3. (Histograms similar to those depicted in Figure 6.3 are presented in Appendix V for the other abrasives).

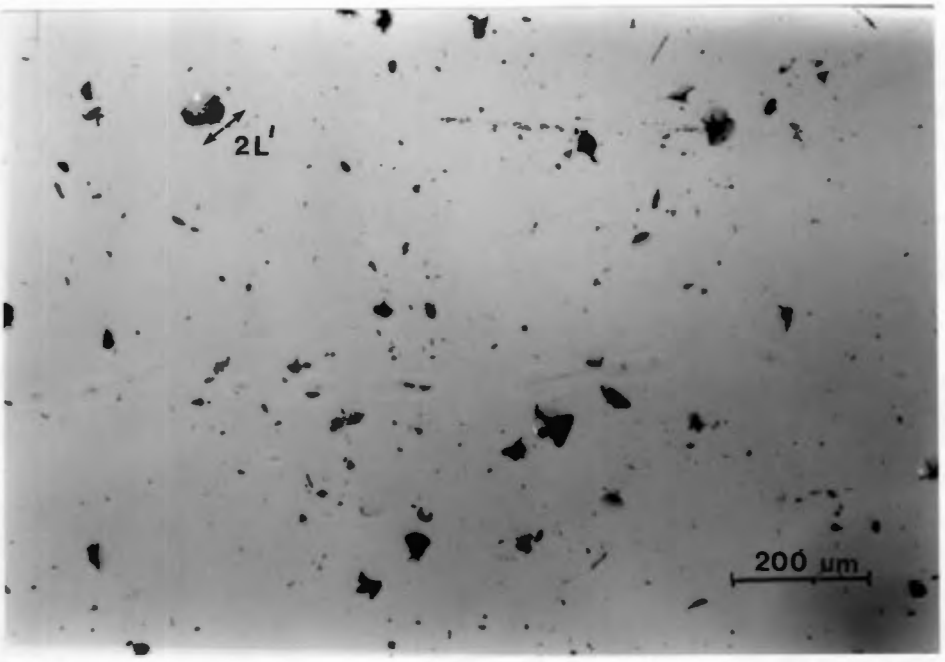

FIGURE 6.2 : An example of the impact damage produced in glass when impacted with 230 µm diamter quartz particles. An example of the damage diameter (2 L') measured, is illustrated by the arrows

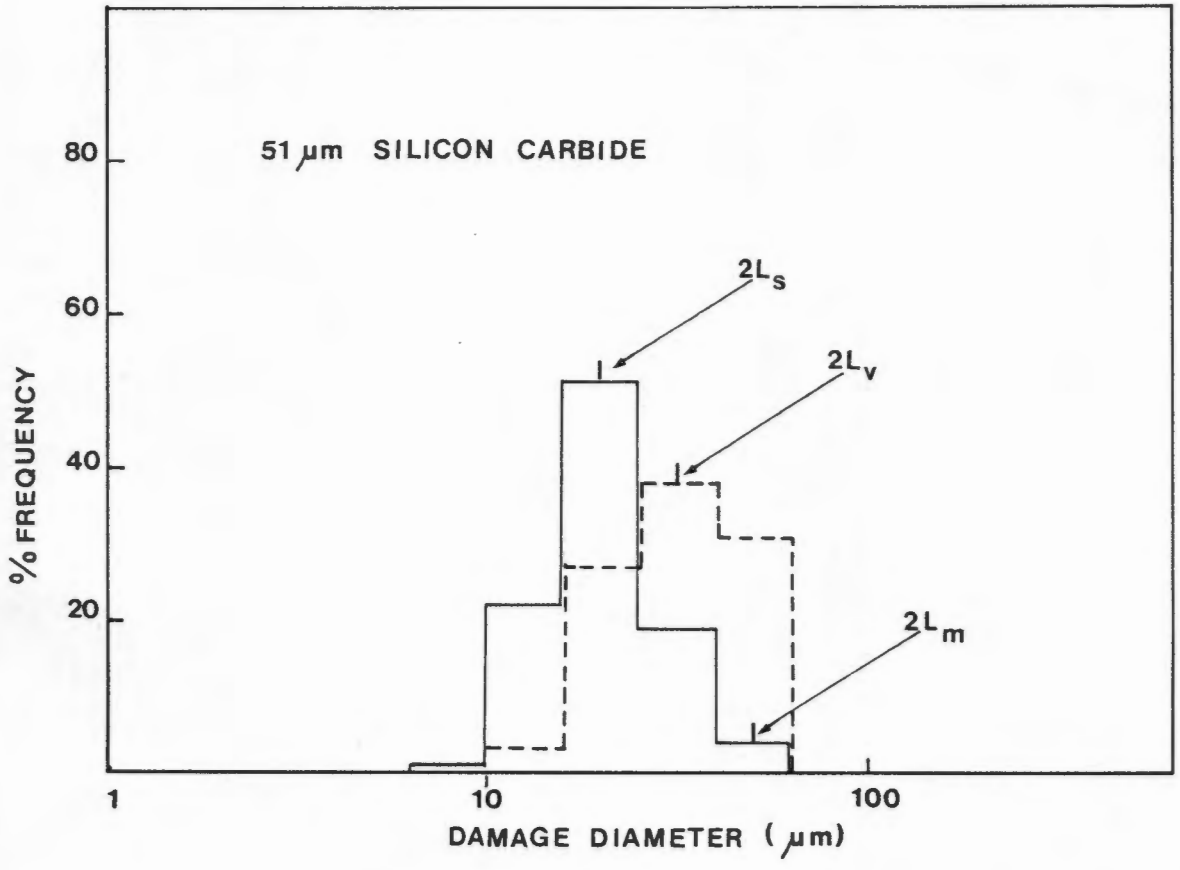

FIGURE 6.3 : The solid line represents the frequency with which damage craters of a certain magnitude occur when glass is impacted with 51 µm diameter silicon carbide particles. The dashed line represents the volumes of material removed.

There is a cut-off point in the measurement of the craters. For example, with the 51 μm diamter silicon carbide, craters with diameters of less than 10 μm could not be reliably measured due to the magnification employed. This means that the frequency with which the small craters occurred would be underestimated.

As is evidenced by the histogram (Figure 6.3) and by the photograph (Figure 6.2), there is a wide variation in the magnitude of the single impact craters. Similarly, since the volume of material removed is equal to L^3, this same variation exists as far as volumes are concerned. A demonstration of the wide range of crater sizes produced by a relatively small range of particle sizes, is obtained when, for example, the 230 μm diameter quartz and the 115 μm diameter quartz are considered. The particles within these size fractions range from 212 to 250 μm (range 38 μm, size ratio 1 to 1.2) and 106 to 125 μm (range 19 μm, size ratio 1 to 1.2) respectively, but the range of measurable crater sizes produced by these particles is much larger: The 230 μm average diameter quartz produced measurable craters ranging in size from 12.6 to 199.45 μm (range 187 μm, size ratio 1 to 16)) and the 115 μm average diameter quartz particles produced craters ranging in measurable size from 12.6 to 126 μm (range 113 μm, size ratio 1 to 10). These ranges of crater sizes become even larger when considering the fact that the small craters could not be measured experimentally.

Gulden's (1980) results also demonstrated this variation in the size of the impact craters and she suggested that this variation was probably a function of particle orientation rather than a function of a target property such as strength, which is unlikely to vary to such an extent. In this study, the majority of the impacting particles are irregular in shape and they may strike the target with a sharp corner, a flat face or a rounded edge. Thus, although the velocity remains the same, the energy transferred per unit area and the extent of damage would vary considerably. In addition, the particle masses are different, with the result that the impact energies will be different. For example, the 51 μm average diameter silicon carbide particles have particles ranging in size from 33 μm to 74 μm (a ratio of 1 to 2.2) and thus a mass range of 6.05×10^{-8}g to 6.80×10^{-7}g (a ratio of 1 to 11.2).

Three of the important crater dimension parameters are the diameter of damage occurring most frequently ($2L_s$), the diameter of damage resulting in the maximum amount of material removal ($2L_v$) and the average diameter of the class containing the largest craters ($2L_m$). The method of obtaining these values is illustrated in Figure 6.3.

The information obtained from Figure 6.3 and the illustrations presented in Appendix V may be summarized as follows:

TABLE 6.1 : Summary of information obtained from the histograms

PARTICLE TYPE	AVERAGE PARTICLE DIAMETER (μm)	DIAMETER OF CRATERS OCCURRING MOST FREQUENTLY ($2L_s$) (μm)	DIAMETER OF CRATERS PRODUCING MAXIMUM VOLUME LOSS ($2L_v$) (μm)	MAXIMUM CRATER DIAMETER PRODUCED ($2L_m$) (μm)
Quartz	230	31	126	200
Quartz	115	19	79	126
Quartz	41	8	15	31
Silicon carbide	115	31	79	126
Silicon carbide	51	19	31	50
Silicon carbide	36	5	12	19
Alumina	120	31	100	126
Zircon	130	31	126	200
Arnot PF	150*	31	79	200
Duvha PF	63*	19	79	126
Matla PF	106*	19	126	126
Kriel PF	49*	19	79	126

* - Nominal values obtained from Figure 5.2

The three damage parameters tabulated above were plotted against average impacting particle diameter, and the relationships are depicted in Figure 6.4.

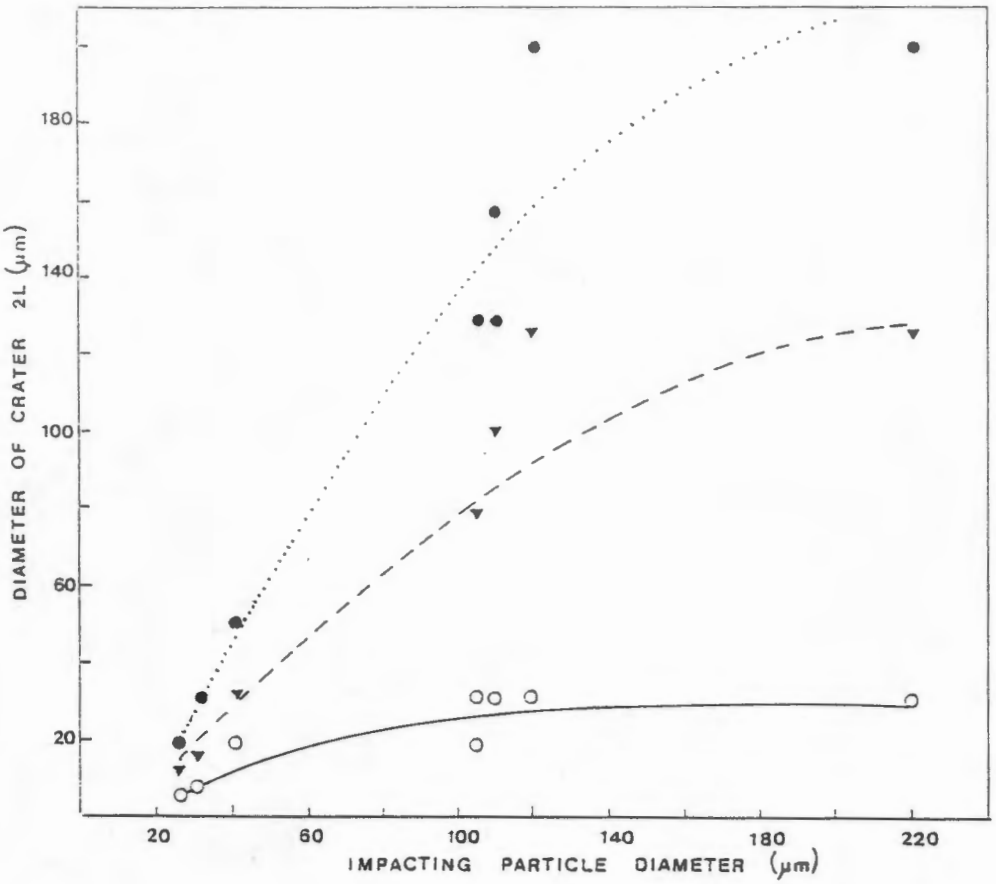

FIGURE 6.4 : The relationships between average impacting particle diameter and $2L_s$ (solid line), $2L_v$ (dashed line) and $2L_m$ (dotted line)

From the data available, there appears to be a levelling-out of the curves as the impacting particle diameter increases. The levelling-out is most marked for the curve of $2L_s$ versus particle diameter. One of the possibilities as to why such a levelling-out should occur may be related to particle fragmentation effects. As previously mentioned (see Section 4.2.2(a)) large particles are more prone to shattering upon impact with the target surface than are small particles, leaving less energy available for the propagation of lateral cracks. Thus, when impacting particles are greater than about 100 μm in diameter, the average lateral crack sizes which they produce become more or less the same. However, the non-linear trends which are suggested by Figure 6.4 should be treated with caution since it may well be that, with a greater number of data

points, a different or more definite relationship between the three aspects of damage size and average particle diameter may emerge.

By plotting the same data that was assembled in order to plot Figure 6.3, cumulatively (from largest to smallest crater), further information may be obtained. Although the discussion which follows again relates to a specific example - 51 μm diameter silicon carbide - it is true of all the abrasives.

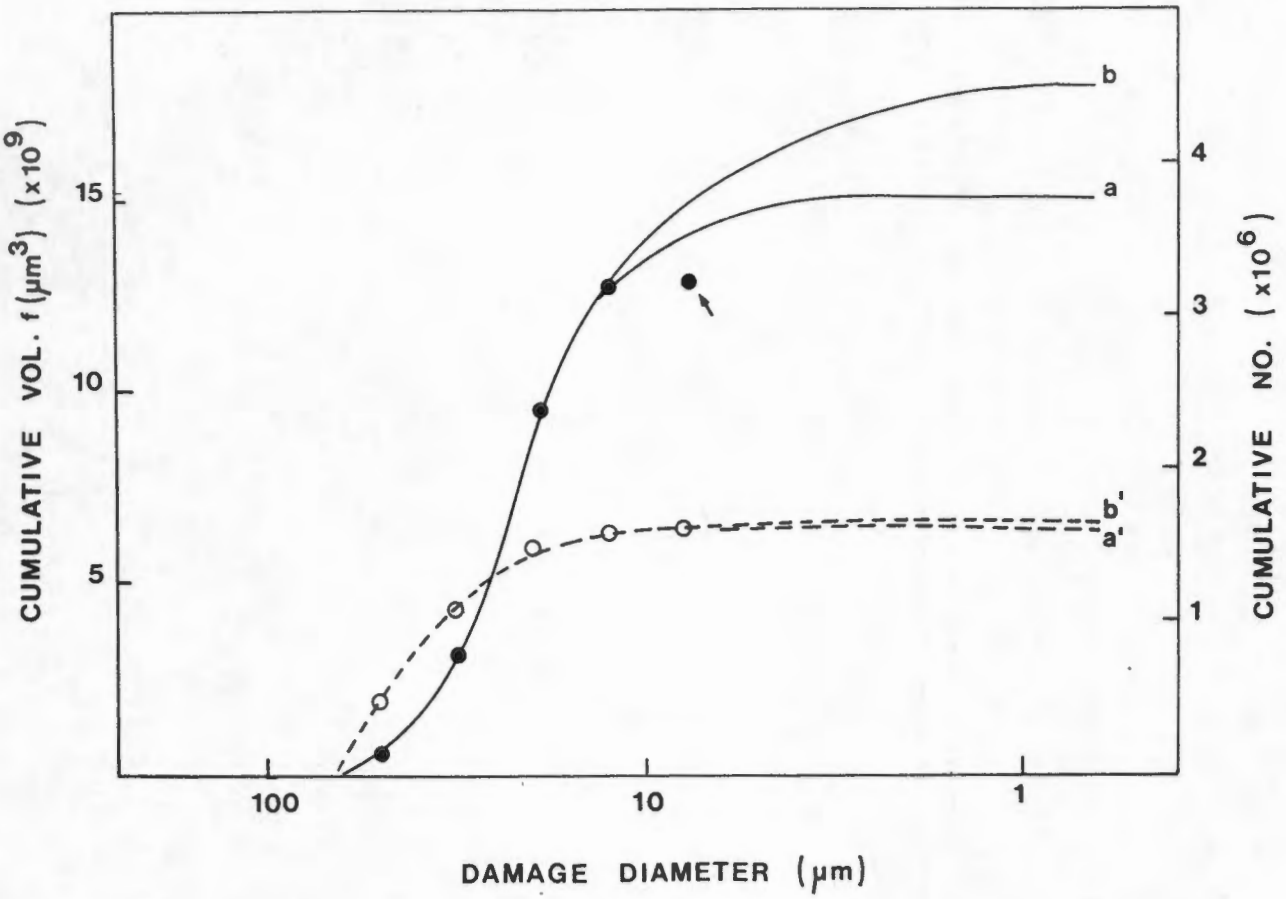

FIGURE 6.5 : Cumulative number (solid lines) and cumulative volume of material removed (dashed lines) versus damage diameter for 51 μm diameter silicon carbide.

Attention is drawn to the fact that the last point (indicated by an arrow in Figure 6.5 above) is not very reliable, which is the result of not necessarily measuring all the small craters in that size class, as was pointed out when discussing Figure 6.3.

Since the smallest craters could not be measured, the total number of craters (and hence the number of particles present in 1g of abrasive

material if assuming that every particle creates a crater) could not be determined from the recorded number of craters alone. However, the total number of craters, even down to the most minute crater, may be estimated in one of two ways:

(i) By graphical extrapolation (ignoring the last point) in which case, for the 51 μm diameter silicon carbide, the total number of craters is estimated to be 3.75×10^6 ('a' in Figure 6.5).

(ii) By calculation, using 51 μm as the average particle diameter. In this instance, the total number of particles, and thus craters, equals 4.50×10^6 ('b' in Figure 6.5).

The graphically determined number of particles (or craters) in most cases corresponds reasonably well with the calculated numbers. The total cumulative volume of material that is removed as a result of particle impact is thus $f(6.24 \times 10^9)$ μm^3 when considering the graphically determined total number of craters and $f(6.26 \times 10^9)$ μm^3 when considering the calculated total number of craters. The difference between the two values is less than a half per cent, and it is thus evident that the contribution by the craters less than 10 μm in diameter (in the case of 51 μm diameter silicon carbide) is immaterial to the total volume of material removed, although their numbers are large - 0.55×10^6 and 1.30×10^6 respectively.

A consideration of the abovementioned data and of Figure 6.5 shows that a very good estimate of the total volume of material that is removed, may be obtained from the craters with measurable dimensions, alone. There is, in fact, no need at all to determine the total number of particles (or craters) in order to estimate the total volume of material that is removed.

The importance of the large craters as contributors to the total volume of material removed, is clearly illustrated in Figure 6.6, where yet again, the 51 μm diameter silicon carbide is taken as a typical example of what is true of all the abrasive media. Based on the graphically extrapolated value for the total number of crater sites, about 10 per cent of the sites (all of which can be measured with ease), are responsible for the removal of 50 per cent of the total volume of material and about 45 percent of the craters are responsible for the removal of 80 per cent of the target material. Another crater dimension which is important, is h, the depth to which lateral cracking occurs. The average value of h can be obtained by comparing the calculated value of volume of target material removed and the actual experimentally determined mass loss (see Section 6.1). Table 6.2 lists the values of h for all the abrasive media.

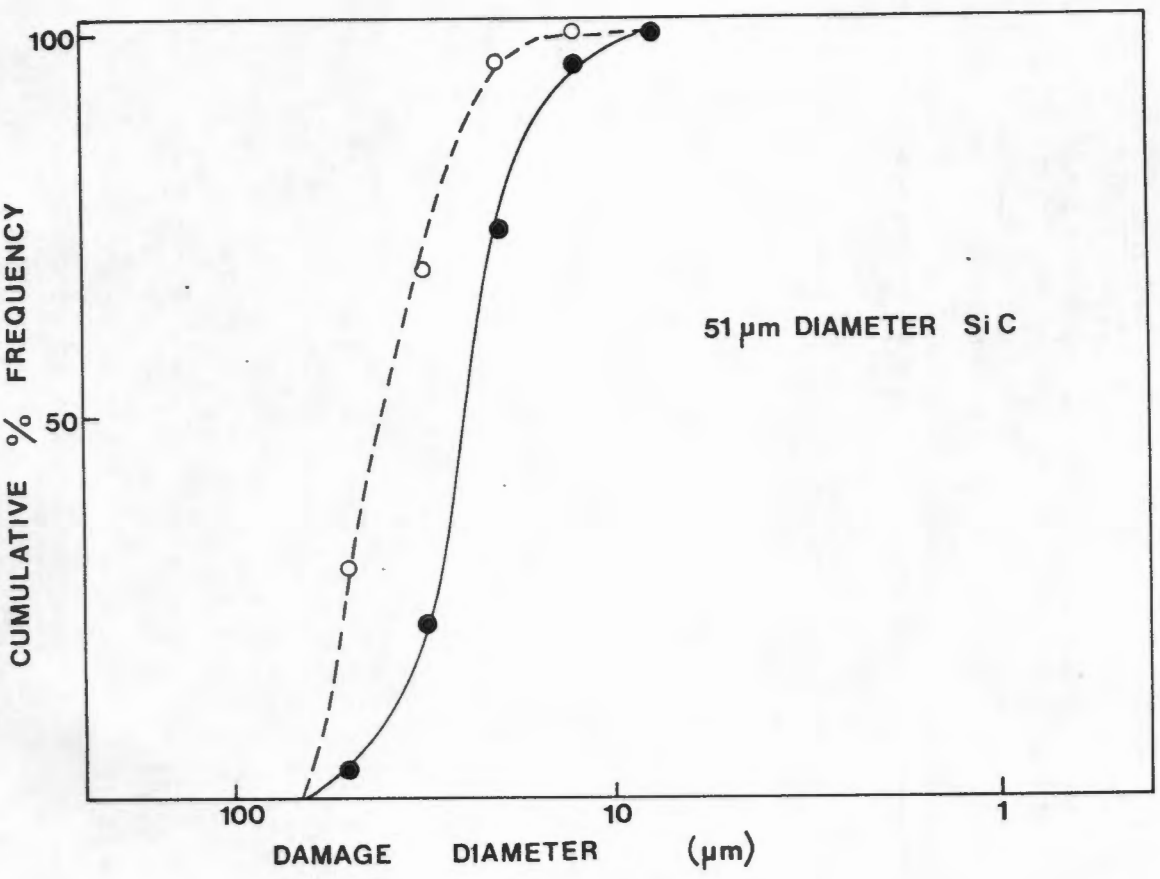

FIGURE 6.6 : Cumulative percentage frequency of number of impact sites (solid line) and volume of material removed (dashed line).

TABLE 6.2 : The total cumulative volume of material removed $f(\mu m)^3$, the erosion rate (mg/g), L_s, h and the ratio $h/2L_s$.

PARTICLE TYPE	TOTAL CUMULATIVE VOLUME OF MATERIAL REMOVED $f(\mu m^3)$	EROSION RATE (mg/g) AT 35 ms^{-1}	L_s (μm)	h (μm)	$h/2L_s$
230 μm Quartz	8.0×10^9	1.45	15.5	11.3	0.36
115 μm Quartz	7.6×10^9	0.70	9.5	6.2	0.33
41 μm Quartz	2.6×10^9	0.26	4	0.1	0.0125
115 μm Silicon carbide	8.4×10^9	0.90	15.5	3.6	0.116
51 μm Silicon carbide	6.6×10^9	0.39	9.5	0.36	0.0189
36 μm Silicon carbide	2.6×10^9	0.13	2.5	0.15	0.03
120 μm Alumina	19×10^9	1.30	15.5	7.2	0.23
130 μm Zircon	8.0×10^9	1.30	15.5	10.7	0.34
Arnot PF	8.2×10^7	0.033	15.5	13.5	0.43
Duvha PF	3.3×10^7	0.012	9.5	9.0	0.47
Matla PF	2.8×10^7	0.0072	9.5	6.2	0.33
Kriel PF	2.3×10^7	0.0070	9.5	5.7	0.30

The values of the total cumulative volume of material removed (determined by measurement of the crater dimension L_s) and the erosion rates determined experimentally for all the particle types are in good agreement, as can be seen from the table above.

It is also evident that, as the particle diameter increases, not only does the depth to which lateral cracking occurs increase, but the ratio $h/2L_s$ also increases. It is interesting to note that the ratios of $h/2L$ for quartz and silicon carbide, calculated from the data reported by Evans et al (1978) are in agreement with the values obtained in this study, despite the fact that they used harder target materials (MgO, MgF_2 and Si_2N_4) and higher velocities (89 - 190 ms^{-1}) than those employed in this investigation. The assumption (made in Section 6.1) that the ratio $h/2L_s$ remains constant for all particle types and sizes is clearly not true. In Figure 6.7 the ratio $h/2L_s$ is plotted as a function of impacting particle diameter and a trend, which may turn out to be linear with the accumulation of more data points, is observed.
There was no correlation between the ratio $h/2L_s$ and the lateral crack length, L_s.

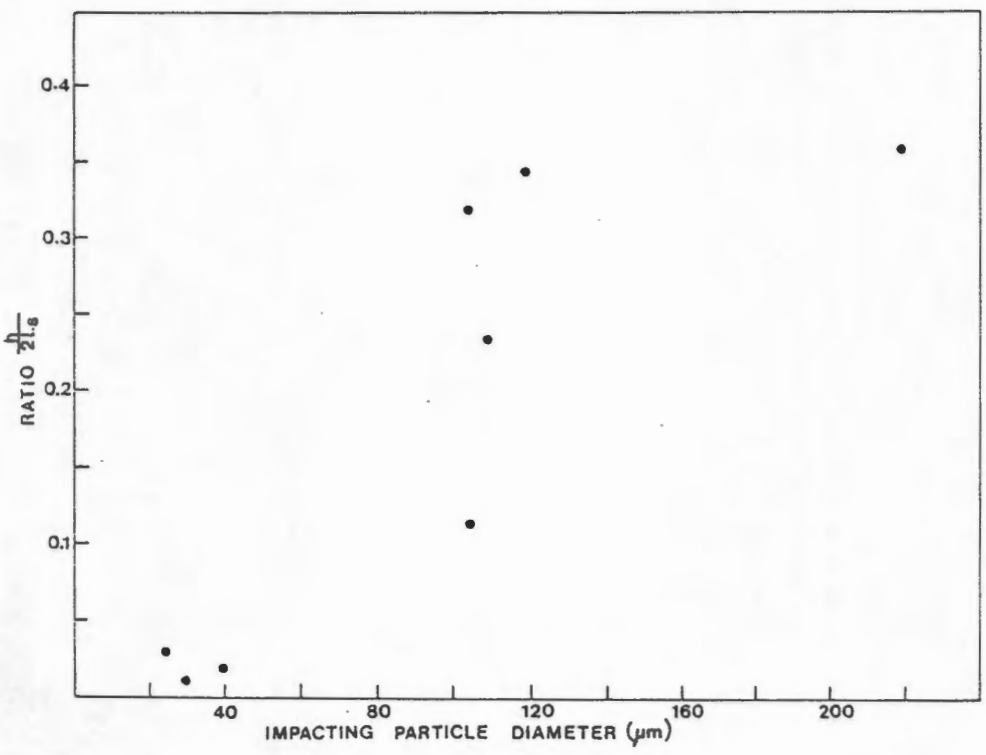

FIGURE 6.7 : The relationship between the ratio $h/2L_s$ and the impacting particle diameter

Three important points emerged as a result of this study.

(i) For any one given particle type, although the range of particle sizes existing within the fraction may be small, the range of crater sizes which the abrasive produces is very large. This effect is probably primarily due to particle orientation effects, i.e. particles may strike the target surface in any orientation - sometimes with a sharp point, sometimes with a flat side.

(ii) The larger crater sites produced by a given abrasive are very important since they are responsible for the removal of most of the target material. Thus, for any given particle size, only a small fraction of those particles produce the bulk of target material removal. It also follows that small particles, even though they may constitute the bulk of the erodent, are irrelevant as contributors to the total volume of material that is removed.

(iii) Finally, the ratio of the depth to which lateral cracking occurs and the radius of the crater does not remain constant, but alters according to the diameter of the particle, with larger particles resulting in craters with higher ratios, that is, steeper craters.

The discrepancies which exist between the erosivity of the pulverized fuels (as predicted in terms of particle size distribution and quartz content) and the actual erosivity of the fuels, can be explained by the results of this study. As has been discussed in this Chapter, it is only a fraction of the particles within a size range which produce larger crater sizes and which remove the majority of the material.

Similarly for the pulverized fuels, it is only a small fraction of the quartz particles present within a screen fraction that is responsible for the majority of the material removal. This clearly illustrates that screen analysis and X-ray diffraction analysis alone are not a sufficiently sensitive means of predicting erosivity, and the actual damage created by the particles must be examined.

By comparison of the actual impact damage, particularly the range of crater parameters L_s, L_v, L_m and h, of the pulverized fuels and of the pure abrasives, suitable replacements for the pulverized fuels for use in accelerated testing could be the 230 μm diameter quartz, 115 μm diameter quartz, 115 μm diameter silicon carbide, 120 μm diameter alumina and 130 μm diameter zircon. However, as discussed in Chapter 5, the influence of particle parameters should also be taken into consideration and with this in mind, the 230 μm diameter quartz, 115 μm diameter silicon carbide and 120 μm diameter alumina should be rejected since their velocity exponents are too low. Zircon was already eliminated from consideration in Chapter 5 as a result of its particle shape, and the 41 μm diameter quartz and 36 μm diameter silicon carbide, which, in terms of particle parameters appear suitable as replacements for the pulverized fuels, are found to be unsuited on examination of the damage produced - the crater sizes were very much smaller than those resulting from pulverized fuel impact.

As a result of this research, the 115 μm diameter quartz was selected as the most suitable replacement, since both the character of the impact damage and its velocity exponent of 3.2 are very similar to that of these pulverized fuels. Although the synergistic effects discussed in Section 4.3.4 could play a role, the increase in erosion rate which a mixture of quartz size ranges would produce is not very great, and the character of the damage produced by the 115 μm diameter quartz alone represents that of the pulverized fuels well. As far as the Arnot pulverized fuel is concerned , the 230 μm diameter quartz would have been the most suitable replacement, in terms of damage parameters, but its velocity exponent is too low ($n = 2.6$), as opposed to that of Arnot pulverized fuel ($n = 3.8$). A compromise must thus be made, and for simplicity's sake, the 115 μm diameter quartz was again selected.

The selection of 115 μm diameter quartz as the replacement also conveniently eliminates such particle parameter effects as hardness which would have to be corrected for, if the candidate materials were to be eroded by a harder abrasive. In addition, quartz is particularly well-suited as a replacement since it is the major erosive constituent occurring naturally in the pulverized fuels. The 115 μm diameter quartz produces erosion rates which are factors of 21, 58, 97 and 100 times greater than those of Arnot, Duvha, Matla and Kriel pulverized fuel, respectively, at 35 ms^{-1}.

CHAPTER 7 : CONCLUSIONS

A simple particle-gas stream erosion apparatus was employed in the characterization and comparison of the erosive behaviour of several pure abrasives and four pulverized fuels. Since high erosion rates were desired, high velocities and an angle of impingement of 90° were employed. In order to be able to relate the experimental conditions to the in-service situation, the effect of variations in velocity and angle of incidence on erosion rate was established. It was found that the maximum in erosion rate occurs at 90° for all the abrasive media and that, in general, there is acceptable agreement between the experimentally determined erosion rates and those predicted by the expression $E_{90}(\sin\alpha)^n$ for angles as low as 35°.

The influence of several particle parameters on erosion rate was investigated since controversies were found to exist as regards some of these parameters. The range of velocity exponent values obtained in this study span those predicted by the models of Evans et al ($n = 3.2$) and Ruff and Wiederhorn ($n = 2.4$) and are comparable to those obtained by other researchers. A definite velocity exponent - particle size dependence exist for quartz and silicon carbide, with the exponent decreasing as particle size increases and the dependence may be expressed by a relationship of the form $n = qD^{-p}$. The erosion rate increases as particle size increases and the particle size exponent obtained in this investigation is in good agreement with the theoretically predicted value of 3.7. Particle density has the effect of increasing the erosivity of a particular particle type and the exponent value obtained as a result of this investigation is 1.30, as compared to the value of 1.20 predicted by the quasi-static model of erosion. Since the target material is softer than all the abrasives, none of the opinions of researchers as to the effect of hardness on erosion rate could be said to be more acceptable.

The major aim of this investigation was to characterize the pulverized fuels in terms of their particle characteristics and to propose a suitable replacement for the pulverized fuels for use in accelerated erosion testing.

Since the erosive characteristics of the pulverized fuels could not be explained in terms of their particle size distributions and quantitative X-ray diffraction analyses alone, a study of the actual impact damage produced by the pulverized fuels (as well as the pure abrasives) was undertaken. This was done by the analysis of the single impact damage events. Note that a single impact study such as this can only be performed on a material such as glass, since a polycrystalline material would obscure the results. It was found that, for a given abrasive, the range of crater sizes produced is an order of magnitude greater than the range of particle sizes. It was established that it is the large crater sites alone which are responsible for most of the material removal, with the small particles contributing very little to the removal processes. As a result of the single impact damage analysis, it became evident that it is not sufficient to consider the particle parameters alone when selecting a suitable replacement for the pulverized fuels.

Based upon consideration of both the particle parameters and several aspects of the damage produced, it can be proposed that 115 μm diameter quartz would be the most suitable replacement for the pulverized fuels for use in accelerated erosion testing. Quartz has the added advantage of being the major erosive constituent occurring naturally in the pulverized fuels.

REFERENCES

1. CHAUDHRI M.M., and BROPHY P.A. (1980): "Single particle impact damage of fused silica", Journal of Materials Science, Vol. 15, pp. 345-352.

2. CHAUDHRI M.M., and WALLEY S.M. (1978): "A high-speed photographic investigation of the impact damage in soda-lime and borosilicate glasses by small galss and steel spheres", Fracture Mechanics of Ceramics, Vol. 3 - Flaws and Testing, Eds: Bradt, Hasselman and Lange, pp. 349-364.

3. DIMOND C.R., KIRK J.N., and BRIGGS J. (1983): "The evaluation of existing models for impact erosion and abrasive wear of ceramic materials", Wear of Materials, pp. 333-339.

4. EVANS A.G. (1979): "Impact damage mechanics : solid projectiles", Treatise on Materials Science and Technology, Vol. 16, pp. 1-67.

5. EVANS A.G., GULDEN M.E., and ROSENBLATT M. (1978): "Impact damage in brittle materials in the elastic-plastic response régime", Proceedings of the Royal Society, London, A361, pp.343-365.

6. EVANS A.G., and WILSHAW T.R. (1976): "Quasi-static solid particle damage in brittle solids - 1. Observations, analysis and implications", Acta Metallurgica, Vol. 24, pp. 939-956.

7. FRITH V., and HECKROODT R.O. (1984): "The reliability of a digitizer system for image analysis", Practical Metallography, Vol. 21, pp. 593-601.

8. GOODWIN J.E., SAGE W., and TILLY G.P. (1969): "Study of erosion by solid particles", Proceedings of the Institute of Mechanical Engineers, Vol. 184, No. 15, pp. 279-292.

9. GULDEN M.E. (1979): "Solid-particle erosion of high-technology ceramics (Si_3N_4, glass bonded Al_2O_3 and MgF_2)", Erosion : Prevention and Useful Applications, ASTM STP 664, American Society for Testing and Materials, pp. 101-122.

10. GULDEN M.E. (1980): "Effect of number of impacts on erosion of polycrystalline MgF_2 in the elastic-plastic response regime", Journal of the American Ceramic Society, Vol. 63, No. 3-4, pp. 121-126.

11. GULDEN M.E. (1981): "Correlation of experimental erosion data with elastic-plastic impact models", Communications of the American Ceramic Society, pp. C59-C60.

12. HEAD W.J., LINEBACK L.D., and MANNING C.R. (1973): "Modification and extension of a model for predicting the erosion of ductile materials", Wear 23, pp. 291-298.

13. HOCKEY B.J., and WIEDERHORN S.M. (1979): "Erosion of cermaic materials : the role of plastic flow", Proceedings of the 5th International Conference on Erosion by Solid and Liquid Impact, pp. 26.1-26.9.

14. HOCKEY B.J., WIEDERHORN S.M., and JOHNSON H. (1978): "Erosion of brittle materials by solid particle impact", Fracture Mechanics of Ceramics, Vol. 3 : Flaws and Testing, Eds: Bradt, Hasselman and Lange, pp. 379-402.

15. KIRCHNER H.P., and GRUVER R.M. (1978): "Localized impact damage in a viscous medium (glass)", Fracture Mechanics of Ceramics, Vol. 3 : Flaws and Testing, Eds: Bradt, Hasselman and Lange, pp. 365-377.

16. KNIGHT C.G., SWAIN M.V., and CHAUDHRI M.M. (1977): "Impact of small steel spheres on glass surfaces", Journal of Materials Science, Vol. 12, pp. 1573-11586.

17. LAWN B.R., and FULLER E.R. (1975): "Equilibrium penny-like cracks in indentation fracture", Journal of Materials Science, Vol. 10, pp. 2016-2024.

18. LAWN B.R., and MARSHALL D.B. (1978): "Indentation fracture and strength degradation in ceramics", Fracture Mechanics of Ceramics, Vol. 3 : Flaws and Testing, Eds: Bradt, Hasselman and Lange, pp. 205-229.

19. MARSHALL D.B., LAWN B.R., and EVANS A.G. (1982): "Elastic-plastic indentation damage in ceramics: The lateral crack system", Journal of the American Ceramic Society, Vol. 65, No. 11, pp. 561-566.

20. MARSHALL D.B., EVANS A.G., GULDEN M.E., ROUTBORT J.L., and SCATTERGOOD R.O. (1981): "Particle size distribution effects on the solid particle erosion of brittle materials", Wear 71, pp. 366-373.

21. MILLS D., and MASON J.S. (1977): "Particle size effects in bend erosion", Wear 44, pp. 311-328.

22. MILLS D., MASON J.S., and TONG K.N. (1983): "The role of penetrative wear in the erosion of pipe bends", Proceedings of the 6th International Conference on Erosion by Liquid and Solid Impact, pp. 58.1-58.7.

23. RAASK E. (1969): "Tube erosion by ash impaction", Wear 13, pp. 301-315.

24. RAASK E. (1979): "Impact erosion wear caused by pulverized coal and ash", Proceedings of the 5th International Conference by Solid and Liquid Impact, pp. 41-1 - 41-7.

25. RITTER J.E., STRZEPA P., JAKUS K., ROSENFELD L., and BUCKMAN K.J. (1985): "Erosion damage in glass and alumina", Journal of the American Ceramic Society, Vol. 67, No. 11, pp. 769-774.

26. ROUTBORT J.L., and SCATTERGOOD R.O. (1980): "Anomalous solid-particle erosion rate of hot-pressed SiC", Journal of the American Ceramic Society, Vol. 63, No. 9-10, pp. 593-595.

27. ROUTBORT J.L., SCATTERGOOD R.O., and KAY E.W. (1980a): "Erosion of silicon single crystals", Journal of the American Ceramic Society, Vol. 63, No. 11-12, pp. 635-640.

28. ROUTBORT J.L., SCATTERGOOD R.O., and TURNER A.P.L. (1980b): "The erosion of reaction-bonded SiC", Wear 59, pp. 363-375.

29. RUFF A.W., and IVES L.K. (1975): "Measurement of solid particle velocity in erosive wear", Wear 35, pp. 195-199.

30. RUFF A.W., and WIEDERHORN S.M. (1979): "Erosion by solid particle impact", Treatise on Materials Science and Technology, Vol. 16, pp. 69-126.

31. SAGE W., and TILLY G.P. (1969) "The significance of particle size in sand erosion of small gas turbines", The Aeronautical Journal of the Royal Aeronautical Society, Vol. 73, pp. 427-428.

32. SARGENT G.A., MEHROTRA P.K., and CONRAD H. (1979): "Multiparticle erosion of pyrex glass", Erosion : Prevention and Useful Applications, ASTM STP 664, American Society for Testing and Materials, pp. 77-99.

33. SCATTERGOOD R.O., and ROUTBORT J.L. (1981): "Velocity and size dependences of the erosion rate in silicon", Wear 67, pp. 227-232.

34. SHELDON G.L. (1970): "Similarities and differences in the erosion behaviour of materials", Journal of Basic Engineering, Transactions of the ASME, pp. 619-626.

35. SHELDON G.L., and FINNIE I. (1966a): "The mechanism of materials removal in the erosive cutting of brittle materials", Journal of Engineering for Industry, Transactions of the ASME, pp. 393-400.

36. SHELDON G.L., and FINNIE I. (1966b): "On the ductile behaviour of nominally brittle materials during erosive cutting", Journal of Engineering for Industry, Transactions of the ASME, pp. 387-392.

37. SHELDON G.L., and KANHERE A. (1972): "An investigation of impingement erosion using single particles", Wear 21, pp. 195-209.

38. SHETTY D.K., WRIGHT I.G., CLAUER A.H., PETERSON J.H., and MERZ W.E. (1982): "Erosive wear of advanced ceramics in coal-slurry streams", Corrosion - NACE, Vol. 38 No. 9, pp. 500-509.

39. SWAIN M.V., and HAGAN J.T. (1976): "Indentation plasticity and the ensuing fracture of glass", Journal of Physics D : Applied Physics, Vol. 9, pp. 2201-2214.

40. TILLY G.P. (1969): "Erosion caused by airborne particles", Wear 14, pp. 63-79.

41. TILLY G.P. (1973): "A two-stage mechanism of ductile erosion", Wear 23, pp. 87-96.

42. TILLY G.P., and SAGE W. (1970): "The interaction of particle and material behaviour in erosion processes", Wear 16, pp. 447-465.

43. UUEMOIS H., and KLEIS I. (1975): "A critical analysis of erosion problems which have been little studied", Wear 31, pp. 359-371.

44. WIEDERHORN S.M. (1979): "Erosion of Ceramics", Proceedings of Conference on Corrosion/Erosion of Coal Conversion System Materials.

45. WIEDERHORN S.M., and HOCKEY B.J. (1983): "Effect of materials parameters on the erosion resistance of brittle materials", Journal of Materials Science 18, pp. 766-780.

46. WIEDERHORN S.M., and LAWN B.R. (1979): "Strength degradation of glass impacted with sharp particles : I. Annealed surfaces", Journal of the American Ceramic Society, Vol. 62, No. 1 - 2, pp. 66-70.

47. WIEDERHORN S.M., and ROBERTS, D.E. (1976), "A technique to investigate high temperature erosion of refractories", Ceramic Bulletin, Vol. 55, No. 2, pp. 185-189.

48. WIEDERHORN S.M., FULLER (Jnr) E.R., BUKOWSKI J.M., and ROBBINS C.R. (1977): "Effect of hydrothermal environments on the erosion of castable refractories", Journal of Engineering Materials Technology, Transactions of the ASME, pp. 143-146.

APPENDIX I

Mineralogical Analysis - The Internal Standard Method

The materials used in preparing the series of mixtures for the calibration curve were:

(a) Blesberg silica (200 mesh 3/78) - a commercially available fine-grained quartz material.

(b) Glass - obtained by crushing container bottles.

(c) Extra pure calcium fluoride (fluorite).

The percentage of quartz present in the mixtures ranged from 2.10 to 31.58 per cent.

Operating Conditions

The Cu tube was operated at 40 kV and 20 mA. Divergence and receiving slits of ½° and an anti-scatter slit of 1° were used. The scanning speed was set at 1°2θ/min, with a time constant of 1. 0.05g CaF_2 was added to 0.95 g of each sample which was then ground in a vibratory agate mill for 10 minutes. The positions at which the peak and background intensities were measured are listed in the table below:

TABLE I : Peak and background intensities measured

PHASE	BACKGROUND	PEAK	BACKGROUND
Quartz (112)	49°	49 - 51°	51°
CaF_2 (220)	46°	46 - 48.3°	48.3°

APPENDIX II

Velocity Measurement

The apparatus, which consists of a common shaft (20 mm long) on which two discs (made from 0.6 mm thick mild steel) are mounted, is placed 10 mm from the exit port of the erosion apparatus. The disc nearest the exit port has a radial slit (1 mm by 10 mm) through which particles pass, eroding the highly polished surface of the second disc.

Ruff and Ives (1975) made two erosion exposures, one with the discs stationary and the other with the discs rotating at a known constant velocity. Measurement of the angular displacement between the erosion marks thus formed gives a measure of the time-of-flight of the particles as they travel from the first disc to the second.

The Ruff and Ives technique was subsequently modified by Wiederhorn and Hockey (1983) by making erosion exposures on the second disc by rotating the apparatus first in one direction and then in the other, the motor speed being kept constant throughout. This modified technique was employed in the present work, and the constant motor speed was monitored by means of a digital tachometer. The velocity of the particles was controlled by the air pressure and was calculated by means of the equation:

$$V = 4\pi r \nu L/S$$

where V = average particle velocity (ms^{-1})
L = 20 mm (the distance separating the 2 discs)
ν = 35 s^{-1} (the disc rotating velocity)
r = 20 mm (radial distance from the disc centre)
S = angular displacement between erosion marks (mm)

The relationship between the average particle velocity and the air pressure may be expressed as a linear relationship of the form:

$$V = a P + c$$

where a and c are constants

P = air pressure (kPa)

V = average particle velocity (ms^{-1})

The values of a and c obtained for the various impacting particle types are listed below.

TABLE II : The constants a and c

PARTICLE TYPE	CONSTANT	
	a	c
Arnot PF	0.103	14.01
Duvha PF	0.085	17.00
Matla PF	0.095	15.38
Kriel PF	0.083	17.91
230 μm Quartz	0.087	17.20
115 μm Quartz	0.089	15.57
41 μm Quartz	0.084	17.49
115 μm SiC	0.114	15.22
51 μm SiC	0.117	16.33
36 μm SiC	0.096	18.42
120 μm Alumina	0.105	13.25
130 μm Zircon	0.098	17.45

A typical example of the type of plot obtained is illustrated in the figure below.

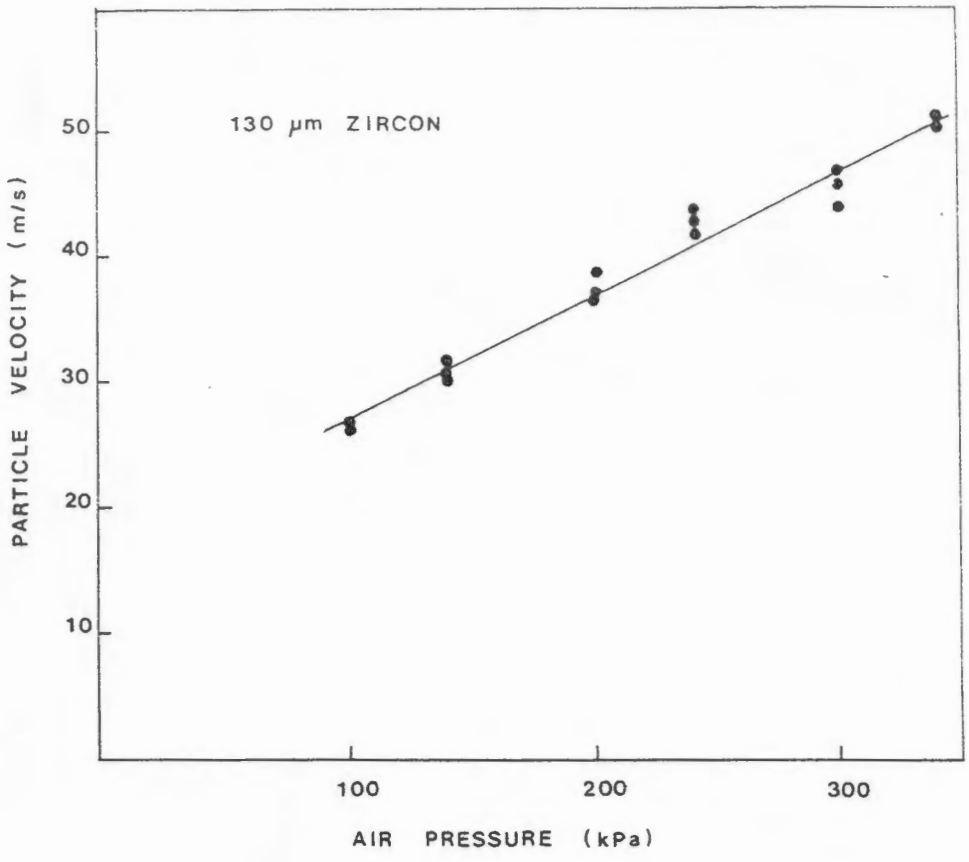

FIGURE II : The measured variation of particle velocity with air pressure. The average distance from the exit port to the rotating discs is 10 mm

It would appear that the linear extrapolation of the form $V = aP + c$ fits the data points very well and the expression can be used for the pressure range 100 kPa to 340 kPa. However, the equation has a large positive y-intercept [a situation found also by Ruff and Ives (1975)] and particle velocities of pressures below 100 kPa must be determined experimentally and not by extrapolation.

APPENDIX III

Erosion rate [milligrams of material lost per gram of abrasive particles (mg/g)] versus particle velocity (ms^{-1}) for the pure abrasives and for the pulverized fuels.

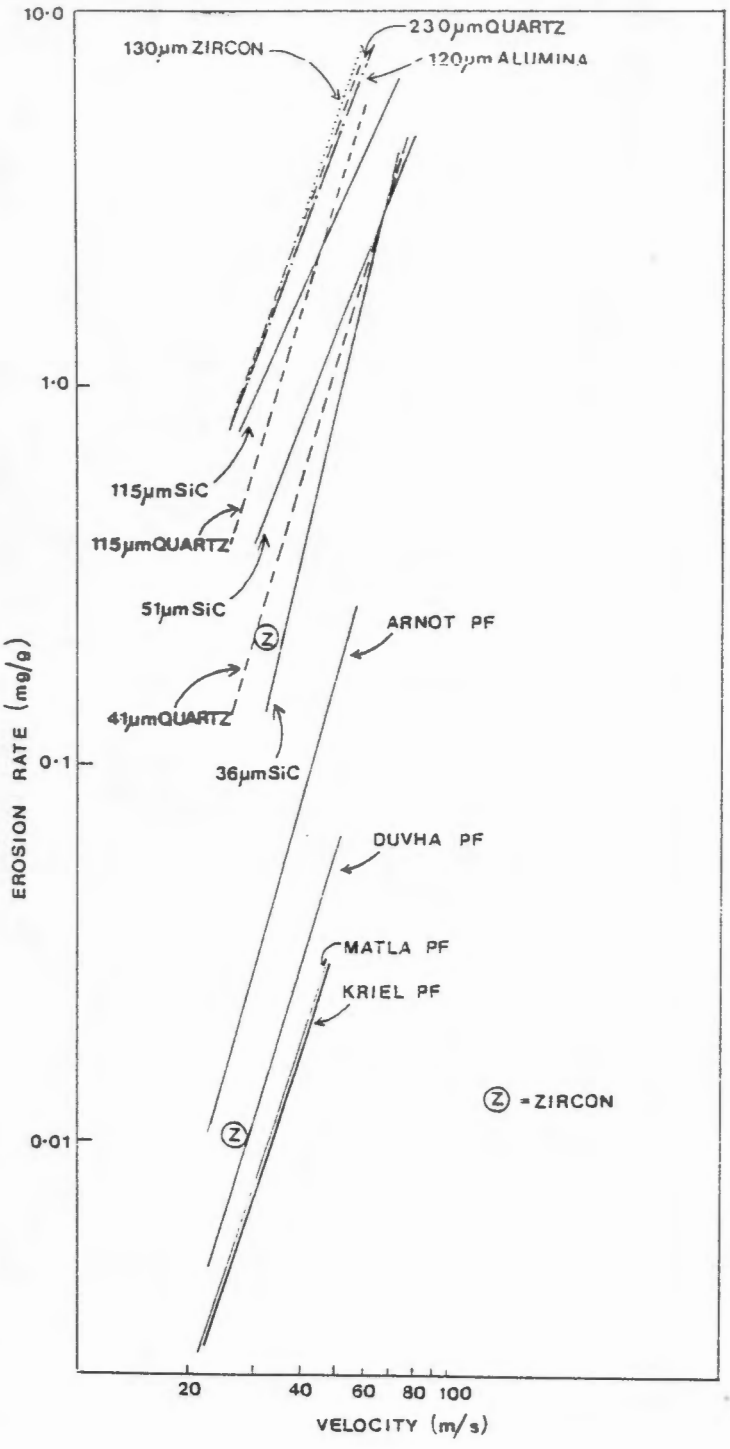

APPENDIX IV

Locations of the power stations, from which the pulverized fuels were obtained, are illustrated in the Figure below.

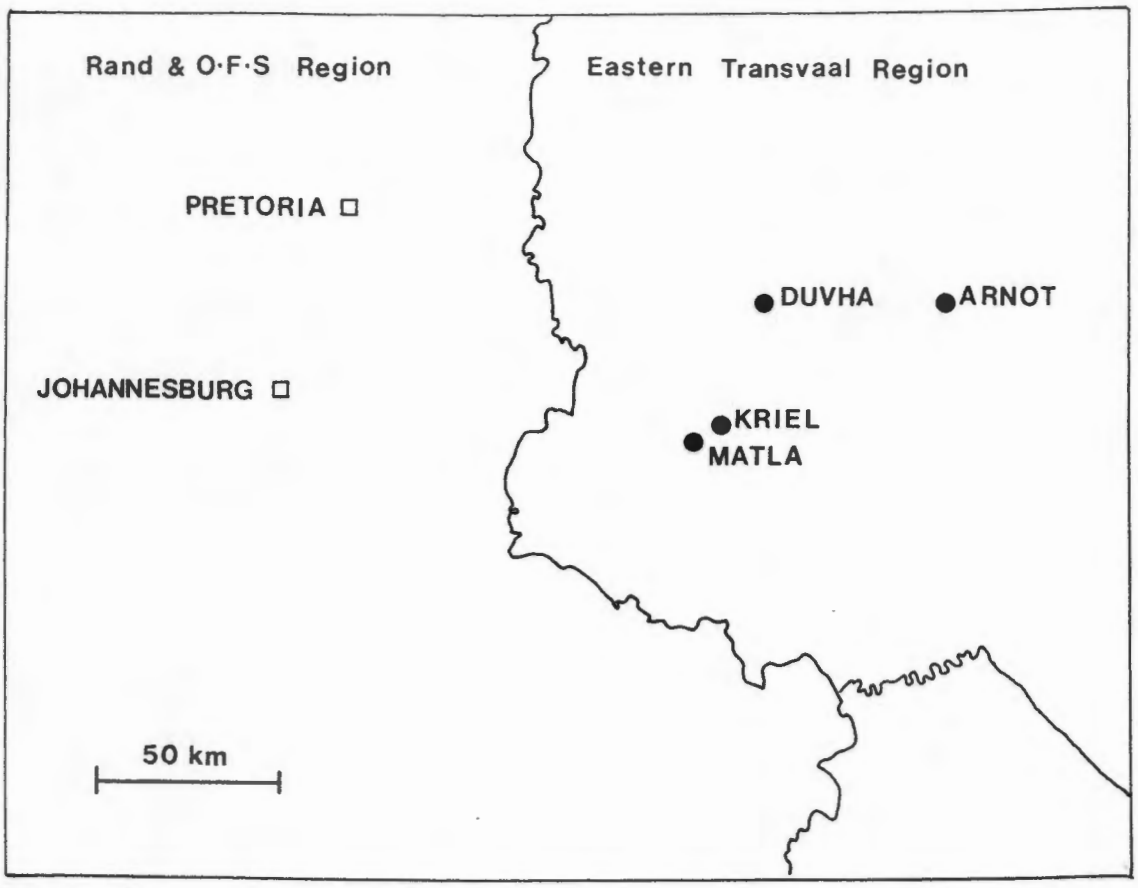

FIGURE III : Locations of the power stations from which pulverized fuel has been analysed.

The following additional information concerning the pulverized fuels was supplied by ESCOM. The information does not have a direct relationship to erosion and has been included for the sake of completeness.

TABLE IIIa : Coal analysis

POWER STATION	ARNOT	DUVHA	MATLA	KRIEL
COLLIERY	ARNOT	DOUGLAS	MATLA	KRIEL
SAMPLE DATE	MARCH 1983	APRIL 1983	JUNE 1982	JUNE 1983
Volatile matter	23,59	25,08	23,08	22,50
Ash	25,74	20,29	25,83	23,87
Moisture	4,04	2,81	4,29	5,50
Sulphur	1,28	1,83	1,16	0,79
Co_2	1,35	1,56	2,78	1,92
Fixed carbon	46,63	51,82	46,80	48,08
Hydrogen	3,37	3,66	3,23	3,17
Nitrogen	1,37	1,45	1,31	1,28

Note the high ash content of the coals

TABLE IIIb : Analysis of the ash obtained from the above coal samples

POWER STATION	ARNOT	DUVHA	MATLA	KRIEL
Silicon (SiO_2)	51,72	48,90	47,50	51,8
Alumium (Al_2O_3)	27,0	30,90	24,90	23,4
Iron (Fe_2O_3)	6,95	5,70	5,0	3,2
Titanium (TiO_2)	1,58	1,90	1,40	1,8
Phosphorous (P_2O_5)	0,92	1,60	0,90	1,5
Calcium (CaO)	6,25	5,20	11,10	11,0
Magnesium (MgO)	1,31	0,60	2,60	2,2
Sodium (Na_2O)	0,88	0,40	0,1	0,3
Potassium (K_2O)	0,51	0,50	1,1	0,6
Manganese (MnO)	0,05	0,04	0,2	0,01
Sulphur (SO_3)	3,78	4,3	4,4	4,2

APPENDIX V

Histograms (per cent volume and per cent number versus diameter of craters (μm)) for the pure abrasives and for the four pulverized fuels. The reproducibility of the results is illustrated in (a).

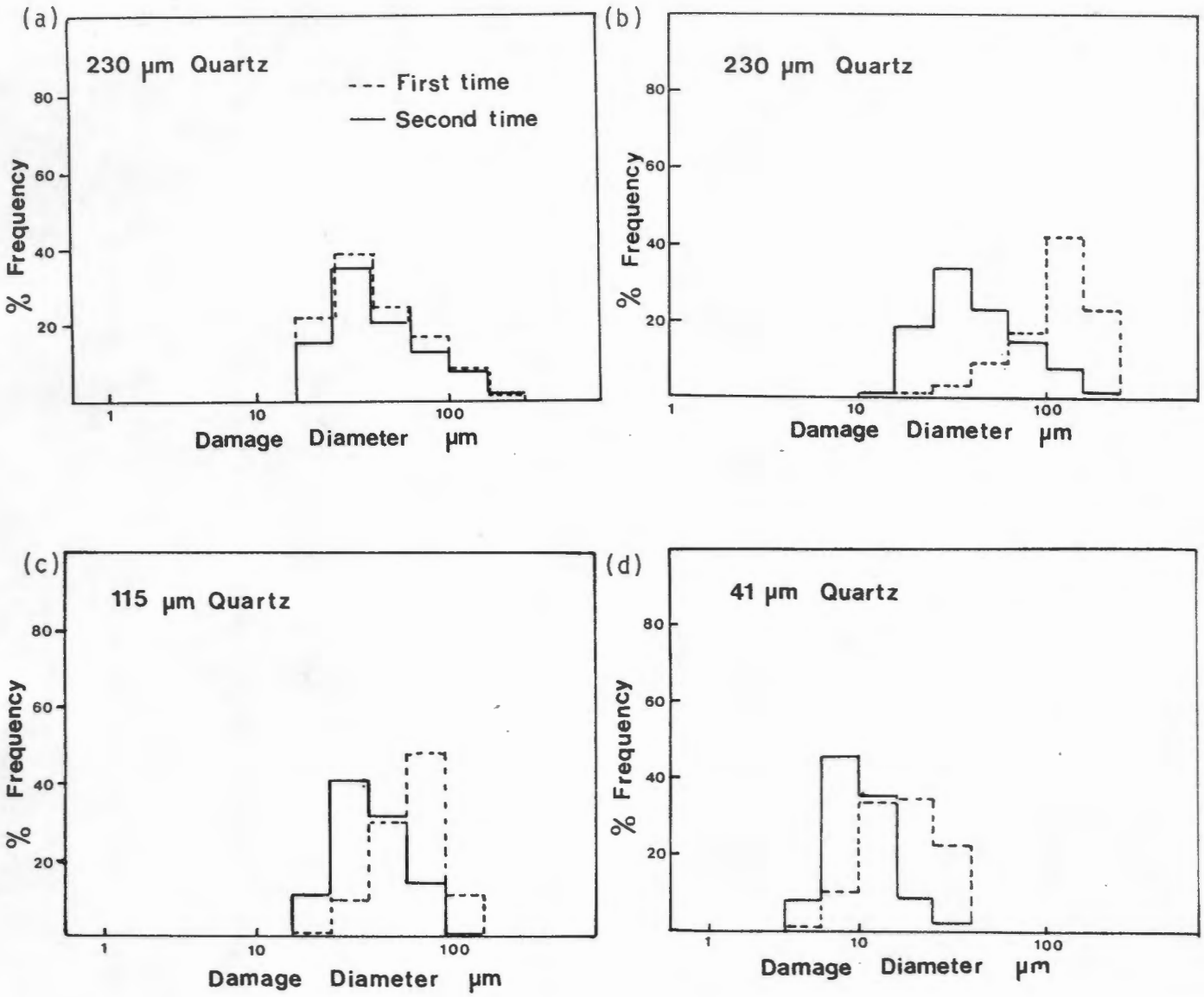

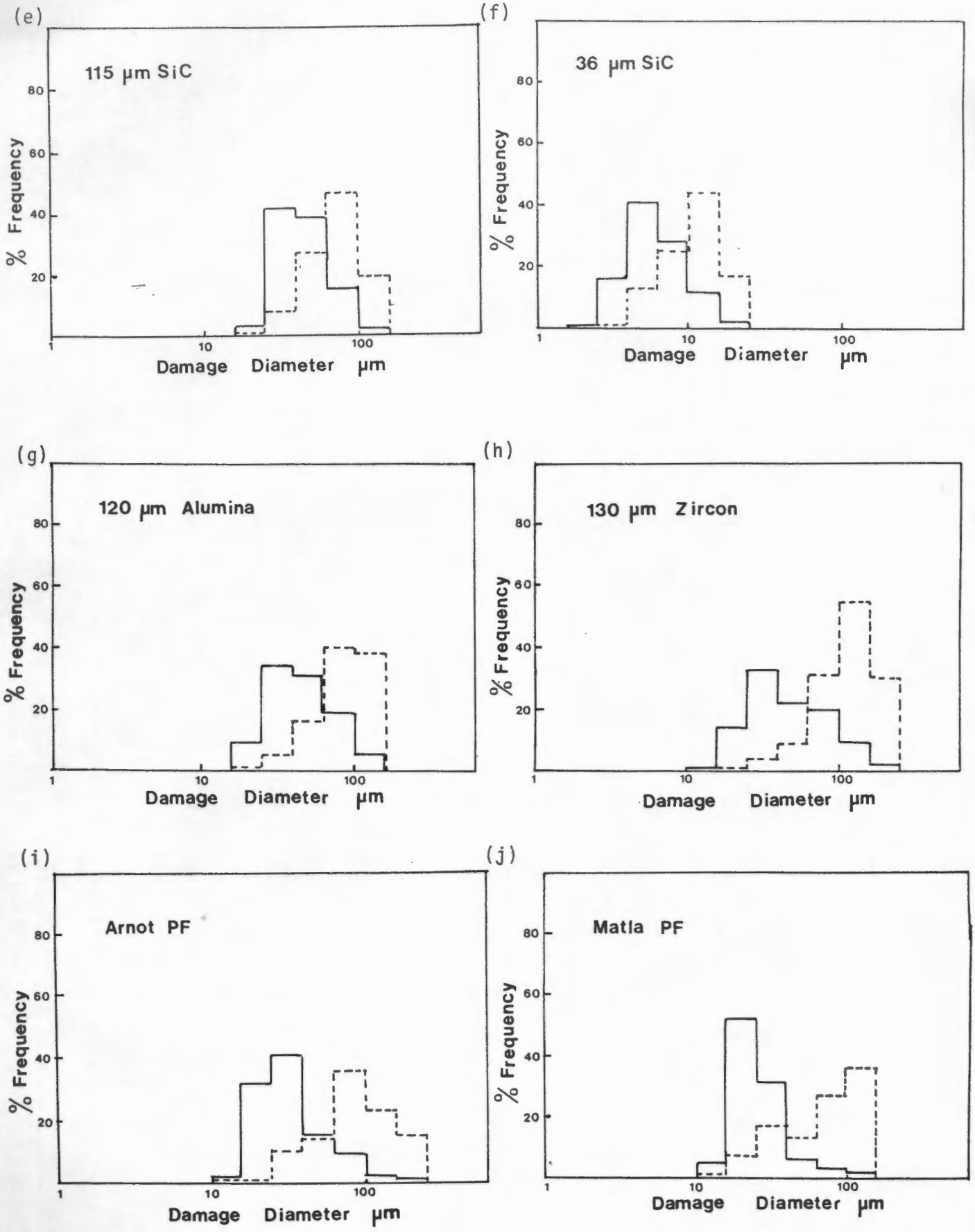
(e)
115 μm SiC
% Frequency
Damage Diameter μm
(f)
36 μm SiC
% Frequency
Damage Diameter μm
(g)
120 μm Alumina
% Frequency
Damage Diameter μm
(h)
130 μm Zircon
% Frequency
Damage Diameter μm
(i)
Arnot PF
% Frequency
Damage Diameter μm
(j)
Matla PF
% Frequency
Damage Diameter μm

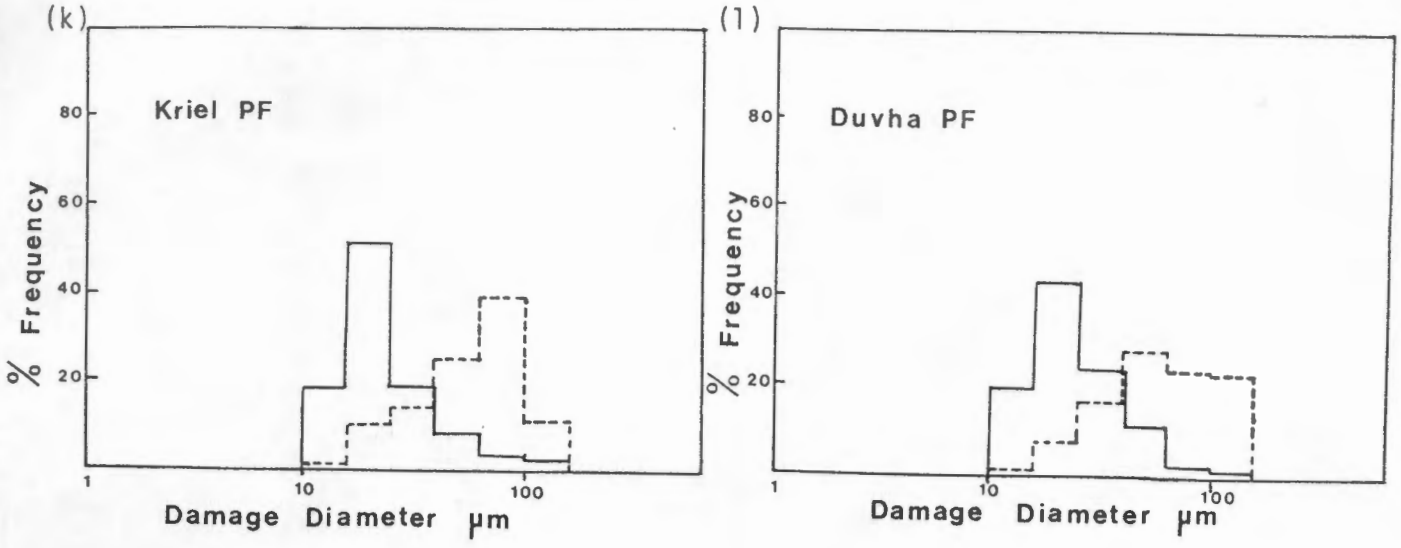
(k)
Kriel PF
% Frequency
80
60
40
20
1
10
100
Damage Diameter µm
(l)
Duvha PF
% Frequency
80
60
40
20
1
10
100
Damage Diameter µm